
Upper Jurassic Geothermal Reservoirs of South Germany

Characterization and novel exploration strategy using an integrated
sequence stratigraphic approach

Dissertation

der Mathematisch-Naturwissenschaftlichen Fakultät

der Eberhard Karls Universität Tübingen

zur Erlangung des Grades eines

Doktors der Naturwissenschaften

(Dr. rer. nat.)

vorgelegt von

Dipl. Geol. Philipp Wolpert

aus Stuttgart

Tübingen

2020

Tag der mündlichen Prüfung:

Dekan: Prof. Dr. Wolfgang Rosenstiel

1. Berichterstatter: Prof. Dr. Thomas Aigner

2. Berichterstatter: Prof. Dr. James H. Nebelsick

Hiermit versichere ich, dass ich die vorliegende Arbeit selbstständig und nur unter Verwendung der angegebenen Hilfsmittel und Quellen angefertigt habe.

Tübingen,

Philipp Wolpert

CONTENT

Content.....	iv
List of figures	vi
List of tables	x
Zusammenfassung.....	1
Abstract	3
1. Introduction	5
1.1 Aims of the Study	6
1.2 Study Area.....	7
1.3 Geological Setting	8
1.3.1 Global Paleogeography	8
1.3.2 Regional Paleogeography (South Germany)	10
1.3.3 Stratigraphic Framework.....	13
1.4 Basin Development & Tectonics.....	15
2. Database and Methodology	17
3. 1D Analysis	19
3.1 Background	19
3.2 Facies Analysis.....	20
3.2.1 Lithofacies Types (LFT)	20
3.2.2 Lithofacies Associations (LFA).....	35
3.3 1D Sequence Stratigraphy	37
3.3.1 Depositional Sequences	37
3.3.2 Observations Core-to-Log Calibration.....	54
Summary of Sequence Stratigraphy	58
3.4 Borehole-Image Interpretation.....	62
3.4.1 Borehole Image Facies	64
3.4.2 Stratal Surfaces Interpreted from Borehole-Image Logs.....	75
3.4.3 Borehole-Image Cycles, Cycle-Sets, and Sequences.....	83
3.4.4 Summary of BHI Interpretation.....	86
3.5 Geothermal Reservoir Types.....	87
4. 2D Analysis	91

4.1	Sequence Stratigraphic Well-Log Correlation.....	91
4.1.1	Correlation panel: Local-scale.....	92
4.1.2	Correlation panel: Regional-scale.....	95
4.1.3	Correlation panel: Basin-scale.....	99
5.	3D Analysis.....	101
5.1	Seismic Interpretation.....	101
5.1.1	Reflector Termination Mapping and Seismic Facies Analysis.....	101
5.1.2	Pseudo stratigraphic layering.....	104
5.1.3	Seismic attribute mapping per zone.....	105
5.1.4	Cut-off definition.....	106
5.1.5	Quantification of reservoir facies vs. non-reservoir facies.....	107
5.1.6	Summary.....	113
5.2	Integration with BHI Logs, Cuttings and Outcrop.....	113
6.	Geological Trend mapping.....	119
6.1	Thickness trends.....	119
6.2	Structural trends.....	121
7.	Synopsis: Geothermal reservoir types and Exploration strategy.....	123
7.1	Distribution of Geothermal Reservoir Types.....	123
7.2	Ranking of reservoir types and integration with dynamic data.....	127
7.3	Inter-well connectivity via high-K streaks.....	129
7.4	Areas of rapid subsidence.....	131
8.	Summary and Conclusions.....	134
	Acknowledgments.....	136
	REFERENCES.....	138

LIST OF FIGURES

Figure 1: Study area showing the North alpine Foreland basin (Molasse Basin). Most of the geothermal developments are in and around the greater Munich area.	8
Figure 2: Paleogeography of Europe (Blakey, 2008)	9
Figure 3: Paleogeographic map of the Upper Jurassic (Malm Zeta 1 +2; modified after Meyer-and Schmidt-Kaler,1989).....	11
Figure 4: Paleogeographic cross-section (modified after Meyer and Schmidt-Kaler, 1990) showing the depositional character and dominating lithological units.	12
Figure 5: Stratigraphic table of South Germany. Modified after Villinger and Fleck (1995), Quenstedt (1858) and ISC (v2018/08).....	14
Figure 6: N-S cross-section of the Molasse basin (Lemcke, 1988).....	16
Figure 7: Interpreted Purbeck lithology and variations.....	19
Figure 8: LFT 1: Claystone	23
Figure 9: LFT 2: Dark, laminated marlstone	23
Figure 10: LFT 3: Lime, bedded mudstones	24
Figure 11: LFT 4: White, thickly bedded and massive lime mudstone	24
Figure 12: LFT 5: White mudstone/ wackestone with fossil-rich clay alternations	25
Figure 13: LFT 6: Well bedded to massive mud-to wackestone	25
Figure 14: LFT 7: Tuberoïd wacke- to packstone.	26
Figure 15: LFT 8: Cm bedded, marly sponge thrombolite float- to rudstone.....	26
Figure 16: LFT 9: Cm- to dm bedded, sponge-thrombolite float- to rudstone	27
Figure 17: LFT 9: Cm to dm bedded, sponge thrombolite float- to rudstone	27
Figure 18: LFT 10: Dm to m bedded sponge-thrombolite float-to-rudstone	28
Figure 19: Sponge-thrombolite float-to-rudstone : detail view.....	28
Figure 20: LFT 11: Massive dolomitic Mud- and Wackestone	29
Figure 21: LFT 12: Chaotic/ brecciated mudstone	29
Figure 22: LFT 13: Well bedded lime-marlstone alternations	30
Figure 23: LFT 14: Bioturbated dolo mudstone	30
Figure 24: LFT 15: Dark, intensively bioturbated, mudstone	31
Figure 25: LFT 16: Bioclastic wackestone and packstone	31

Figure 26: LFT 17: Wackestone with dolo packstone filled burrows	32
Figure 27: LFT 18: Bioclastic-peloidal-oolitic Packstones.....	32
Figure 28: LFT 19: Peloidal-oolitic grainstones.....	33
Figure 29: LFT 20: Coral floatstone	33
Figure 30: LFT 21: Flat pebble conglomerate and reworked surface	34
Figure 31: LFT 22: Algal boundstone	34
Figure 32: Main Lithofacies Associations modified after (Meyer and Schmidt-Kaler, 1989)	35
Figure 33: Sedimentological characteristics of S 1(Malm Alpha to top Beta).....	39
Figure 34: Large scale sequence 1 (S1) comprising the Malm alpha to top beta interval.	40
Figure 35: Sedimentological characteristics of S 2(Malm Gamma to top Epsilon interval).	43
Figure 36: Bed thickness index tentatively used to differentiate the Malm Delta-Epsilon interval.....	44
Figure 37: Large scale sequence 2 (S 2) comprising the Malm Gamma to top Epsilon interval.....	45
Figure 38: Sedimentological characteristics of S 3(Malm Zeta interval).	48
Figure 39: Sequence 3, comprising the Malm zeta intervals.	49
Figure 40: Sedimentological characteristics of S 4 (Malm Zeta to Purbeck interval).	52
Figure 41: Sequence 4, comprising the Malm Zeta to Purbeck interval.....	53
Figure 42: Storey bioturbation after Wetzel (1981) compared to the Top Upper Jurassic Sequence Boundary observed in research well Moosburg SC 4.....	55
Figure 43: Top Malm sequence boundary interpreted from research well Moosburg SC4.	56
Figure 44: Overview of the well Moosburg SC4 and the interpreted large scale sequences.	59
Figure 45: General sequence stratigraphic interpretation for the Upper Jurassic (modified after Leinfelder et al., 1994).....	61
Figure 46: Linking core-based facies with the borehole image facies.....	62
Figure 47: Borehole image facies type: Well-bedded limestone	64
Figure 48: Borehole image facies type: Clasts and debris.....	65

Figure 49: Borehole image facies type: Bioclast debris	66
Figure 50: Borehole image facies type: Bioturbation	67
Figure 51: Borehole image facies type: Olistolith.....	68
Figure 52: Borehole image facies type: Sponge bioherm	69
Figure 53: Borehole image facies type: Corals	70
Figure 54: Borehole image facies type: Karst.....	71
Figure 55: Borehole image facies type: Vuggy macropores	72
Figure 56: Undefined borehole image facies	73
Figure 57: Stratal surfaces from image logs: Highly indented surfaces	76
Figure 58: Stratal surfaces from image logs: Truncation surfaces.....	77
Figure 59: Stratal surfaces from image logs: Concordat surfaces	78
Figure 60: Stratal surfaces from image logs: Draping surfaces	79
Figure 61: Statal surfaces as proximal-distal indicators.....	80
Figure 62: Multi-proxy BHI workflow to identify large scale sequences	82
Figure 63: Sequence boundaries identified from borehole image logs.....	83
Figure 64: Cycles and cycle sets	84
Figure 65: Reservoir Type: Karst.....	87
Figure 66: Reservoir Type: Vuggy porosity.....	88
Figure 67: Reservoir Type: Dolomitization.....	88
Figure 68: Reservoir Type: Bioturbation	89
Figure 69: Reservoir Type: Bioherm debris	89
Figure 70: Reservoir Type: Fractures	90
Figure 71: Reservoir Type: Faults	90
Figure 72: Local correlation in approx. dip orientation.	94
Figure 73: Orientation of dip section on a regional correlation scale.	95
Figure 74: Orientation of dip section with paleogeography and structural elements.	96
Figure 75: Regional correlation in approx.. dip orientation.....	98
Figure 76: Basin-wide correlation in approx. dip orientation (A=proxima, B=distal).....	100
Figure 77: Seismic facies and reflector termination classification after Mitchum and Vail (1977). Marked in red are the most frequently occurring features of this study.	102

Figure 78: Seismic line showing the uninterpreted and interpreted section. Seismic facies analysis and reflector terminations show basin, reef/bioherm, and reef/bioherm debris as well as three large scale depositional sequences (S1-S3) and a fault. 103

Figure 79: Pseudo-stratigraphic layering scheme. Top Upper Jurassic and Top Middle Jurassic are interpreted surfaces, whereas the layers in between are calculated based on the thickness map and seismic resolution. 104

Figure 80: Seismic attribute mapping per zone. The example shows the first results for zone 1, with high reflectivity in purple and low reflectivity in yellow/red colors..... 106

Figure 81: Cut-off definition via cursor-tracking mode. (A) Adjusted attribute map compared simultaneously with the seismic line (B) to define the threshold for basin and reef/bioherm (C). 107

Figure 82: Sum of magnitude map for zone 1 108

Figure 83: Sum of magnitude map for zone 2..... 108

Figure 84: Sum of magnitude map for zone 3..... 109

Figure 85: Sum of magnitude map for zone 3..... 109

Figure 86: Sum of magnitude map for zone 4..... 110

Figure 87: Sum of magnitude map for zone 5..... 110

Figure 88: Sum of magnitude map for zone 5..... 111

Figure 89: Sum of magnitude map for zone 6..... 111

Figure 90: Sum of magnitude map for zone 7..... 112

Figure 91: Summary seismic attribute maps visualizing bioherm growth during the Upper Jurassic. 113

Figure 92: Integration of borehole image facies associations to validate the seismic interpretation..... 114

Figure 93: Borehole cuttings to validate the borehole image interpretation. 115

Figure 94: Key observation from the seismic interpretation compared with outcrop analogs. 116

Figure 95: Size and dimensions of bioherm-complex and basins..... 117

Figure 96: Bioherm complex from the Swabian Alb with an internal lagoon (from Chiracal, 2020). 117

Figure 97: Individual bioherm buildup (from Chiracal, 2020) 118

Figure 98: Thickness map of the complete Upper Jurassic Malm. 119

Figure 99: Potential Karst map interpreted from caliper data.....	120
Figure 100: Pre-Permian geological map of Western Europe.....	121
Figure 101: Permian and Mesozoic Tectonic Units	122
Figure 102: Geothermal reservoir type 1: Karst.....	123
Figure 103: Geothermal reservoir type 2: Shallow water facies.....	124
Figure 104: Geothermal reservoir type 3: Bioturbation	125
Figure 105: Geothermal reservoir type 4: Dolomite around clay/marl baffles	125
Figure 106: Geothermal reservoir type 5: Bioherm debris (proximal)	126
Figure 107: Geothermal reservoir type 6: Fractures and faults.....	127
Figure 108: Schematic fluid flow behavior (matrix or high-K) in the subsurface.	130
Figure 109: Dry geothermal wells south of Munich (modified from Ziegler, 1990)	131
Figure 110: Comparison of seismic dip line from Freigham and Königsdorf.....	133

LIST OF TABLES

Table 1: Summary of lithofacies types (LFT).	21
Table 2: Lithofacies types (LFT) and Facies Associations (LFA).....	36
Table 3: Summary BHI Facies Types	74
Table 4: Reservoir types Integration of dynamic data.....	129

ZUSAMMENFASSUNG

Diese Studie untersucht systematisch die geothermischen Reservoireigenschaften der etwa 500-600 m mächtigen Karbonate des Oberjura im Untergrund des Molassebeckens, wo nur bestimmte Intervalle zum geothermischen Aquifer beitragen. Daher integriert diese Studie alle relevanten Aspekte der geothermischen Reservoircharakterisierung nach einem 1-D (Bohrkern und Well-Logs), 2-D (Korrelationen), 3-D Ansatz (seismische Interpretation und Integration). Dieser hierarchische Workflow, der auf Erfahrungen der Kohlenwasserstoffindustrie im Bereich der Reservoircharakterisierung aufbaut, wurde an die Bedürfnisse der Geothermie angepasst, um die Eigenschaften und die Verteilung der Reservoirtypen zu verstehen. Der Workflow besteht aus folgenden Schritten: (1) Faziesanalyse an Bohrkernen, (2) Borehole Image- und Well-Log Interpretation, (3) Sequenz-stratigraphisches Rahmenwerk, (4) Interpretation des Ablagerungsmilieus, (5) Identifizierung potentieller Reservoirtypen und (6) Integration dynamischer Daten.

Zweiundzwanzig Lithofaziestypen wurden bei der Faziesanalyse dokumentiert, sowie drei Ablagerungssequenzen für den Oberjura und eine für die Purbeck Formation. Große Teile der Kernstecke wurden einem tiefen Ablagerungsmilieu (unterhalb der Sturmwellenbasis) zugeordnet. In obersten Teil der Abfolge ist jedoch ein Wechsel zu einem flacheren, höher-energetischen Ablagerungsmilieu zu beobachten, unter anderem mit deutlichen Auftauchanzeiger.

Ein innovativer Multi-Proxy-Workflow für die Interpretation von Borehole Image Logs in Karbonaten bietet neue Möglichkeiten, die Beobachtungen der Bohrkernbeschreibung mit den Image Logs zu integrieren. Die vertikale Abfolge von neun verschiedenen Borehole Image Faziestypen sowie ein semi-quantitatives Charting der stratalen Oberflächen lieferten wichtige Einblicke in die sequenz-stratigraphische Entwicklung und die Charakterisierung von geothermischen Reservoirtypen.

Das Resultat der 3D-Seismik Analyse ist ein „Best-Practice“ Workflow zur Unterscheidung der drei dominierenden seismischen Faziestypen, basierend auf ihrer Reflektionsintensität. Dadurch kann zwischen potentieller Reservoirfazies und Nicht-Reservoirfazies unterschieden werden. Die Ergebnisse der 1-D- und 2-D-Analyse wurden

schrittweise integriert, um die Interpretation auf verschiedenen Skalen zu validieren. Die dadurch gewonnenen Erkenntnisse können bei der Exploration von neuen geothermischen Projekten im Molassebecken angewendet werden und liefern wichtige Erkenntnisse um das Fündigkeitsrisiko einschätzen zu können.

Die lokale, regionale und beckenweite sequenz-stratigraphische Korrelation zeigt unter anderem deutliche Mächtigkeitsvariationen der oberjurassischen Karbonate. Die Integration paläotektonischer Aspekte in die sequenz-stratigraphische Interpretation trägt zum Verständnis dieser Mächtigkeitsvariationen bei. Zusammen mit den Mächtigkeitsvariationen wurde auch eine Veränderung der Ablagerungsräume und der Faziestypen dokumentiert. All diese Faktoren beeinflussen die Entstehung, Eigenschaften und Verteilung potentieller geothermischer Reservoirtypen.

Letztlich ermöglicht die Integration dynamischer Daten ein Ranking der geothermischen Reservoirtypen basierend auf dem dominierenden Permeabilitätstyp : (1) "High-K" und (2) "Matrix-dominated". Diese Studie zeigt, dass das untersuchte oberjurassische geothermische Feld eine Kombination aus strukturellen und stratigraphischen Fallen ist. Deshalb ist das sequenz-stratigraphische Rahmenwerk, welches die Entstehung und Verteilung der Reservoirtypen und Zuflüsse im genetischen Kontext betrachtet, ein entscheidendes Element für eine erfolgreiche und nachhaltige geothermische Entwicklungsstrategie in Karbonaten des Süddeutschen Oberjura.

ABSTRACT

This study systematically investigates the geothermal reservoir properties of the approximately 500-600 m thick Upper Jurassic carbonates in the subsurface of the Molasse basin, where only specific intervals contribute to the geothermal aquifer. Therefore, this study integrates all relevant aspects of geothermal reservoir characterization in carbonates following an 1-D (core and well data) to 2-D (correlations) to 3-D (seismic interpretation and integration) approach. This hierarchical workflow, which is based on reservoir characterization workflows established by the hydrocarbon industry is then modified to understand the characteristics and distribution of geothermal reservoir types involving the following steps: (1) core-based facies analysis, (2) borehole image and well log analysis, (3) sequence-stratigraphic framework, (4) interpretation of depositional environments, (5) identification of potential reservoir types and (6) integration of dynamic data.

The core-based facies analysis reveals twentytwo lithofacies types, three depositional sequences for the Upper Jurassic and one for the Upper Jurassic/Lower Cretaceous Purbeck Formation. Large parts of the interpreted depositional environment correspond to a relatively deep (below storm-wave base) deposetting. Towards the top of the succession, a change to a shallower, higher water energy environment is observed, with clear indications of exposure.

A newly established multi-proxy workflow for borehole image interpretation in carbonates reveals novel opportunities to link the core-based observations with the borehole images and shows how to maximize the value of information of such logs. The vertical stacking of nine distinct borehole image facies types, as well as a semi-quantitative charting of stratal surfaces, provided new insights into the sequence-stratigraphic development and the characterization of geothermal reservoir types.

The evaluation of the 3D seismic survey yielded a best practice approach to differentiate three dominating seismic facies types based on their reflectivity and to differentiate between potential reservoir facies and non-reservoir facies. The results of the 1-D and 2-D analysis were used to validate the interpretation on various scales and draw

conclusions, that can be applied directly to the early exploration stage of emerging geothermal projects in the Molasse basin.

The local, regional and basin-wide sequence-stratigraphic correlation show thickness variations of the Upper Jurassic carbonates. The integration of paleotectonic aspects into the sequence-stratigraphic interpretation adds to the understanding of these thickness variations. Along with the thickness variations, a change of depositional environment and facies types were documented. All these factors affect the characteristics and the distribution of potential geothermal reservoir types.

Ultimately, the integration of dynamic data allows a ranking of the geothermal reservoir types and a subdivision into “high-k dominated” and “matrix-dominated” geothermal reservoir types. It shows that the investigated Upper Jurassic geothermal field of the study area is a combination of structural and stratigraphic traps. The sequence stratigraphic context explains the distribution of the preferential fluid pathways and is a crucial element for a successful and sustainable geothermal development strategy in Upper Jurassic carbonates.

1. INTRODUCTION

Carbonates of the Upper Jurassic are the most important target for deep geothermal exploration in the Molasse Basin/Germany (Böhm et al., 2010; Böhm et al., 2011; Böhm, 2012a; Homuth et al., 2015; Wolfgramm et al., 2011). They are buried 2500-4000m in the Munich metropolitan area. High flow rates (>100 l/sec) and high temperatures (>100°C) are the requirements for electric power generation and domestic heating. The Upper Jurassic Malm aquifer offers both; hence geothermal exploration in the Molasse basin is thriving to accomplish Munich's ambitious vision to cover domestic heating demand exclusively through renewable energy by 2040 (www.swm.de).

Upper Jurassic carbonates of South Germany are traditionally subdivided into two simplified magna-facies types: (1) well-bedded marly carbonates and (2) massive carbonates (Geyer and Gwinner, 1984; Gwinner, 1976). The massive carbonates often associated with karstification, dolomitization, and fractures, and are therefore considered as the best potential geothermal reservoir facies. The well-bedded marly carbonates are non-reservoir facies and act as aquitards (Böhm, 2012a)). The massive carbonates are predominantly formed by sponge/microbial biohermal buildups associated with a deeper shelf environment of deposition (below storm wave base) (Leinfelder et al., 1996; Leinfelder, Krautter et al., 1994; Pawellek and Aigner, 2003a, 2003b; Ruf et al., 2005b). Towards the top of the Upper Jurassic carbonate succession, the sponges are successively replaced by corals and other shallow water components like ooids and peloids, which are now the primary buildup-building components (Meyer, 1994a). This change from an M-factory to a T-factory (Schlager, 2005) is most likely related to sea-level fall at the end of the Upper Jurassic (Haq et al., 1987). The sequence stratigraphic analysis of the fully-cored reference well Moosburg SC4 reveals 3 large scale depositional sequences (S1-S3), that can also be identified on a seismic scale. Internal heterogeneities of the massive lime- and dolostones (bioherms), as well as the sequence stratigraphic architecture, have a significant impact on reservoir types, distribution, and properties. Highest flow rates are often linked with (1) karstification, (2) dolomitization, and/or (3) faults and fractures and are therefore of significant interest.

1.1 Aims of the Study

The improvement of the geothermal exploration strategy for Upper Jurassic carbonates in the greater Munich area and the Molasse Basin is the main objective of this study. Several non-economic dry-holes located south of Munich (e.g., Gelting-Geretsried, Mauerstetten, and Iking), highlight the need to better understand the subsurface and the geothermal carbonate reservoir (Dussel et al., 2018).

This study deals with the following fundamental questions to improve the geothermal exploration and development of Upper Jurassic carbonates in the South German Molasse Basin:

1. What are the geothermal reservoir types?
2. Where are these reservoir types located (in a sequence stratigraphic context)?
3. What is controlling the formation of the geothermal sweet-spots?
4. Is the presence of geothermal sweet-spots predictable?
5. Why are the geothermal wells south of Munich dry?
6. Where is the southern border of the productive aquifers?

Therefore, a systematic approach from 1-D sedimentological observations to 2-D correlations, 3-D seismic interpretation, and integration with dynamic data was applied. The workflow is based on the work from Kearns and Tinker (1997) and was adapted to focus on the geothermal requirements. The key elements are:

- Documentation of the Upper Jurassic facies types and depositional sequences.
- Borehole image facies interpretation and the link with core-based facies types.
- Establishment of a sequence-stratigraphic framework.
- Seismo-stratigraphic analysis and borehole image facies integration.
- Identification of potential geothermal reservoir types.
- Geothermal property mapping.

1.2 Study Area

Most of the geothermal exploration activity takes place directly in the Munich metropolitan area, in the surrounding communities, and further to the south towards the Alps (Figure 1). The Upper Jurassic carbonates are buried to a depth of 2500 - 3500m in the Munich area and up to 5000m further to the South. 30km NW of Munich, close to the city Landshut an der Isar, the research well Moosburg SC4 is located. It is the only well that recovered a continuous section of core from the Upper Jurassic and the Purbeck Formation (Meyer, 1994b), and yields invaluable information to better understand the subsurface of the Molasse Basin. The Upper Jurassic carbonates crop out to the North at the Swabian and Franconian Alb which are excellent areas for outcrop analog studies. Facies types, fossils, depositional environments, sequence stratigraphic architecture, geobody dimensions, and orientations can be studied in great detail and provide invaluable information to better understand the subsurface of the Molasse basin (Aigner and Schauer, 1998; Bartenbach, 2008; Bold, 2010; Fügel, 2009; Geyer and Gwinner, 1984; Gwinner, 1976; Koch et al., 1994; Koch and Heuschkel, 2016; Olivier et al., 2004; Pawellek, 2001; Pawellek and Aigner, 2003a, 2003b; Pawellek and Aigner, 2004; Pross et al., 2006b; Ruf et al., 2005a; Ruf et al., 2005b)

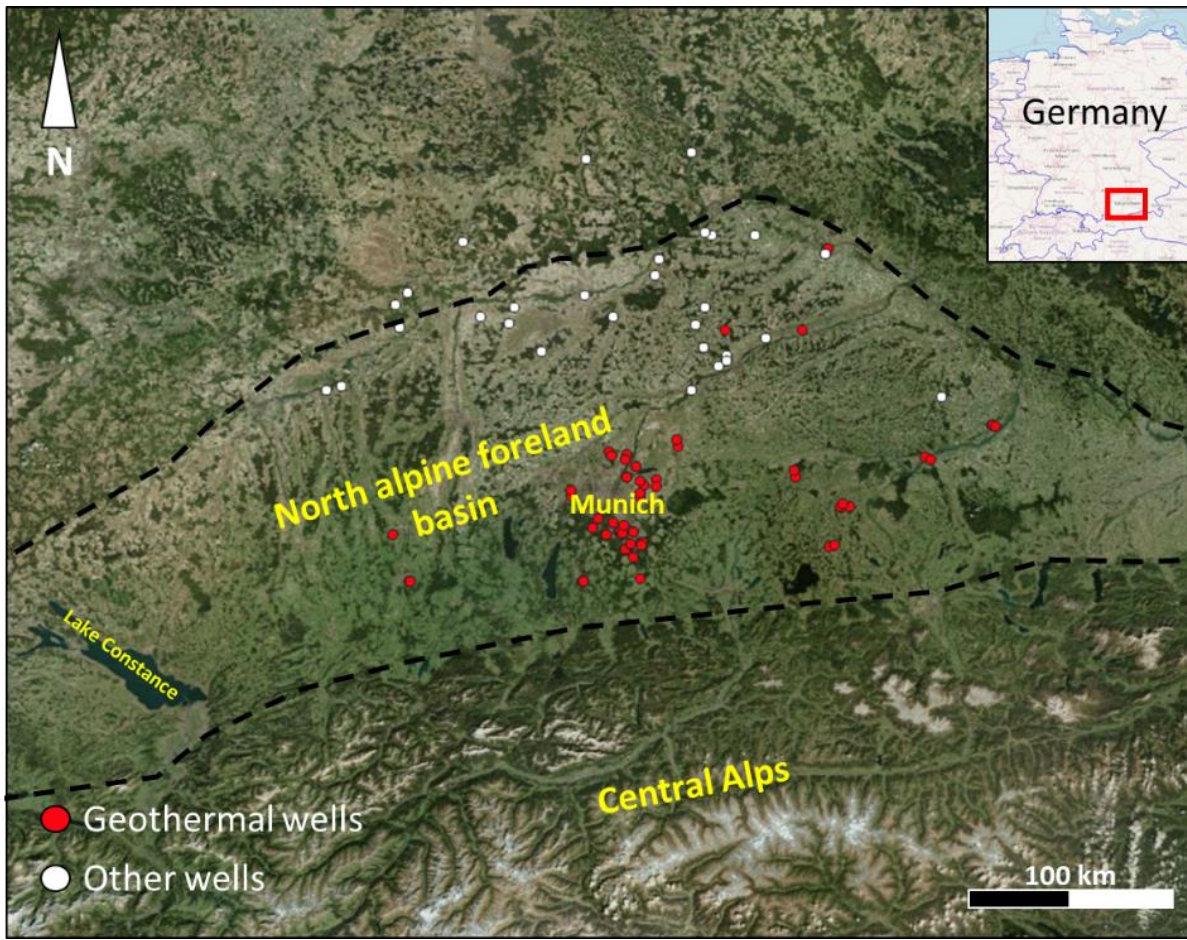


Figure 1: Study area showing the North alpine Foreland basin (Molasse Basin). Most of the geothermal developments are in and around the greater Munich area.

1.3 Geological Setting

1.3.1 Global Paleogeography

During the Jurassic, the Tethys ocean separated the northern continents (Laurasia) from Gondwana. It was an episode of increased igneous activity and rifting (Scotese, 2001). In the Late Jurassic, the Central Atlantic Ocean was a narrow ocean that separated Africa and North America (Figure 2, A), and Gondwana started to break apart (Blakey, 2008; Scotese, 2001). Large parts of the continental edges were flooded, forming epicontinental shelf seas (Figure 2, light blue rims of continents).

Introduction

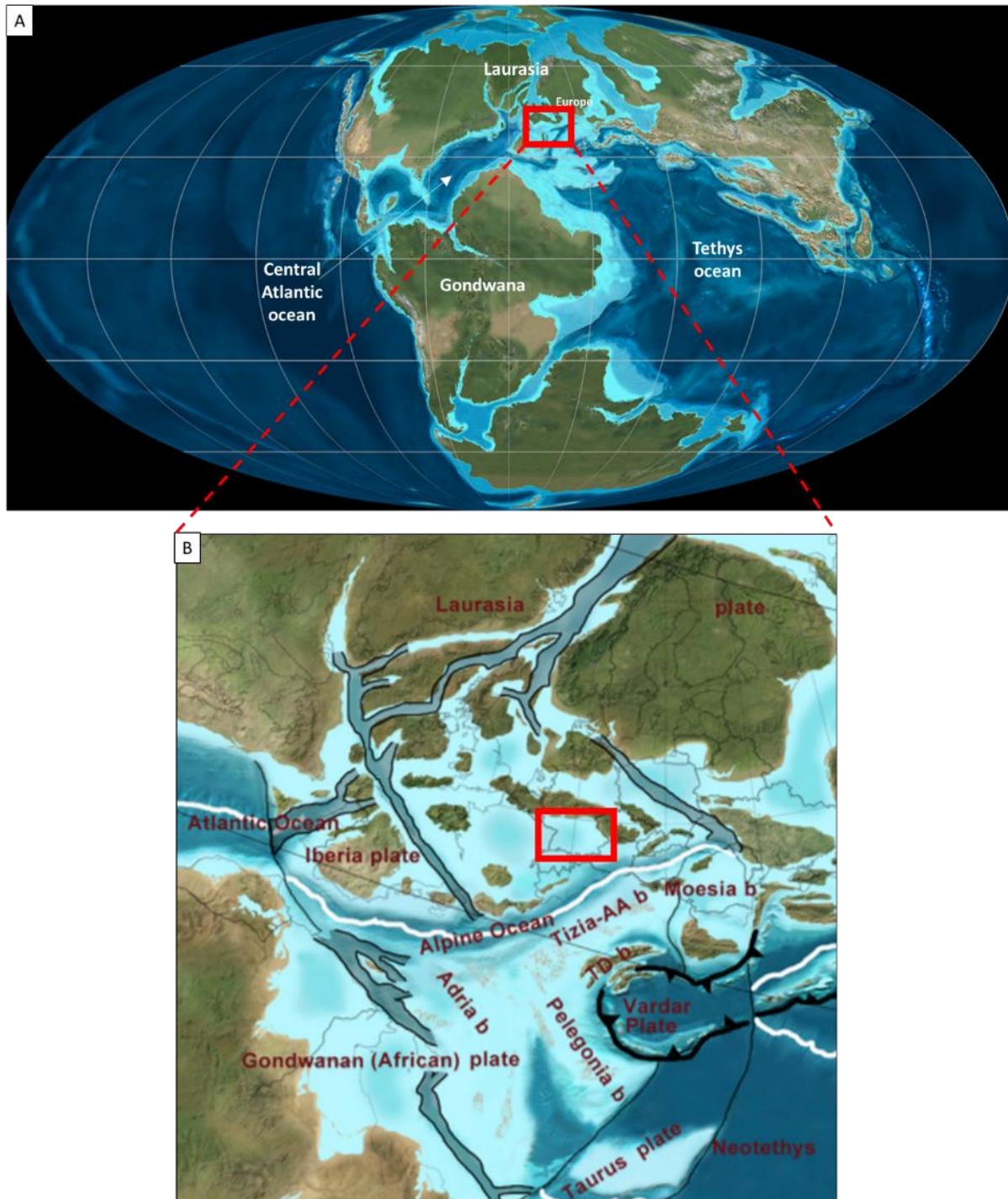


Figure 2: Paleogeography of Europe (Blakey, 2008)

(A) Overview of the Upper Jurassic showing the northern edge of the Tethys ocean, the opening of the Central Atlantic Ocean and the surrounding landmasses. (B) The study area of south Germany marked with the red square.

According to many authors (Leinfelder, 1994; Meyer & Schmidt-Kaler, 1990; Pawellek and Aigner, 2003b; Ziegler, 2001) the Upper Jurassic of South Germany was part of

Introduction

such an epicontinental shelf area (Figure 2, B). To the North, the shelf was separated from the boreal sea by an island archipelago (formed by the London Brabant Massif, Rhenish Massif, and the Bohemian Massif) and connected to the Tethys Ocean in the South (Meyer, 1994a; Meyer, R. K. F. and Schmidt-Kaler, H., 1990). The epicontinental shelf seas, along with a tropical to a subtropical and relatively hot and dry climate, favored the deposition of carbonates (Leinfelder, Krautter et al., 1994; Leinfelder, R., 1993; Leinfelder, R. R., Nose, M. et al., 1993).

1.3.2 Regional Paleogeography (South Germany)

The Upper Jurassic of Southern Germany can be subdivided into three large paleogeographic areas: the Swabian, the Franconian, and the Helvetic facies. In general, the Helvetic facies represents a basin environment, the Swabian facies a sponge-dominated deeper part of the carbonate platform/ramp, and the Franconian facies comprises more shallow-water facies (e.g., corals). The paleogeographic context for the Upper Jurassic of South Germany is shown in Figure 3 and discussed in great detail in (Meyer and Schmidt-Kaler, 1989, 1990).

Three overall depositional environments are present:

- (1) continental environment
- (2) transitional environment
- (3) marine environment

The continental environment is represented by the Rhenish Land to the North-West and the Bohemian massif to the East. The continental environment turns into a transitional zone, which is characterized by tidal mudflats. The marine environment is dominated by carbonates and represents the Upper Jurassic of South Germany. The three arrows in Figure 3 indicate the main direction of terrigenous input (Meyer and Schmidt-Kaler, 1989, 1990).

Introduction

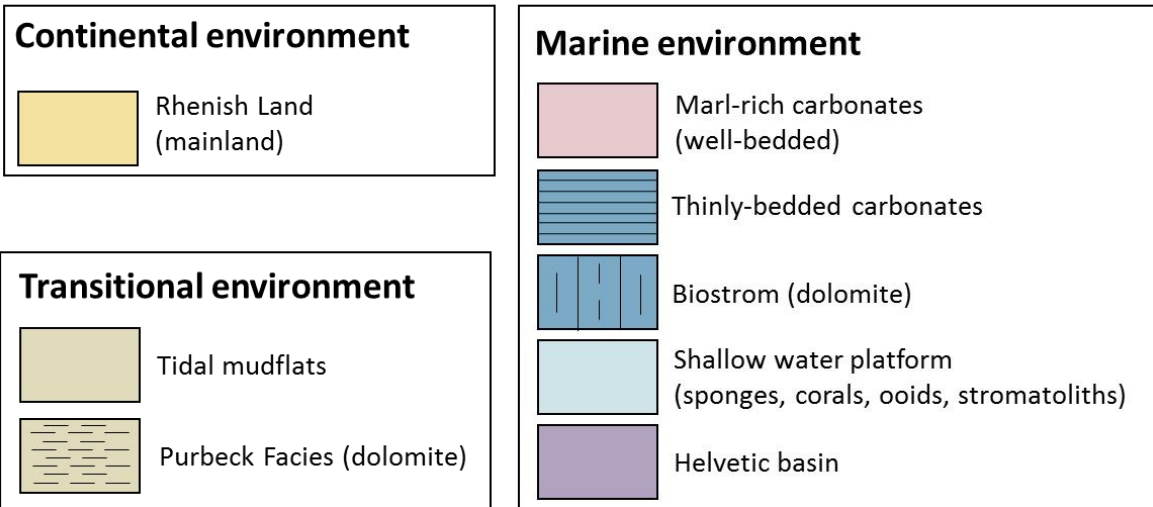
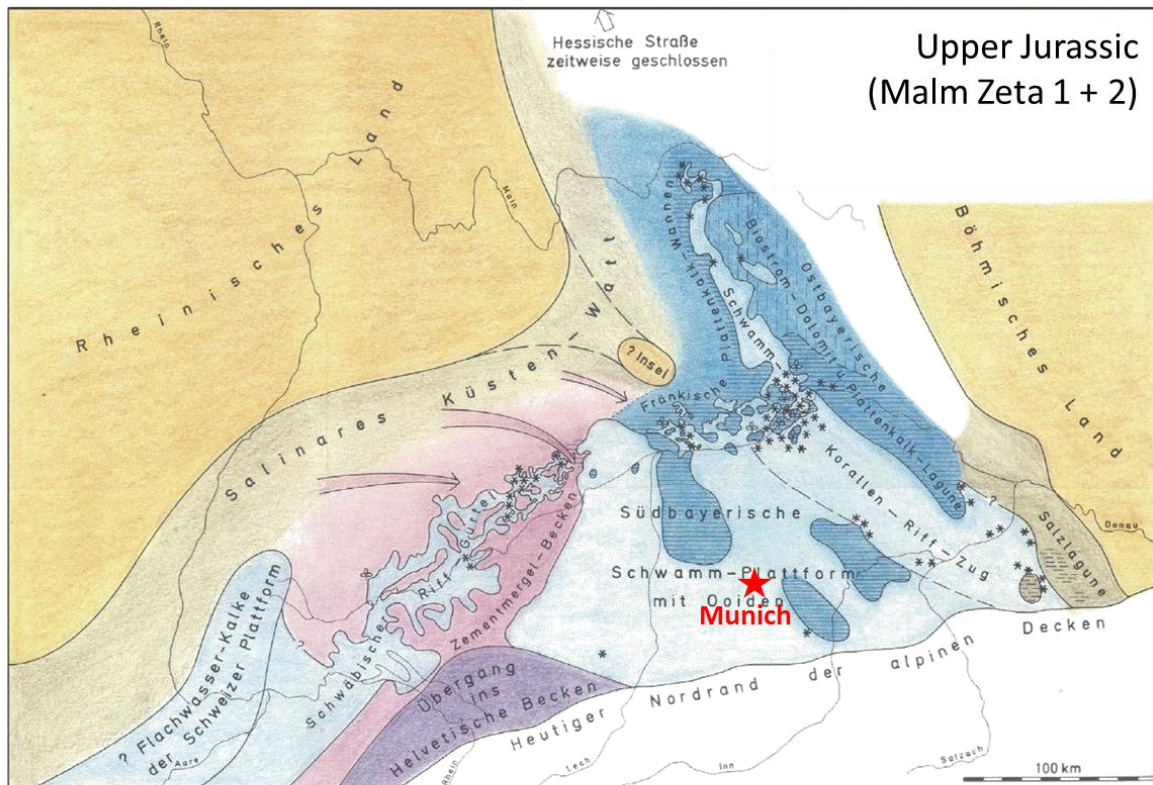


Figure 3: Paleogeographic map of the Upper Jurassic (Malm Zeta 1 + 2; modified after Meyer and Schmidt-Kaler, 1989)

The red star shows the greater Munich metropolitan area. According to Meyer and Schmidt-Kaler (1989), this area was part of a shallow-water, sponge, and coral-dominated platform with ooids and stromatoliths during the Uppermost Jurassic (Zeta 1 + 2).

The Upper Jurassic consists of two major lithofacies types that are (1) well-bedded carbonates and (2) massive carbonates (Geyer and Gwinner, 1984; Gwinner, 1976; Ziegler, 1977). The massive carbonates are mainly comprised of sponges,

Introduction

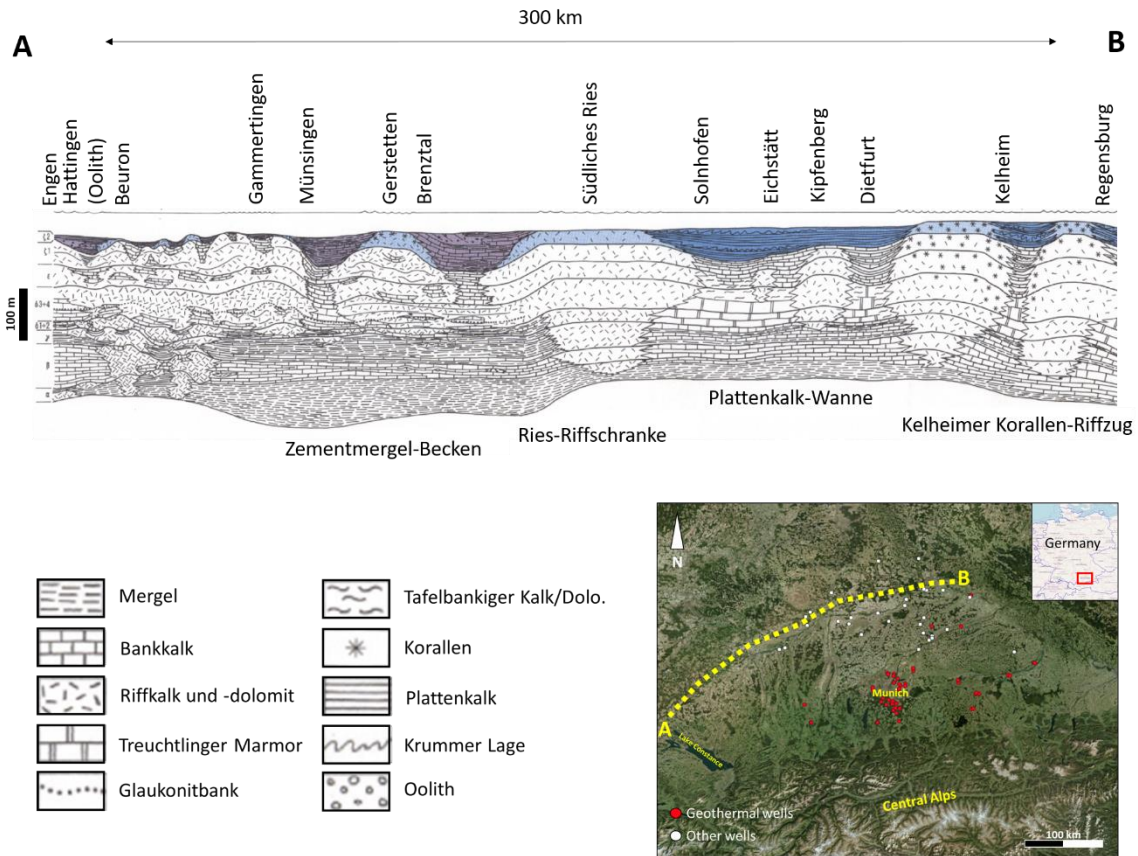


Figure 4: Paleogeographic cross-section (modified after Meyer and Schmidt-Kaler, 1990) showing the depositional character and dominating lithological units.

thrombolites and microbial crusts, formed in a relatively deep shelf environment (below fair-weather wave base) as bioherms or mounds (Gwinner, 1976; Leinfelder et al., 1996; Leinfelder, Krautter et al., 1994; Leinfelder, R., 1993; Meyer and Schmidt-Kaler, 1989; Pawellek and Aigner, 2003b; Ziegler, 1977). During the further evolution of the Upper Jurassic, the sponges as main-bioherm building organisms are commonly replaced by corals. Furthermore, the presence of ooids, peloids, and reef debris wedges in the uppermost part can be observed, indicating a shallower depositional environment (Meyer, 1994a; Meyer and Schmidt-Kaler, 1989, 1990). Clastic input (e.g., clay, silt) was derived from the Rhenish Massif in the North (Gygi, 1986; Meyer and Schmidt-Kaler, 1989) and partly from the Swiss Platform in the West (Olivier et al., 2004, Pittet et al., 2000; Pittet and Strasser, 1998).

Figure 4 shows a simplified schematic cross-section through the Molasse Basin (approximately NE-SW orientation). The depositional environment is deeper to the SW (dominated by sponges, mostly below fair-weather wave base) and shallower to the NW (presence of corals and shallow water facies). The Upper Jurassic of South Germany is a highly heterogeneous system comprised of biohermal buildups, which

are separated by inter-biohermal basins, but also by intra-biohermal basins (Chiracal, 2019; Leinfelder, R. R., Nose, M. et al., 1993; Meyer and Schmidt-Kaler, 1989). The complexity of this depositional environment is observed on several scales and further discussed in chapter 5 (seismic interpretation) as it concerns the development of geothermal reservoir types and their distribution.

1.3.3 Stratigraphic Framework

The Upper Jurassic of South Germany (also known as “Malm” or “White Jurassic”) conformably overlays the Middle Jurassic Dogger and is between 450 m to 600 m thick. It is partly overlain by the Purbeck Formation (in the subsurface of the Molasse basin) but also by an unconformity followed by Cretaceous deposits. The Upper Jurassic Malm is of Oxfordian to Tithonian age, which corresponds to approximately 15-18,5 Ma years (Figure 3). The variation in the absolute age is mainly caused by a re-evaluation of the German stratigraphic commission (Deutsche Stratigraphische Kommission, 2016) and the uncertainty of age of the Purbeck Formation (currently classified as Upper Jurassic/Cretaceous). (Lesić, 2019) deals with the Purbeck Formation of South Germany in detail and, e.g. (Niebuhr and Pürner, 2014) with the actual classification of the German stratigraphic commission and the subdivision of the Upper Jurassic into Formations.

Introduction

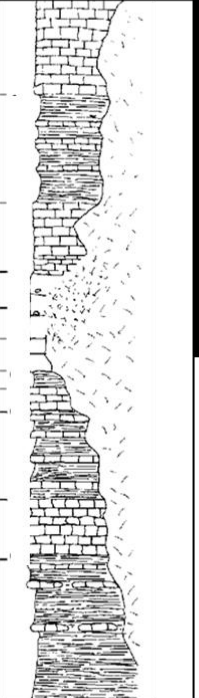
Series	Chrono- stratigraphy	Age (ma) (ISC, v2018/08)	Lithostratigraphy (Villinger & Fleck (1995) and Quenstedt (1858))					
Upper Jurassic (Malm)	Tithonian	145.0-152.1	Hangende Bankkalke	ζ 3	ti1			
	Kimmeridgian	152.1-157.8	Zement- mergel	Weißjura ζ	ζ 2		ki5	
			Liegende Bankkalke		ζ 1		ki4	
			Obere Felsenkalke	W ε				ki3
			Untere Felsenkalke	Weißjura δ	δ 4			Ki 2.4
					δ 3			Ki 2.3
					δ 2			Ki 2.2
	δ 1				Ki 2.1			
	Lacunosa- mergel	Weißjura γ			ki1			
	Oxfordian	157.8-163.5	Wohlgeschichtete Kalke	W β			ox2	
Impressa- Mergel			Weißjura α			ox1		

Figure 5: Stratigraphic table of South Germany. Modified after Villinger and Fleck (1995), Quenstedt (1858) and ISC (v2018/08)

Figure 5 shows the lithostratigraphic classification after (Quenstedt, 1858) and (Villinger and Fleck, 1995).

The Quenstedt classification is based on outcrop observations and ammonite zones. However, it is still the most suitable to characterize the subsurface because it represents alternating intervals that are dominated by marls or by carbonates, respectively.

Viewed by an explorationist, these changes of composition can be detected by: (1) wireline well logs (e.g., gamma-ray), (2) seismic reflectors and (3) constrained by borehole image logs to identify stratigraphic surfaces and marker beds.

Hence, for the reason of applicability in subsurface reservoir characterization, the original Quenstedt classification is used in this study.

1.4 Basin Development & Tectonics

The Molasse basin formed during the late stages of the Alpine orogeny. It represents a typical asymmetric foreland basin that dips to the south and continues at least 50km underneath the nappes of the Alps (Allen and Homewood, 1986; Bachmann et al., 1987; Bachmann and Müller, 1992). The northernmost limit of the basin was situated approximately 20-30 km to the north of the Swabian and Franconian Alb. Crystalline basement blocks of the Bohemian massif (e.g., the Landshut Neuötting High) represent the eastern limit of the Molasse basin (Sissingh, 1997). The basement is of Variscan age and consists of gneisses and granites (Bachmann et al., 1991). They were uplifted and eroded during the Late Carboniferous resulting in an SW-NE oriented graben and troughs system (Ziegler, 1990; Ziegler and Dèzes, 2006). During the Jurassic, these preexisting basement structures were reactivated (extensional phase), resulting in differential subsidence and rotation of fault-bounded blocks (Wetzel et al., 2003). Especially in carbonate environments, which are highly sensitive to changes in accommodation space (Schlager, 1993), the reactivation of preexisting basement faults can be related to facies changes (e.g., (Warnecke and Aigner, 2019; Wetzel et al., 2003).

According to (Moeck, 2014) the Upper Jurassic Malm carbonates of South Germany can be classified as an “orogenic belt geothermal play type”, which is buried deep enough to reach high temperatures in the greater Munich area (Agemar et al., 2012; Böhm et al., 2013; StMWIVT, 2010).

Figure 6 shows an N-S oriented cross-section and the strata overlying the crystalline basement (Lemcke, 1988).

Introduction

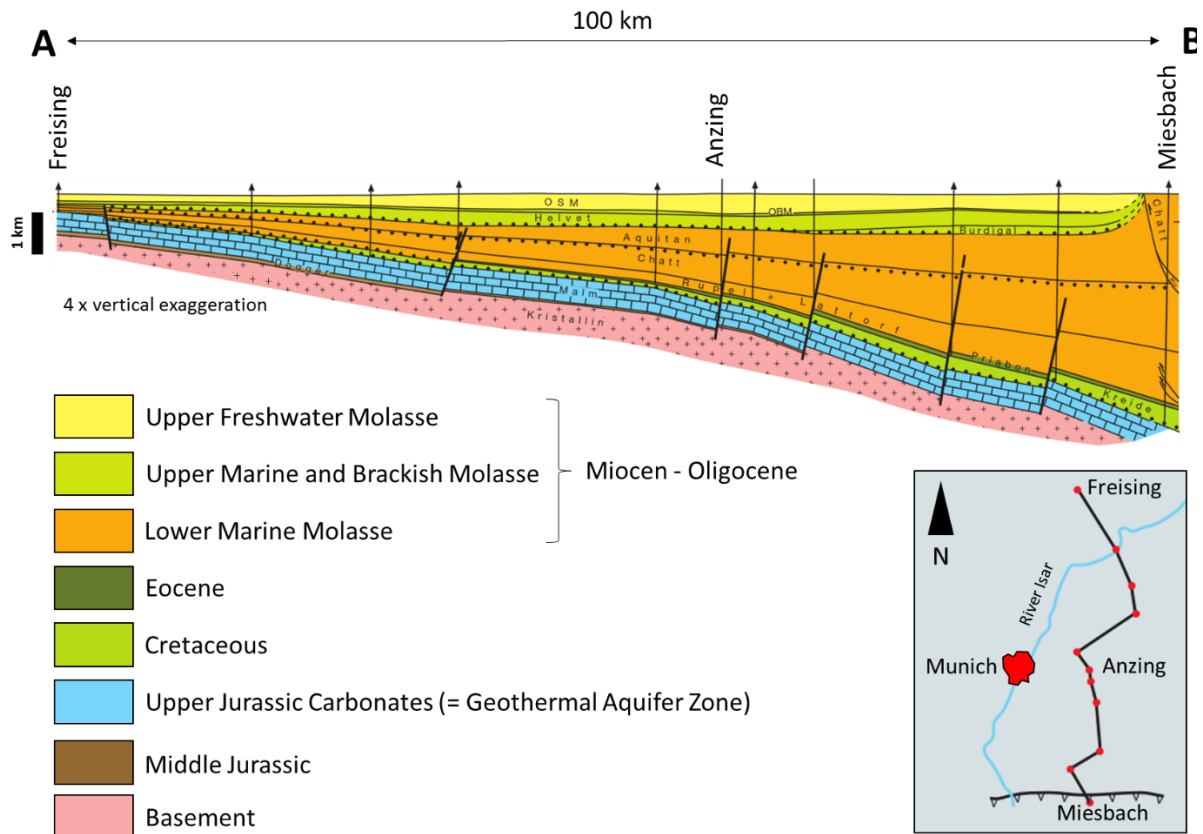


Figure 6: N-S cross-section of the Molasse basin (Lemcke, 1988).

The Malm carbonates (blue) are cropping out at the Swabian and Franconian Alb and are buried towards the south due to the Alpine orogenesis.

2. DATABASE AND METHODOLOGY

The research well Moosburg SC4 is the only fully cored well through the entire Upper Jurassic of South Germany (TD 1585, 20m) and is used as reference well for this study as no core data is available from any of the geothermal wells in the greater Munich area. Additionally, cored intervals from four hydrocarbon wells were investigated. In total 785 m of core from the Upper Jurassic were systematically logged with a resolution of 1:20. Textural composition (Dunham texture), lithology, grain size, components, sedimentary structures, and rock color were recorded, interpreted and digitized with WellCAD 5.1. A core-to-log calibration was performed, comparing the gamma-ray signal with the sedimentological changes, sequence stratigraphic trends and marker beds. Forty-six rock samples were collected and used for thin section analysis (microfacies).

Borehole image logs were analyzed and interpreted from 12 geothermal wells following a standard workflow (Pöppelreiter, García-Carballido, Kraaijeveld, 2010b), but with a focus on borehole image facies. To verify the interpretation and linked the borehole image facies with core-based facies, borehole cuttings from three geothermal wells were integrated into the interpretation.

The 3D seismic volume from the Freigham geothermal field, covering an area of 4.2 km x 5.5 km) was interpreted in terms of seismic reflector termination mapping, seismic facies, sequence stratigraphy, and seismic attributes. The wells Freigham Th1 and Th2 were tied into the seismic to verify and compare the results of the interpretation.

Dynamic data from flowmeter tests is linked with the borehole image interpretation and the seismic to identify geothermal reservoir types. Geothermal reservoir types are ranked according to the dominating permeability type.

Three Master Theses, one Bachelor Thesis, and one scientific research project are part of this overall study, covering the following special aspects:

- MSc.-Thesis Eigler (2018): Brenztal-Trümmerkalk, Facies Analysis, Sequence Stratigraphy and 3D-Modelling. Upper Jurassic carbonate debris as new potential geothermal play type in the Molasse Basin

Database and Methodology

- BSc.-Thesis Chiracal (2018): Sedimentological core description and wall panel interpretation of Upper Jurassic carbonates. Focus on geobody dimensions and porosity trends of bioherm debris wedges.
- MSc.-Thesis Lesić (2019): The Purbeck Formation of the Molasse Basin. Subsurface Facies, Log and Sequence Analysis
- Scientific research project Chiracal (2019): Using aerial photography to investigate the size and dimensions of biohermal build-ups of Upper Jurassic carbonates of the Swabian Alb exposed by weathering. Comparison of outcrop dimensions with seismic attribute interpretation
- MSc.-Thesis Arlat (2020): Regional Geologic Trends and Geothermal Reservoir Potential of Upper Jurassic Carbonates in the Molasse Basin.

3. 1D ANALYSIS

3.1 Background

The greater Munich area is under intense geothermal development to reach the goals of Vision 2040 (www.swm.de); however, there is no core data available from any of the geothermal wells to calibrate the well-log or seismic interpretations.

The Upper Jurassic of South Germany is very well studied in outcrops of the Swabian and Franconian Alb both by stratigraphers and by sedimentologists (Aigner and Schauer, 1998; Bartenbach, 2008; Bold, 2010; Fügel, 2009; Geyer and Gwinner, 1984; Gwinner, 1976; Koch et al., 1994; Koch and Heuschkel, 2016; Pawellek, 2001; Pawellek and Aigner, 2003a, 2003b; Pawellek and Aigner, 2004; Pross et al., 2006b; Ruf et al., 2005a; Ruf et al., 2005b), but consistent lithofacies descriptions of the subsurface in the Molasse basin are still missing. This lack of information can lead to severe misinterpretations, as shown in Figure 7. The exact position of the Purbeck Formation, and therefore the Top Upper Jurassic (Malm), is often inconsistently picked, even within the same geothermal field. The wells A and B are only 2,5 km apart and yet show fundamental differences in lithology for the Purbeck Formation and the Upper Jurassic. The same problem is observed for Well C, which is approx. 20 km to the NE. The misinterpretation of Purbeck/Top Malm has a direct influence on stratigraphic interpretation and, therefore, on reservoir thickness and properties.

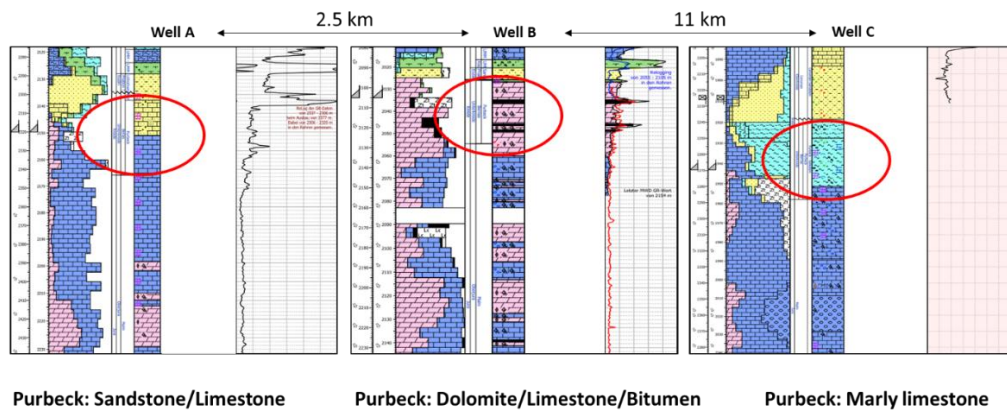


Figure 7: Interpreted Purbeck lithology and variations.

3.2 Facies Analysis

The research well Moosburg SC4 is the only fully-cored well through the Bavarian Molasse, that recovered a complete succession of Upper Jurassic carbonates, including the contact to the Middle Jurassic at the base and the Purbeck Formation at the top. Additionally, a continuous gamma-ray log was acquired. The well has been described and interpreted stratigraphically by (Meyer, 1994a) and (Böhm et al., 2011). However, a sedimentological study, including facies and sequence stratigraphy, was still missing.

Therefore, the core was logged in a 1:20 scale with a focus on sedimentological structures, components, lithology, facies, pore types, cyclicity, depositional environment, and sequence stratigraphy. The aim of the core description is to derive a lithofacies and cycle hierarchy, that can be transferred into the subsurface of the Munich area, and to calibrate it with wireline logs to assist with the 2-D log correlation (Kearns and Tinker, 1997). Especially the link between the core-based facies, the borehole image facies, and the gamma-ray are of major interest to improve the understanding of the geothermal reservoirs.

3.2.1 Lithofacies Types (LFT)

Twentytwo lithofacies types were identified for the Upper Jurassic Malm and the Upper Jurassic/Cretaceous Purbeck Formation of research well Moosburg SC4. They are summarized in Table 1 below and shown in detail in Figure 8 to Figure 31. The characterization of lithofacies types follows the classification from (Pawellek, 2001; Pawellek and Aigner, 2004) and includes the Dunham texture, fossil content, components, sedimentary structures, visible porosity but also bed thickness, contacts, and other important observations. The aim is to recognize the core-based lithofacies types from the core via distinct diagnostic features that can be captured by micro-resistivity borehole image logs from the geothermal wells of the greater Munich area.

1D Analysis

Table 1: Summary of lithofacies types (LFT).

Litho Facies Types	Facies (F)	Stratigraphic interval	Bed thickness	Basal contact	Sedimentary structures/ Observations	Biological Structures
LFT 23	Sandstone	Gault (Cretaceous)	cm	gradual	not observed	not observed
LFT 22	Algal Boundstones	Purbeck	dm	sharp	Wavy-bedding	algal lamination
LFT 21	Flat pebble conglomerate and reworked surface	Purbeck	cm - dm	erosive	rip-up clasts or chaotic brecciation	not observed
LFT 20	Coral Floatstone	Zeta 4-5	dm	sharp	massive with branched corals	coral in living position
LFT 19	Peloidal-oolitic grainstones	Zeta 4-5, Purbeck	dm	sharp or erosional	cross-bedding	not observed
LFT 18	Bioclastic-peloidal-oolitic Packstones	Zeta 4-5, Purbeck	dm	sharp or erosional	cross bedding	bioturbation
LFT 17	Wackestones with packstone filled burrows	Zeta 4-5, Purbeck	dm	sharp	1-2 cm thick burrows, filled with coarse grained bioclast-rich packstones (often dolomitised)	bioturbation, <i>Thalassinoides</i> type burrows
LFT 16	Bioclastic wackestones and packstone	Zeta 4-5, Purbeck	cm -dm	sharp	massive with fine shell and bioclast debris	
LFT 15	Very dark, intensively bioturbated, black pebble dominated wackestones	Zeta 4-5, Purbeck	dm - m	gradual	destratified, very dark, greenish, black pebbles	intensively bioturbated
LFT 14	Bioturbated Mudstones	Gamma, Zeta 2, Zeta 4-5, Purbeck	dm -m	gradual	wavy bedding	bioturbation
LFT 13	Well bedded Mudstones	Zeta 1, Zeta 2, Zeta 3	m	sharp	bedding with horse tail structures (dissolution seams)	not observed
LFT 12	Chaotic bedded, reworked (slump-slide) Mudstones	Zeta 1, Alpha	dm - m	erosional	brecciated, reworked chaotic mudstones, syn-sedimentary deformation, deformed bedding	not observed

1D Analysis

LFT 11	Massive dolomitic Mud- and Wackestones	Gamma,Delta,Epsilon,Zeta 1, Zeta 4-5, Purbeck	dm	sharp	massive	not observed
LFT 10	Dm-thick to massive sponge-thrombolite Float-to-Rudstone	Delta,Epsilon	dm - m	gradual	massive	not observed
LFT 9	Cm-to dm bedded, sponge-thrombolite Float-to-Rudstone	Delta,Epsilon	cm - dm	gradual	massive	not observed
LFT 8	Cm-thin bedded, marl rich sponge-thrombolite Float-to-Rudstone	Delta,Epsilon	cm	gradual	thin-bedded, laminated	not observed
LFT 7	Tuberoid and bioclast debris wackestones	Gamma, Zeta 1	cm - dm	gradual	massive	sparse bioturbation
LFT 6	Well bedded to massive bioclast debris rich wackestones	Beta,Gamma,Zeta 4-5, Purbeck	dm - m	sharp	parallel bedding	not observed
LFT 5	White mudstones/wackestones with fossil-rich clay alternations	Beta,Gamma	dm	sharp	parallel bedding, cm thin laminated clay intervals	not observed
LFT 4	White, thick-bedded and massive mudstone	Beta, Purbeck	dm - m	sharp	parallel bedding	not observed
LFT 3	Grey, bedded mudstones	Alpha, Beta, Zeta 4-5, Purbeck	cm - dm	sharp	parallel bedding, lamination	very sparse bioturbation
LFT 2	Dark, clay-rich, laminated mudstones	Alpha	cm - dm	sharp	lamination	some bioturbation, chondites type burrows
LFT 1	Clay, fissile shale	all intervals	mm - cm	sharp	lamination	not observed

1D Analysis

LFT	Lithofacies	Texture (Dunham)	Reservoir Characteristics	Common Features	Depositional Environment
1	Claystone	n.a.	<ul style="list-style-type: none"> No porosity No permeability 	<ul style="list-style-type: none"> Thinly-laminated Brittle Loose, rubble 	<ul style="list-style-type: none"> Low water energy

Figure 8: LFT 1: Claystone

LFT	Lithofacies	Texture (Dunham)	Reservoir Characteristics	Common Features	Depositional Environment
2	Dark, laminated marlstone	Mudstone	<ul style="list-style-type: none"> No porosity No permeability 	<ul style="list-style-type: none"> Well bedded Bioturbation Chondrites (A) (B) Sponge fragments (C) 	<ul style="list-style-type: none"> Low water energy Below storm wave base Distal outer platform/ ramp

Figure 9: LFT 2: Dark, laminated marlstone

1D Analysis

LFT	Lithofacies	Texture (Dunham)	Reservoir Characteristics	Common Features	Depositional Environment
3	Lime, bedded mudstones	Mudstone	<ul style="list-style-type: none"> No porosity No permeability 	<ul style="list-style-type: none"> Well bedded Bioturbation (A) 	<ul style="list-style-type: none"> Low water energy Below storm wave base Distal outer platform/ ramp

Figure 10: LFT 3: Lime, bedded mudstones

LFT	Lithofacies	Texture (Dunham)	Reservoir Characteristics	Common Features	Depositional Environment
4	White, thickly bedded and massive lime mudstone	Mudstone	<ul style="list-style-type: none"> No porosity No permeability 	<ul style="list-style-type: none"> Thickly bedded Bright, white color Sparse bioturbation (A) 	<ul style="list-style-type: none"> Low water energy Below storm wave base Distal outer platform/ ramp

Figure 11: LFT 4: White, thickly bedded and massive lime mudstone

1D Analysis

LFT	Lithofacies	Texture (Dunham)	Reservoir Characteristics	Common Features	Depositional Environment
5	White mudstone/wackestone with fossil-rich clay alternations	Mudstone, Wackestone	<ul style="list-style-type: none"> No porosity No permeability 	<ul style="list-style-type: none"> Frequent, thin bedded clay alternations (A) Crinoids (B) Ammonites (C) Belemnites (D) 	<ul style="list-style-type: none"> Low water energy Below storm wave base Distal outer platform/ramp

Box 579

Box 596

Box 596 (detail)

Box 580 (detail)

Box 580 (detail)

Box 583 (detail)

Figure 12: LFT 5: White mudstone/ wackestone with fossil-rich clay alternations

LFT	Lithofacies	Texture (Dunham)	Reservoir Characteristics	Common Features	Depositional Environment
6	Well bedded to massive mud-to wackestone	Mudstone, Wackestone	<ul style="list-style-type: none"> No porosity No permeability 	<ul style="list-style-type: none"> Thickly-bedded Bioclasts (A) Tuberoïdes (B) 	<ul style="list-style-type: none"> Low water energy Below storm wave base Distal outer platform/ ramp

Box 558

Box 571

Slab 560

Slab 560 (detail)

Slab 570 (detail)

Figure 13: LFT 6: Well bedded to massive mud-to wackestone

1D Analysis

LFT	Lithofacies	Texture (Dunham)	Reservoir Characteristics	Common Features	Depositional Environment
7	Tuberoid wacke-to packstone	Wacke-stone to pack-stone	<ul style="list-style-type: none"> No porosity No permeability 	<ul style="list-style-type: none"> Tuberoïdes (A) Bioclasts (B) Shells (C) 	<ul style="list-style-type: none"> Low water energy Below storm wave base Distal outer platform/ramp

Box 566

Slab 566

Slab 583

Slab 579

Figure 14: LFT 7: Tuberoid wacke- to packstone.

LFT	Lithofacies	Texture (Dunham)	Reservoir Characteristics	Common Features	Depositional Environment
8	Cm bedded, marly sponge-thrombolite Float-to-Rudstone	Float-stone, Rud-stone	<ul style="list-style-type: none"> Vuggy (A) and moldic (B) porosity Low permeability 	<ul style="list-style-type: none"> Very thin bedded Marly Sponges (C) Thrombolites (D) 	<ul style="list-style-type: none"> Low water energy Below storm wave base Distal outer platform/ramp

Box 503 Box 504

Box 488

Slab 502

Slab 479

Figure 15: LFT 8: Cm bedded, marly sponge thrombolite float- to rudstone

1D Analysis

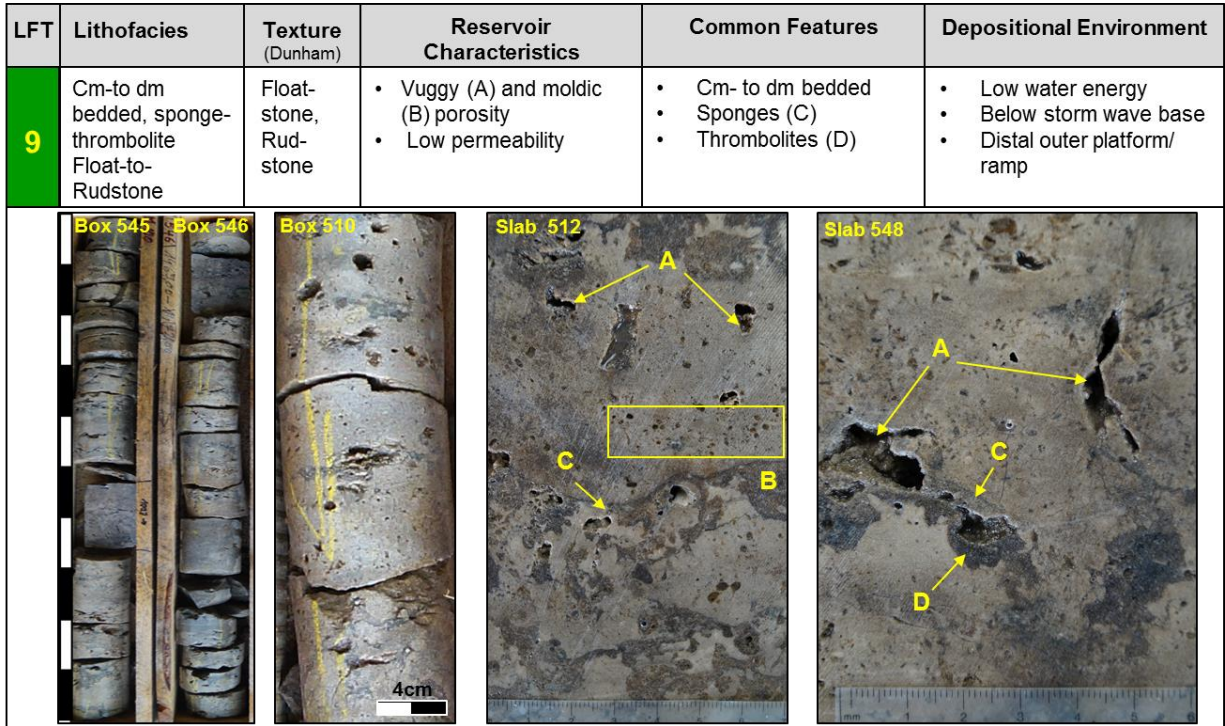


Figure 16: LFT 9: Cm- to dm bedded, sponge-thrombolite float- to rudstone

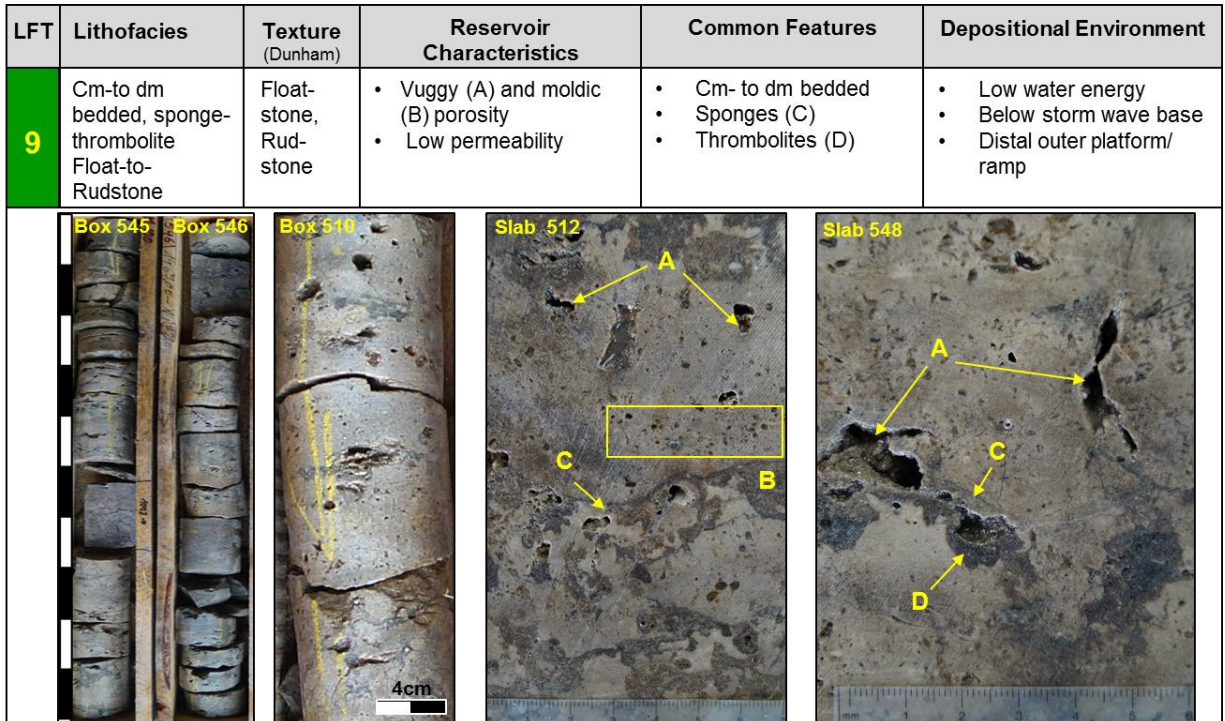


Figure 17: LFT 9: Cm to dm bedded, sponge thrombolite float- to rudstone

1D Analysis

LFT	Lithofacies	Texture	Reservoir Characteristics	Common Features	Depositional Environment
10	Dm to m bedded sponge-thrombolite Float-to-Rudstone	Float-stone, Rud-stone	<ul style="list-style-type: none"> Vuggy (A) and moldic (B) porosity Low permeability 	<ul style="list-style-type: none"> Cm- to dm bedded Sponges (C) Thrombolites (D) 	<ul style="list-style-type: none"> Low water energy Below storm wave base Distal outer platform/ ramp

Figure 18: LFT 10: Dm to m bedded sponge-thrombolite float-to-rudstone

Sponge – thrombolite float- to rudstone: detail view and comparison

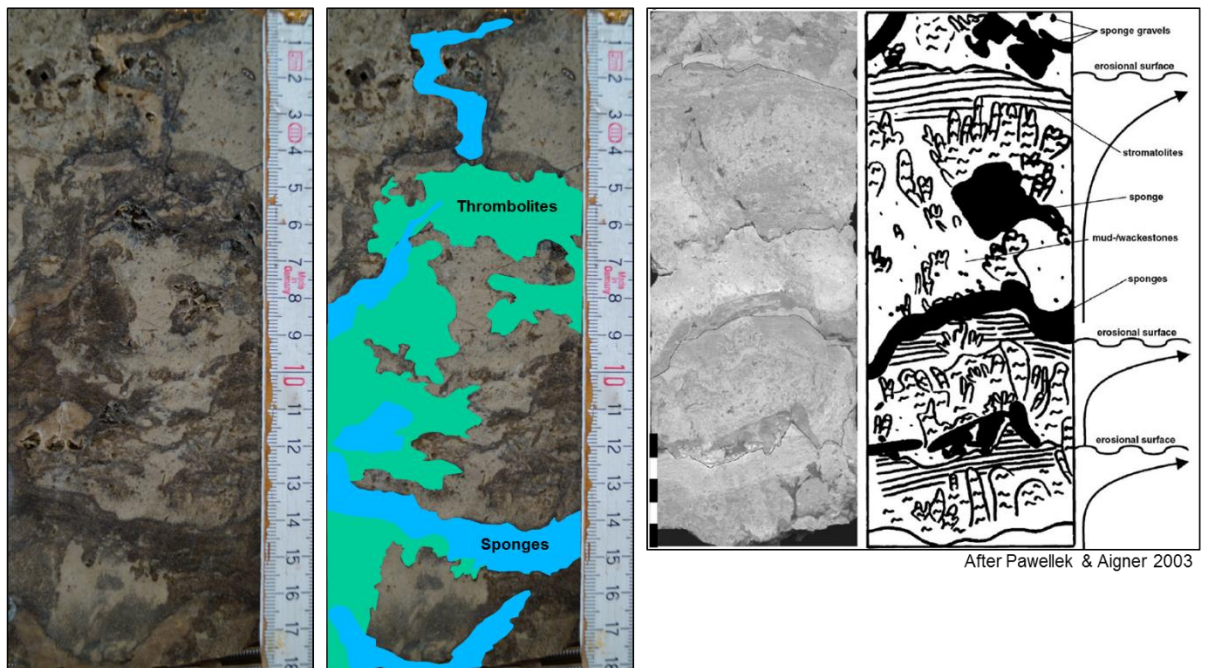


Figure 19: Sponge-thrombolite float-to-rudstone : detail view

1D Analysis

LFT	Lithofacies	Texture	Reservoir Characteristics	Common Features	Depositional Environment
11	Massive dolomitic Mud- and Wackestone	Mudstone, Wackestone	<ul style="list-style-type: none"> Poor to moderate porosity poor permeability Moldic por (C), rare vuggy porosity (D) 	<ul style="list-style-type: none"> Tuberoides (A) Bioclasts (B), sponge fragments? Bioclast debris 	<ul style="list-style-type: none"> Low water energy Below storm wave base Distal outer platform/ ramp

Figure 20: LFT 11: Massive dolomitic Mud- and Wackestone

LFT	Lithofacies	Texture (Dunham)	Reservoir Characteristics	Common Features	Depositional Environment
12	Chaotic/ brecciated mudstone	Mudstone	<ul style="list-style-type: none"> No porosity No permeability Possible fracture porosity 	<ul style="list-style-type: none"> Mudstone clasts (A) with lamination Syn-sedimentary deformed mudstones (B) 	<ul style="list-style-type: none"> Low water energy Below storm wave base Slope Gravity flow (slide/slump)

Figure 21: LFT 12: Chaotic/ brecciated mudstone

1D Analysis

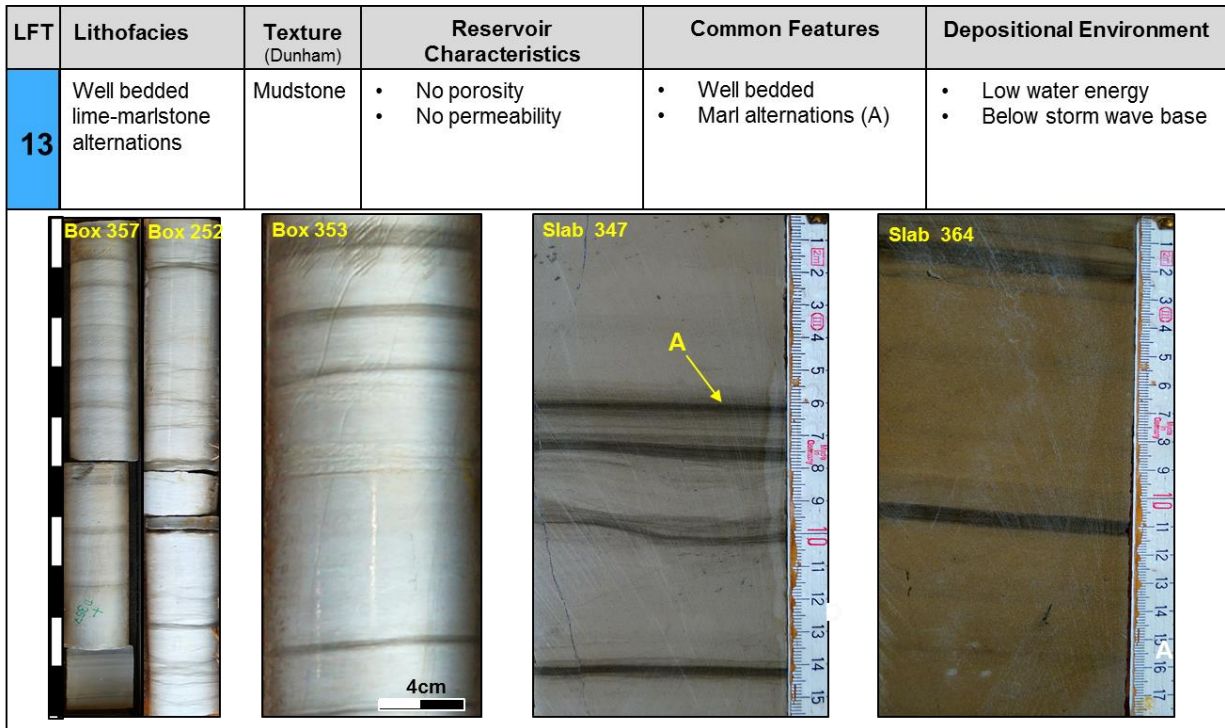


Figure 22: LFT 13: Well bedded lime-marlstone alternations

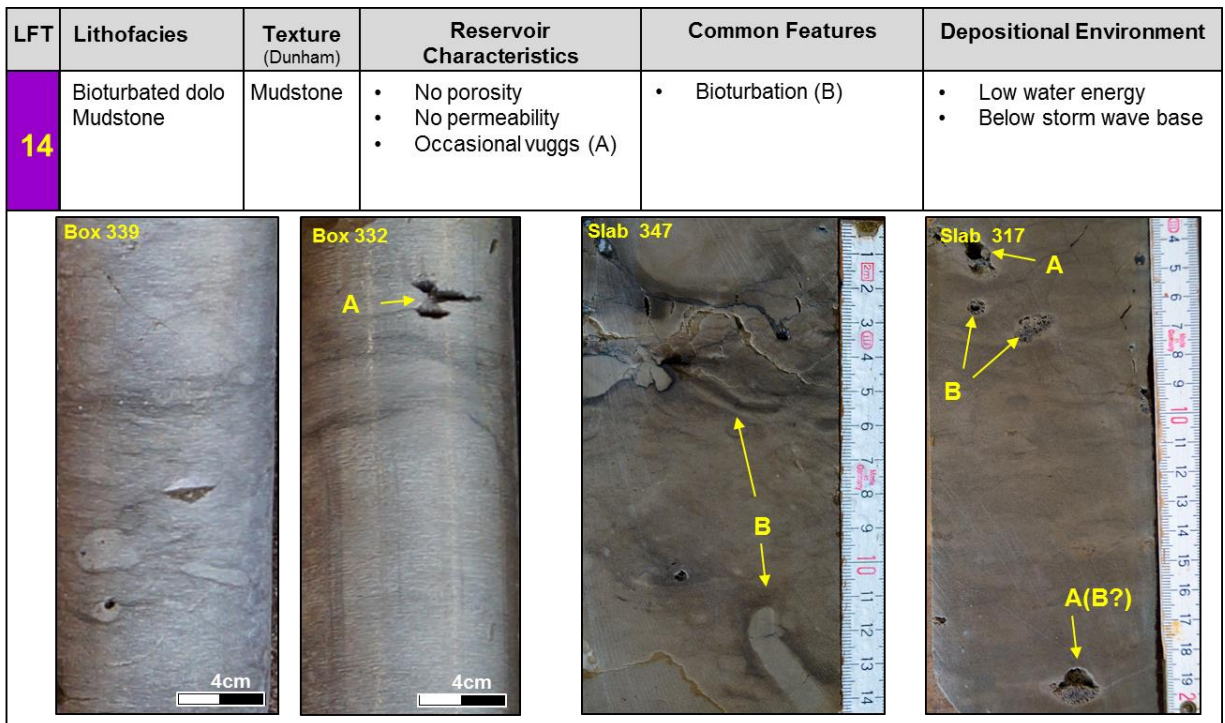


Figure 23: LFT 14: Bioturbated dolo mudstone

1D Analysis

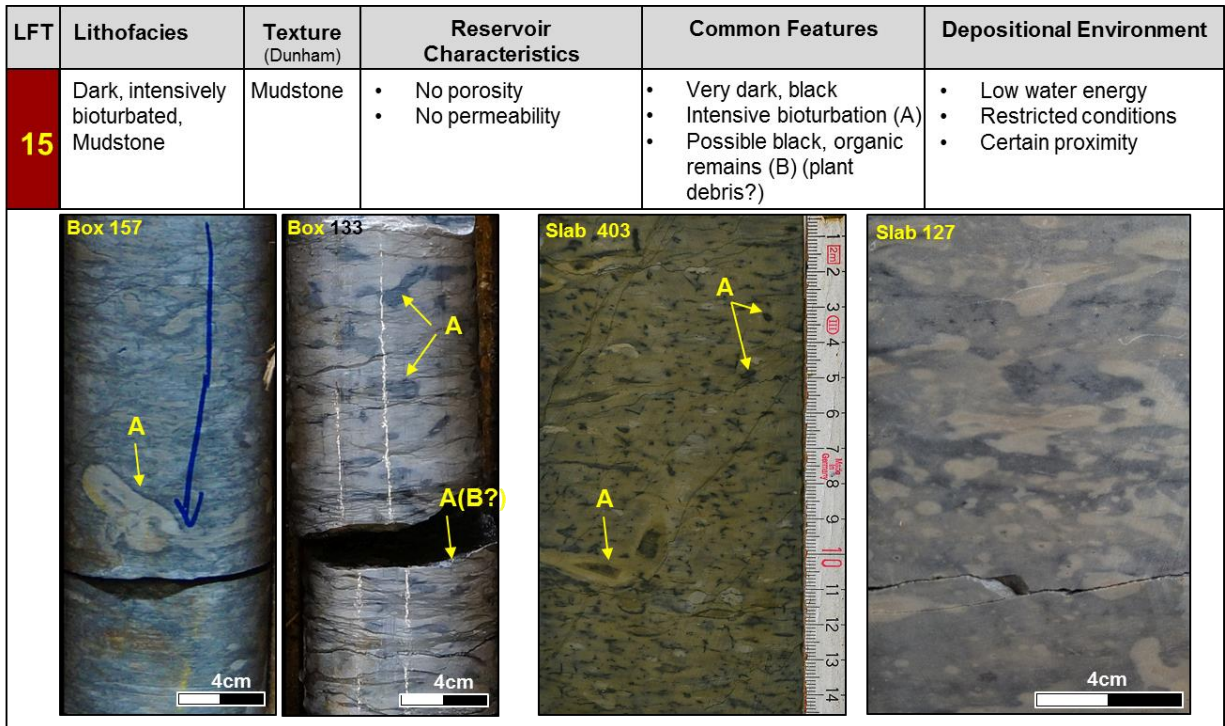


Figure 24: LFT 15: Dark, intensively bioturbated, mudstone

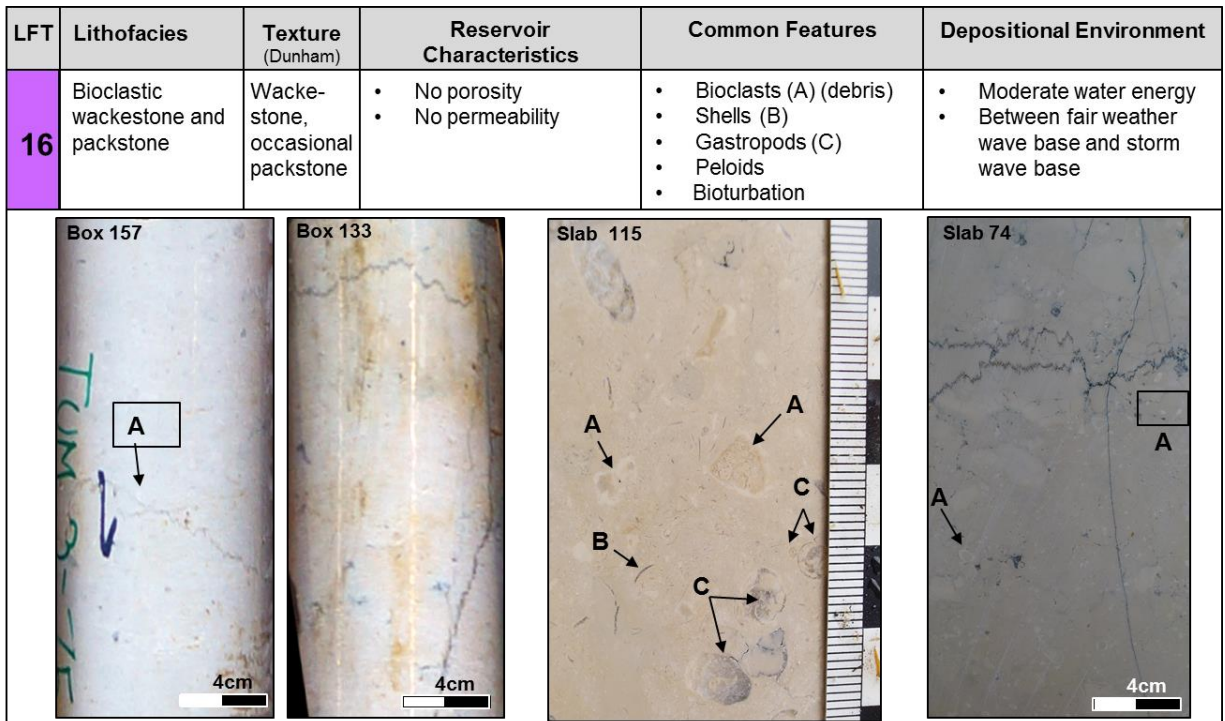


Figure 25: LFT 16: Bioclastic wackestone and packstone

1D Analysis

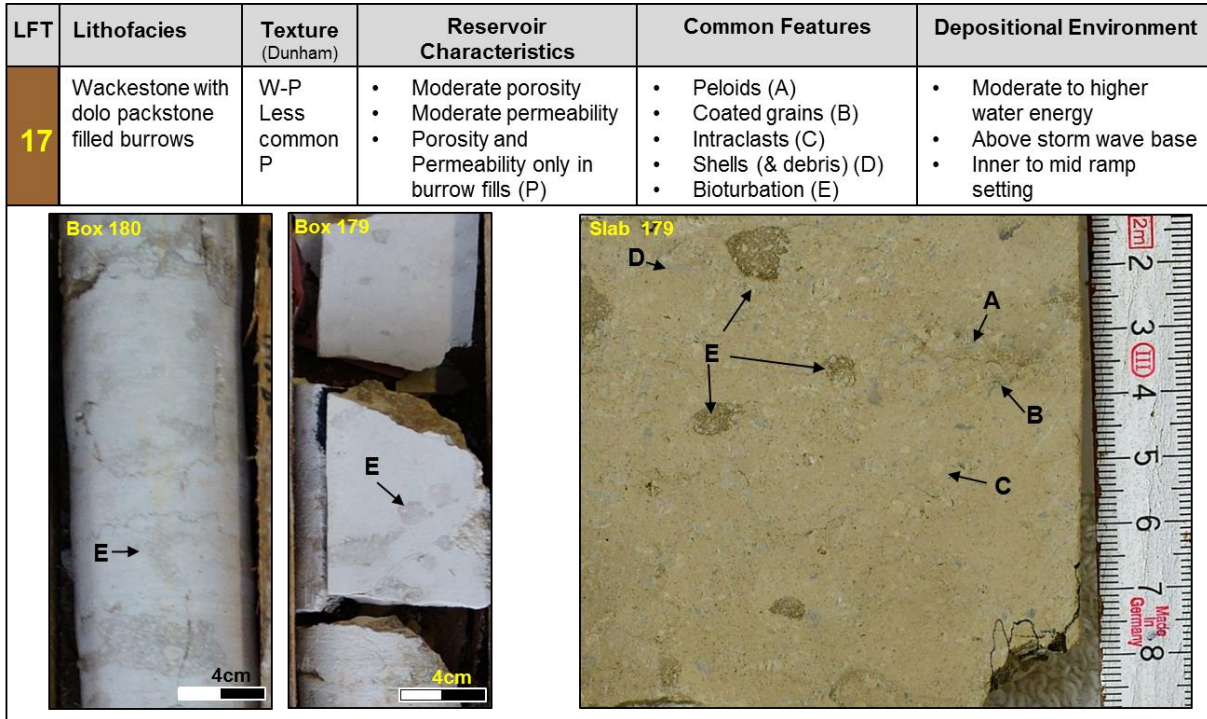


Figure 26: LFT 17: Wackestone with dolo packstone filled burrows

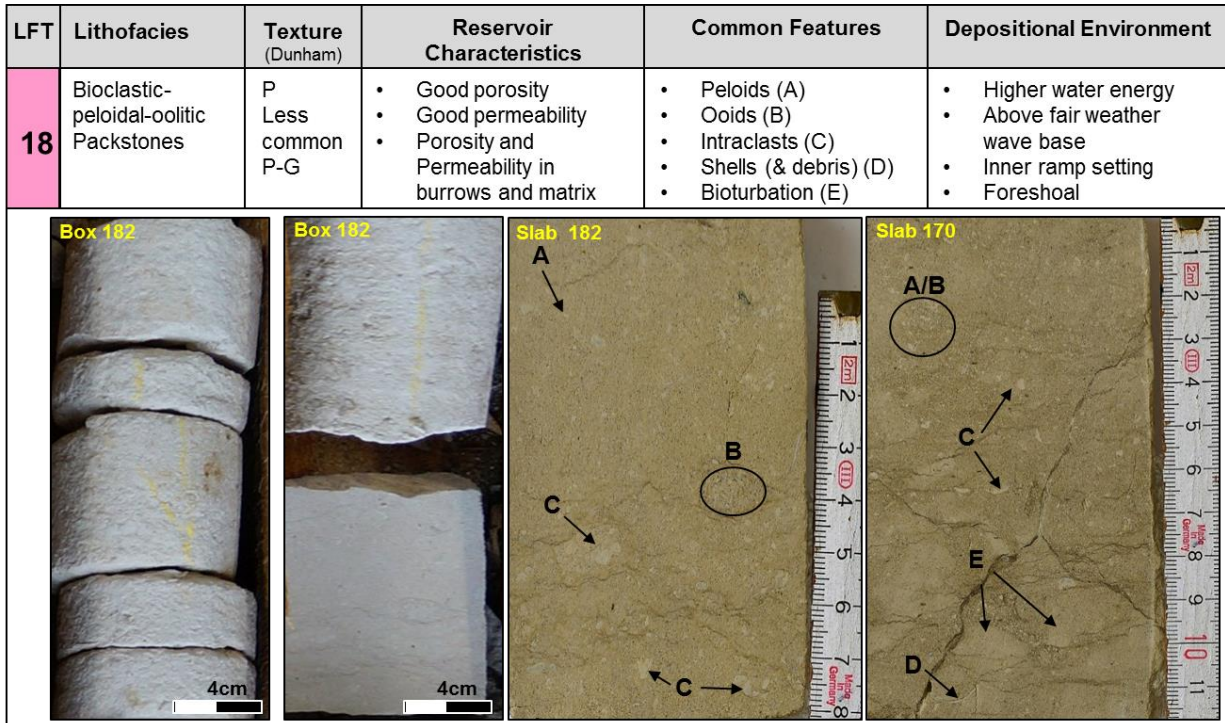


Figure 27: LFT 18: Bioclastic-peloidal-oolitic Packstones

1D Analysis

LFT	Lithofacies	Texture	Reservoir Characteristics	Common Features	Depositional Environment
19	Peloidal-oolitic grainstones	G Less common P	<ul style="list-style-type: none"> • Good porosity • Good permeability 	<ul style="list-style-type: none"> • Peloids (A) • Ooids (B) • Intraclasts (C) • Cross-bedding(D) 	<ul style="list-style-type: none"> • Higher water energy • Above storm wave base • Inner ramp setting • Shoal

Figure 28: LFT 19: Peloidal-oolitic grainstones

LFT	Lithofacies	Texture	Reservoir Characteristics	Common Features	Depositional Environment
20	Coral floatstone	F with P Matrix	<ul style="list-style-type: none"> • Low-Medium porosity • Low-Medium perm. 	<ul style="list-style-type: none"> • Coral (A) • Peloids • Bioclast debris 	<ul style="list-style-type: none"> • Above fair weather wave base • Moderate to high water energy • Proximal ramp setting

Figure 29: LFT 20: Coral floatstone

1D Analysis

LFT	Lithofacies	Texture (Dunham)	Reservoir Characteristics	Common Features	Depositional Environment
21	Flat pebble conglomerate and reworked surface	Rudstone, Breccia	<ul style="list-style-type: none"> No porosity No permeability ➤ But important marker surfaces 	<ul style="list-style-type: none"> Erosive contact (A) Reworked clasts (B) Black pebbles (C) Desiccation cracks (D) 	<ul style="list-style-type: none"> Exposure High water energy Shallow setting

Figure 30: LFT 21: Flat pebble conglomerate and reworked surface

LFT	Lithofacies	Texture (Dunham)	Reservoir Characteristics	Common Features	Depositional Environment
22	Algal Boundstone	Boundstone	<ul style="list-style-type: none"> No porosity No permeability 	<ul style="list-style-type: none"> Fine lamination Wavy bedding 	<ul style="list-style-type: none"> Very shallow setting Peri-tidal

Figure 31: LFT 22: Algal boundstone

3.2.2 Lithofacies Associations (LFA)

Lithofacies types are grouped into lithofacies associations which are genetically related (Walker and James, 1992). Geyer and Gwinner (1984) are distinguishing two lithofacies associations for the Upper Jurassic, which is the “massive facies” and the “normal facies”. The massive facies represents the sponge-dominated bioherms, and the normal facies correspond to the well-bedded basin facies in-between. Böhm et al. (2011) describe an additional “transitional zone,” which includes bioherm debris wedges.

Figure 32 shows a modified cross-section from Meyer and Schmidt-Kaler (1989), where four lithofacies associations can be recognized : (A) shallow-water, (B) bioherm debris, (C) bioherm, and (D) basin. These four facies associations can clearly be observed in the core description, borehole image logs, and outcrop analogs. Bioherm, bioherm debris, and basin can be interpreted from 3D seismic.

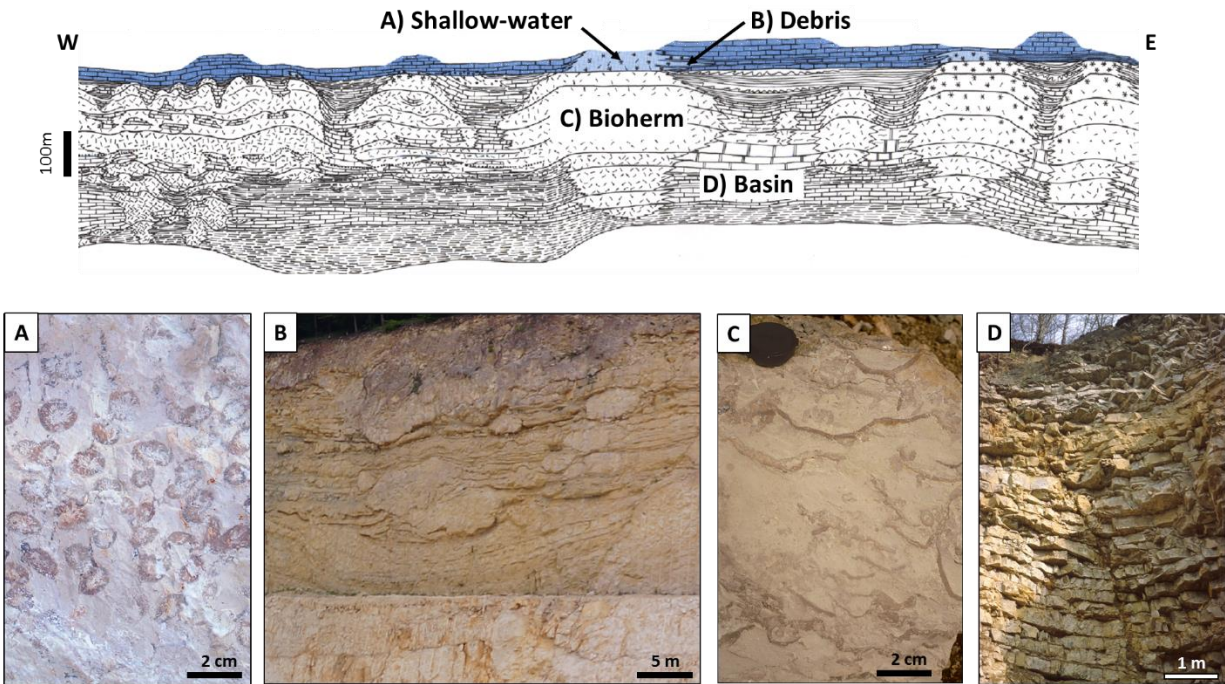


Figure 32: Main Lithofacies Associations modified after (Meyer and Schmidt-Kaler, 1989)

1D Analysis

Table 2 summarizes the lithofacies types (LFT) from the research well Moosburg SC 4 and shows the corresponding lithofacies facies association (LFA).

Table 2: Lithofacies types (LFT) and Facies Associations (LFA).

Code	Lithofacies Types (LFT)	Facies Association (LFA)
LFT 23	Sandstone	n.a. (terrestrial, Cretaceous)
LFT 22	Algal Boundstones	FA 1: Shallow-water
LFT 21	Flat pebble conglomerate and reworked surface	FA 1: Shallow-water
LFT 20	Coral Floatstone	FA 1: Shallow-water
LFT 19	Peloidal-oolitic grainstones	FA 1: Shallow-water
LFT 18	Bioclastic-peloidal-oolitic Packstones	FA 1: Shallow-water
LFT 17	Wackestones with packstone filled burrows	FA 1: Shallow-water
LFT 16	Bioclastic wackestones and packstone	FA 1: Shallow-water
LFT 15	Very dark, intensively bioturbated, black pebble dominated wackestones	FA 1: Shallow-water
LFT 14	Bioturbated Mudstones	FA 4: Basin
LFT 13	Well bedded Mudstones	FA 4: Basin
LFT 12	Chaotic bedded, reworked (slump-slide) Mudstones	FA 2: Bioherm debris
LFT 11	Massive dolomitic Mud- and Wackestones	FA 3: Bioherm
LFT 10	Dm-thick to massive sponge-thrombolite Float-to-Rudstone	FA 3: Bioherm
LFT 9	Cm-to dm bedded, sponge-thrombolite Float-to-Rudstone	FA 3: Bioherm
LFT 8	Cm-thin bedded, marl rich sponge-thrombolite Float-to-Rudstone	FA 3: Bioherm
LFT 7	Tuberoid and bioclast debris wackestones	FA 2: Bioherm debris
LFT 6	Well bedded to massive bioclast debris rich wackestones	FA 4: Basin
LFT 5	White mudstones/wackestones with fossil-rich clay alternations	FA 4: Basin
LFT 4	White, thick-bedded and massive mudstone	FA 4: Basin
LFT 3	Grey, bedded mudstones	FA 4: Basin
LFT 2	Dark, clay-rich, laminated mudstones	FA 4: Basin
LFT 1	Clay, fissile shale	FA 4: Basin

3.3 1D Sequence Stratigraphy

The sequence stratigraphic interpretation of Upper Jurassic carbonates of South Germany is challenging, especially in the subsurface of the Molasse basin but also in outcrops of the Swabian and Franconian Alb. Because most of Upper Jurassic carbonates were deposited in a relatively deep carbonate ramp/platform, situated below-average storm wave base (Pawellek and Aigner, 2003a, 2003b), classical sequence stratigraphic surfaces, such as sequence boundaries (Handford and Loucks, 1993; van Wagoner et al., 1988; van Wagoner et al., 1990) tend to be only poorly developed. However, a sequence stratigraphic interpretation in this deeper-water realm of the Upper Jurassic is still possible, as shown by Pawellek and Aigner; 2003a, Pawellek and Aigner, 2003b; Pawellek and Aigner 2004; Ruf et al. 2005; Pross et al., 2006. The key to unlocking the sequence-stratigraphic development is not to search for sharp stratal surfaces alone, but to focus as well on more subtle, transitional facies shifts referred to as “turnarounds” (Schlager, 1993, Kearns and Tinker, 1997).

3.3.1 Depositional Sequences

Following the methodology and nomenclature after (Catuneanu et al., 2011), four large scale depositional sequences (S1-4) were interpreted for the research well Moosburg SC4. Three large scale sequences comprise the Upper Jurassic Malm. One large scale sequence represents the Purbeck Fm. The following section shows each interpreted sequence and highlights characteristic diagnostic features.

Sequence 1 (S 1) from 1569.70m – 1501.10m

Observations

The Upper Jurassic Malm Alpha starts with the glauconitic marls (marker bed) at the base (Meyer, 1994b), as shown in Figure 34. Above the glauconitic marls, the argillaceous limestones of the Malm Alpha interval are very dark in color, thin-bedded and frequently interbedded with cm thick clay-marl layers. Almost the complete succession of the Malm Alpha consists of mudstones, as only very few components are present. At 1553.50m, decomposed sponge remains are present (Figure 33, pic.3). The thin clay-marl layers from the base of the Malm Alpha up to 1546.00m often contain abundant belemnites.

1D Analysis

Bioturbation can be observed as well, dominated by Chondrites- type burrows. Above 1546.00m abundance of belemnites decreases rapidly and the color of the limestones becomes brighter, turning into a solid white. Bed thickness is also increasing to a more massive, several dm thick beds. Crinoids can be observed towards the top of the Malm Alpha as well as occasional very fine-grained tuberoid debris. The Malm Beta interval starts at 1514.50m and consists of white, several dm thick, very clean mudstones. From 1506.00m onwards very fine tuberoid debris is present and constantly increasing towards the top of the Malm Beta. At 1505.30m the content of tuberoid debris is so high, that the limestones are now classified as wackestone. The top of the Malm Beta interval is marked by the presence of the first prominent marl and clay layers, which form part of the Platynota marls (marker bed) and correspond to the Malm Gamma interval.

Interpretation

Sequence stratigraphically the Malm Alpha and Beta intervals are interpreted as a transgressive (blue) and regressive (red) hemi-sequence. The transgressive hemi sequence dominates. The base of the Malm Alpha, the glauconitic marls is interpreted as SB (sequence boundary). Thin bedded, dark, clay-rich mudstones with some fine bioturbation are interpreted as LST (low stand system tract). During relatively low sea levels an enhanced input of terrigenous debris, nutrients and clay can be observed (Pross et al., 2006a) The high amount of clay is clearly visible on the GR track. The presence of tuberoid debris, a decrease in clay (visible on the GR track) and a change in bedding style from thin-bedded to dm-thick bedding characterizes the TST (transgressive system tract). The HST (high stand system tract) is represented by the massive, white mudstones of the Malm Beta, indicating open marine conditions. The contact to the overlying Platynota marls of the Malm Gamma is interpreted as SB.

1D Analysis

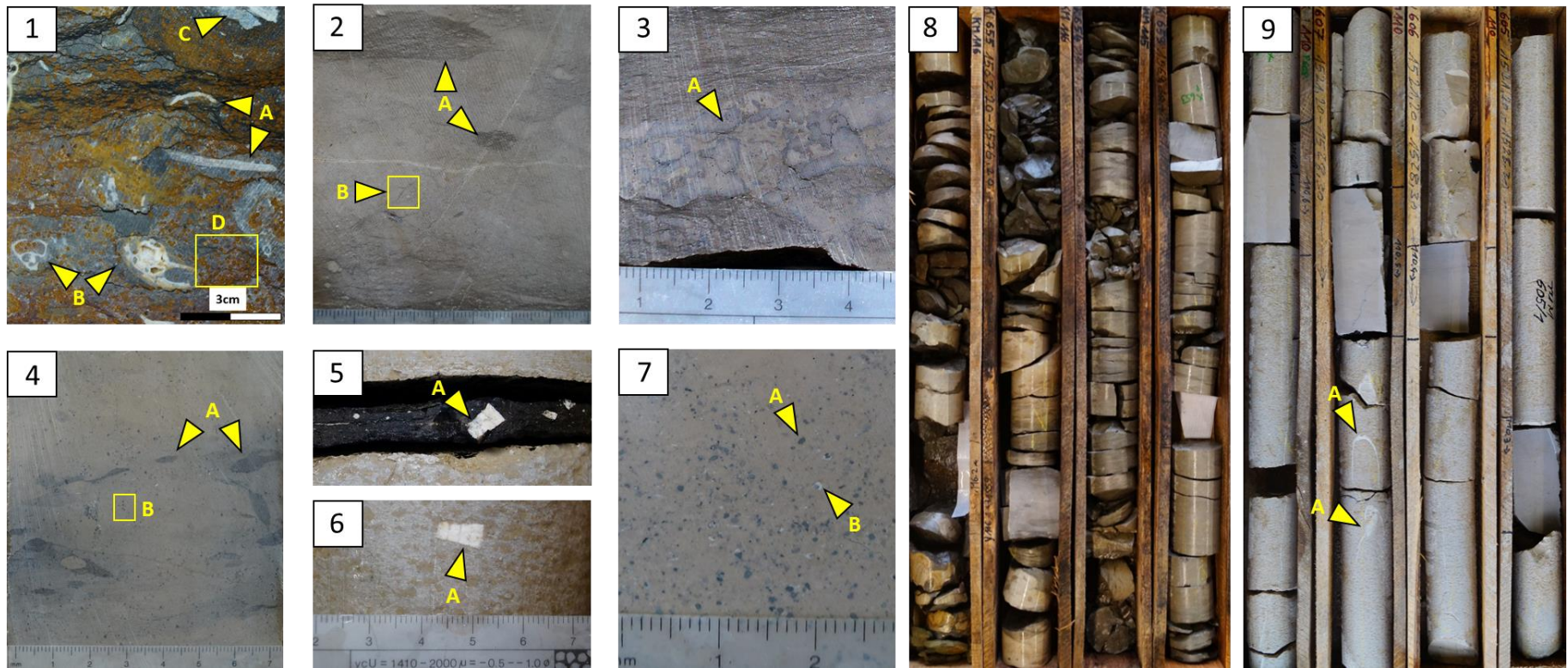


Figure 33: Sedimentological characteristics of S 1 (Malm Alpha to top Beta).

(1): Slab 658 from the Dogger shows a reworked texture with large shells (A), gastropods (B), intraclasts (C) and abundant Iron-Ooids (D). (2): Slab 655 from the Malm represents a dark, bioturbated mudstone. Bioturbation consists of larger burrows (A) as well as abundant subtle fine burrows interpreted as chondrite type burrows (B). (3): Slab 640. Dark, clay-rich mudstone with decomposed sponge remains (A). (4): Slab 621 is a mudstone with dark burrows (A). The mudstone is slightly whiter in color, fine-grained tuberoid debris (black spots) can be observed as well (B). (5; slab 597) and (6; slab 596) show crinoids (A), often concentrated in thin clay layers (5) but also present in the massive mudstone (6). (7): Slab 557 shows abundant fine-grained tuberoid debris (A) and some fine-grained white bioclast debris (tubiphytes debris?). (8) shows the core traces from KM 116 from the base of the Malm Alpha. The core consists of dark, thin-bedded mudstones with occasional thin clay intervals. (9): KM 110 from the top of the Malm Alpha interval. The mudstones are much whiter in color, more massive and dm-thick bedded. Natural fractures (A) (calcite filled) are only present in this interval of the Malm Alpha.

1D Analysis

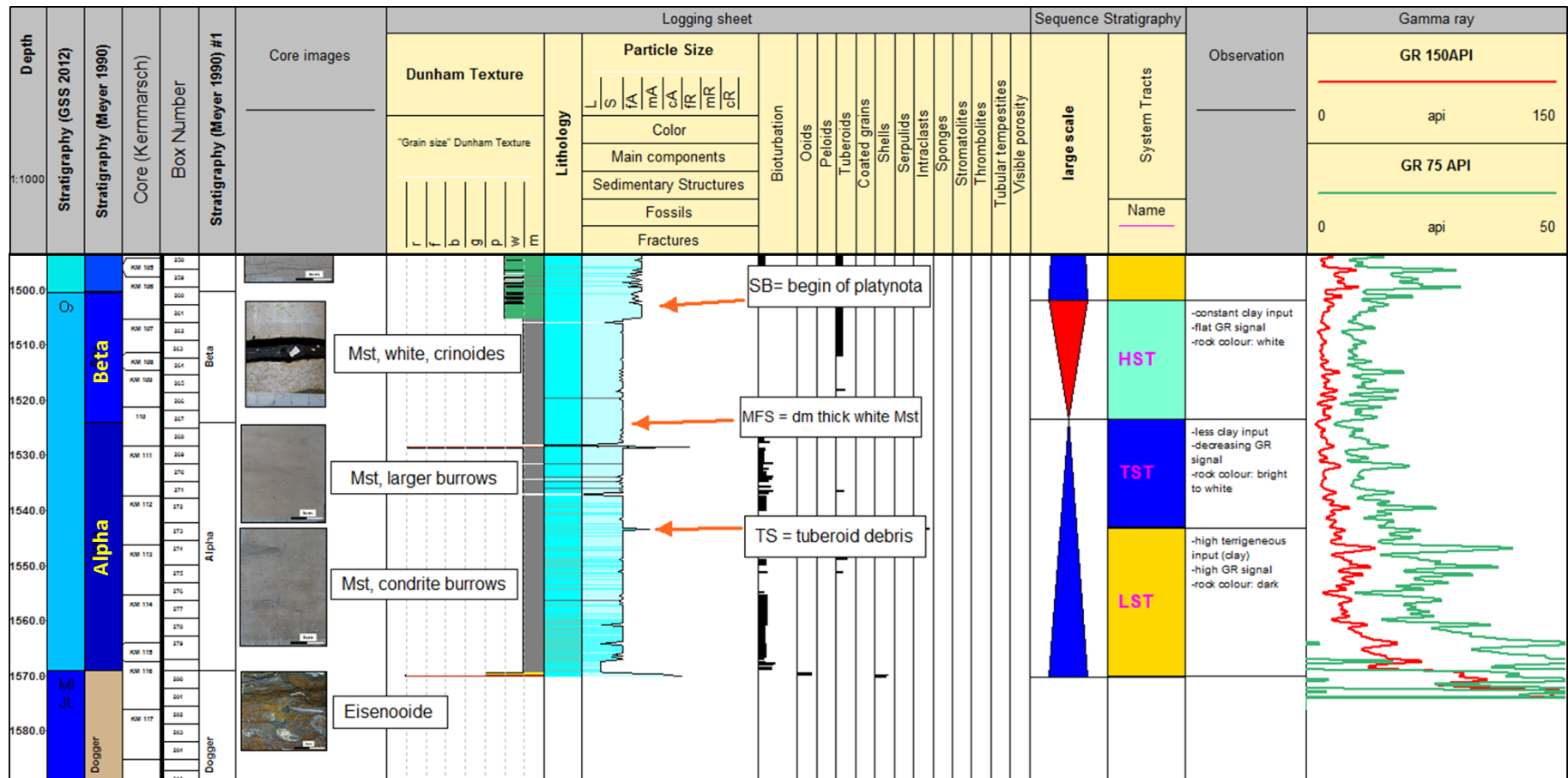


Figure 34: Large scale sequence 1 (S1) comprising the Malm alpha to top beta interval.

The gamma-ray signature shows high values at the lower sequence boundary and is constantly decreasing, as a result of decreasing terrestrial (clay) input and more open marine conditions. The maximum flooding zone has low gamma-ray values and consists of several dm-thick, white limestones. The gamma-ray values are increasing again towards the top. The upper sequence boundary is the base of the Platynota marls, which is reflected by a pronounced gamma-ray peak.

Sequence 2 (S 2) from 1363.90m – 1502.00m

Observations

The Platynota marls of the Malm Gamma form the base of S 2. Frequent alternations of cm-thin clay-marl layers are typical for the Gamma interval. The Crussoliensis marls at the top of the Gamma can be clearly recognized as well (Meyer, 1994b). The increased content of clay minerals is very well visible on the GR-log. The Platynota marls at the base and Crussoliensis marls at the top of the Malm Gamma are 2 very important stratigraphic marker beds, also for other wells in the subsurface of the Molasse basin because of their characteristic GR signature. A sharp contact with the overlying Malm Delta-Epsilon interval is present. It consists almost exclusively of a succession of completely dolomitized sponge-thrombolite float-to rudstone, interbedded with massive dolomites. Significant differences in the bedding style are observed and described in more detail in Figure 36. Based on this observation, a further subdivision of the Malm Delta-Epsilon interval is possible. The top of the Malm Epsilon is a sharp contact with a chaotic bedded mudstone breccia.

Interpretation

The Malm Gamma interval, in general, is very clay-rich. The presence of the Platynota marls at the base of the Malm Gamma is a very prominent and sudden sedimentological change and interpreted as sequence boundary (SB). Figure 35, pic. 8 shows the abundance of marl and clay layers. The Malm Gamma is interpreted as a low stand systems tract (LST). During the LST the base level is lowered, and more terrigenous input occurs. A sharp contact is present at the top of the Gamma interval (Figure 35, pic. 3) interpreted as a transgressive surface (TS). The Malm Delta interval represents the transgressive system tract (TST). Sponge-thrombolite float-to rudstone is the main facies type for this interval. The massive presence and almost basin-wide extension (Meyer, 1994b) of sponges indicate improved living conditions for these filtering organisms. As sponges are very susceptible to clay input (Leinfelder, 1994, 1993) a rising sea level would inhibit such an input (Pross et al., 2006a), allowing the sponge bioherms to grow and extend. A very thin-bedded zone, described by (Böhm, 2012b) as “core discing” is tentatively interpreted as maximum flooding zone (MFZ) There is already a trend in bed

1D Analysis

thickness visible as described in Figure 36 and Figure 37. The regressive hemi sequence, the high stand systems tract (HST), shows a gradual change in bed thickness: from very thin-bedded, marly (close to the MFZ) to several dm thick-bedded sponge-thrombolite float-to rudstone and massive dolomites at the top. The upper sequence boundary (SB) is a sharp, erosive contact with a chaotic-bedded mudstone breccia (Zeta 1).

Figure 36 shows a variation of bed-thickness for the Malm Delta and Epsilon interval. Usually, the Malm Delta and Epsilon interval can be further subdivided (e.g., Delta 1,2,3 and 4). In well Moosburg SC 4 the dolomitization makes it very difficult to recognize distinct criteria for this subdivision. Therefore, these intervals were summarized and classified as one Malm Delta-Epsilon interval (Meyer, 1994b).

However, a significant difference in bed thickness can be observed, as shown in Figure 36. Three main categories of bedding style are present (1): very thin-bedded and marl rich intervals (blue), (2) cm-to dm thick-bedded, and (3) dm-thick bedded intervals. Böhm (2012) described the very thin-bedded and marl rich intervals as “core discing”. The intervals affected by core discing can also be recognized with the gamma-ray log as they have higher values. There is a clear, superordinate trend: from thick-bedded to thin-bedded (marly) and vice versa. This bed-thickness trend can be interpreted in sequence stratigraphic context as a transgressive (blue triangle) hemi-sequence, the thin-bedded interval (“core discing”) as the maximum flooding zone, followed by the regressive hemi-sequence which is represented by a gradual increase in bed thickness.

1D Analysis

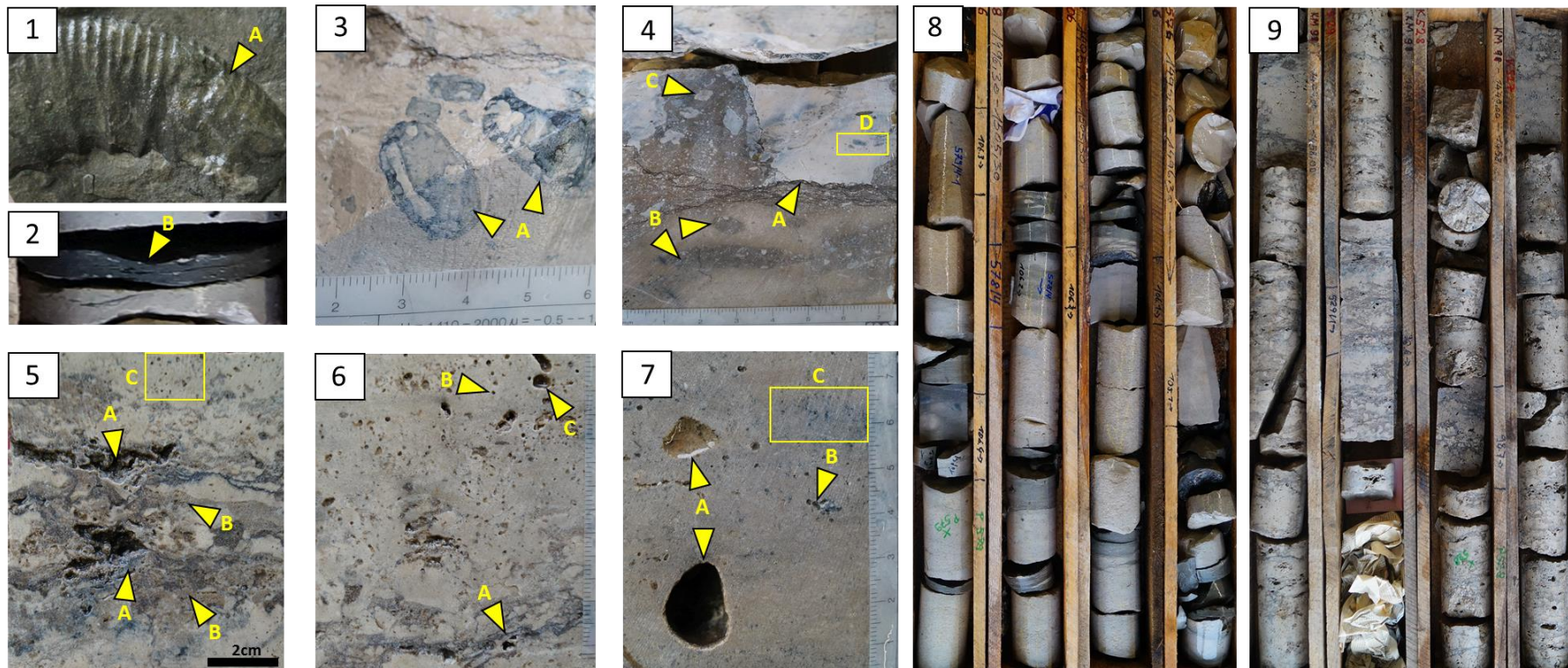


Figure 35: Sedimentological characteristics of S 2 (Malm Gamma to top Epsilon interval).

(1): Slab 580: Ammonite (A) from the Platynota marls. (2): Box 583 shows thin marls-clay layers that are typical for the Malm Gamma interval. Belemnites and Ammonites are often concentrated in these thin, marl layers. (3): Box 557 shows large (several cm) tuberooids. They are associated with decomposed sponge remains (Fritz, 1958; Wagenplast, 1972), hence indicating the proximity to sponge bioherms. (4): A very sharp contact is visible at slab 555 (A). Tuberooid debris (D) and intraclasts (C) cut into the bioturbated wackestone (B). This is interpreted as a sequence boundary and described as the boundary between the Malm Gamma and Delta interval (Meyer, 1994b). (5): Sponges (A) and thrombolites are very common in the Malm Delta and Epsilon intervals as shown in slab 529. Large vugs (A) and moldic pores (C) are very common as well. (6): Slab 532 contains sponges (A) and fine tuberooids (B) as well as moldic pores. (7): Slab 533 with large vugs (A), moldic pores (B) and dark tuberooids (C). The frequent dark marl-clay alternations are characteristic for the Malm Gamma interval as shown in (8). (9): The Malm Delta-Epsilon interval consists almost exclusively of sponge-thrombolite float-to rudstone with abundant vuggy and moldic porosity.

1D Analysis

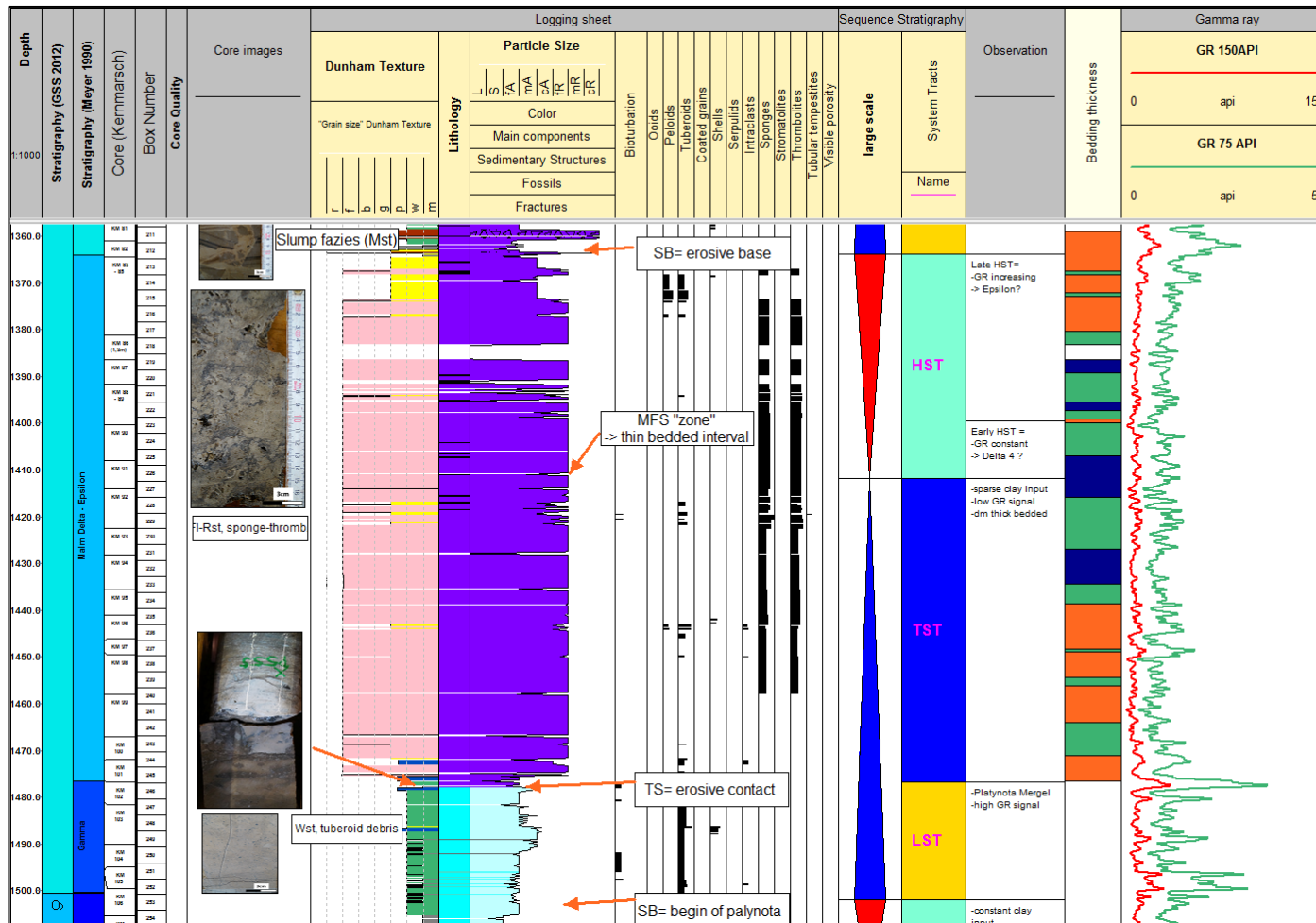


Figure 37: Large scale sequence 2 (S2) comprising the Malm Gamma to top Epsilon interval.

The gamma-ray signal of S2 shows at the base two characteristic peaks, which correspond to the *Platynota* and *Crussoliensis* (Meyer, 1994a). The gamma-ray (0-150 API, red) is relatively low and shows a blocky character. Slightly higher values and a "saw teeth" pattern can be observed around the maximum flooding zone. The upper sequence boundary shows a pronounced peak, which is an erosive contact to a thick carbonate breccia interval.

Sequence 3 (S 3) from 1363.90m – 1140.00m

Observations

The base of large scale sequence 3 is the erosive contact with the chaotic bedded mudstone breccia. This brecciated interval is 30m in thickness and consists of laminated dolomitic-mudstones, which are reworked or deformed. According to (Meyer, 1994b), this is the beginning of the Malm Zeta 1 interval. Well bedded, laminated dolomitic-mudstones follow upwards in the succession. From 1288m onwards, a gradual increase of bioturbation can be observed with an intensively bioturbated zone at 1256m. The intensive bioturbation results in destratification, reworked/disrupted bedding. High GR values are associated with this zone. Well bedded laminated mudstones follow the succession with a change in lithology at 1226m from dolomite to limestone. The laminated mudstones are white in color, and frequent alternations with cm thin marl beds can be observed. This succession is approximately 70 thick, with no major changes in composition, components or texture. Only core 31 to 34 are slightly darker in color (probably higher clay content) and hence have a more pronounced GR signal. Bioturbation starts from 1158m onwards, shells and shell debris, and corals are present. Other abiogenic components are peloids, ooids, and intraclasts, indicating a change of the depositional environment. The top of S3 is represented by core box 179-177. This interval is shown in more detail in Figure 42 and represents the upper sequence boundary (SB) of S3.

Interpretation

The chaotic bedded mudstone breccia consists of several intervals. Most of the mudstone clasts are laminated (Figure 38, Pic 1) and angular, thus have been lithified before transportation. Also, deformed mudstone beds are present and syn-sedimentary fractures. They are interpreted as gravity deposits down a slope, probably a series of several slides and slumps. Therefore, this Interval is interpreted as low stand system tract (LST). The transgressive system tract (TST) consists of well-bedded, laminated mudstones indicating a rising sea level and a quiet environment of deposition. From 1289 m onwards bioturbation sets in gradually. A constant increase of the GR values can be observed as well, with a maximum peak at 1256m. This zone is intensively bioturbated, dolomitized, and interpreted as maximum flooding zone (MFZ), as shown in Figure 38,

1D Analysis

(3). The early stage of the high stand system tract (HST) consists of well-bedded lime mudstones with frequent marl alternations (Figure 38, (2) and (3)). From 1151.4m onwards, the late HST shows a gradual change of facies. Peloids, ooids, shells, and corals are more frequent, indicating a much shallower environment of deposition. The upper sequence boundary (SB) of S 3 is interpreted at a distinct surface with stony bioturbation shown in Figure 42. This hiatus in sedimentation might even be an indicator for exposure associated with dolomitization and the pronounced gamma-ray peak.

1D Analysis

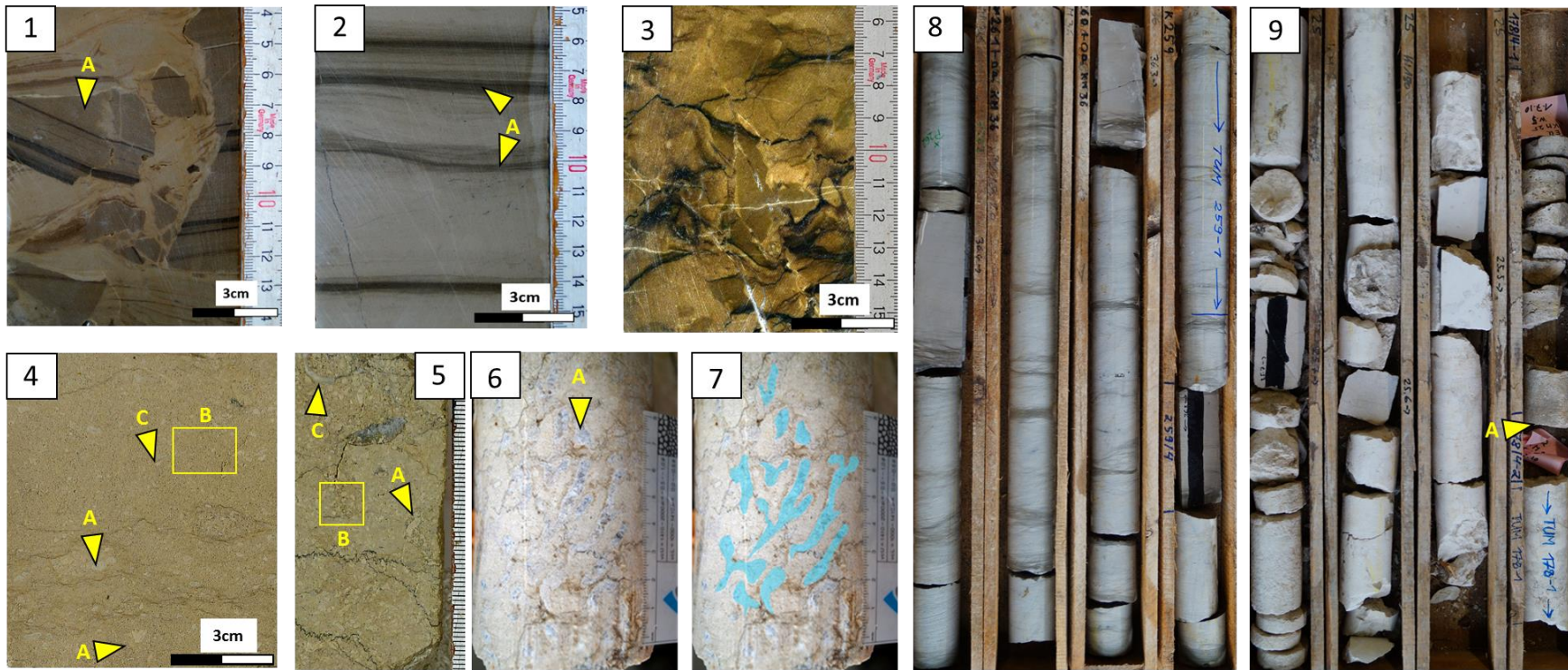


Figure 38: Sedimentological characteristics of S 3 (Malm Zeta interval).

(1): Slab 416 shows an example of the chaotic bedded mudstone breccia interval. Large clasts (A) of laminated mudstone are present, surrounded by mud. This interval is almost 30m in thickness and interpreted as gravity flow down a slope, like a slump or a slide. (2): Slab 347 is a well-bedded limestone with cm-thin marl alternations (A). (3): Slab 311 shows an intensively bioturbated dolo-mudstone. Due to the bioturbation, the bedding is disrupted-de-stratified. This sample is from the interpreted maximum flooding zone (MFZ). (4): Slab 182 shows a peloids-oid (B) dominated packstone with intraclasts (A) and shells (C). (5) is a zoom-in into slab 180 showing intraclasts (A), peloids and ooids (B) shells (C) in more detail. (6) shows the base of core 184, a coral in living position (A) The branches of the coral are highlighted in blue (7). (8): Core 36 shows the well-bedded mudstones with the frequent marl alternations. (9): Core 25 represents the top of the Malm succession with the interpreted sequence boundary (SB) top Malm shown with the yellow arrow (A). The top Malm SB is further explained in Figure 42..

1D Analysis

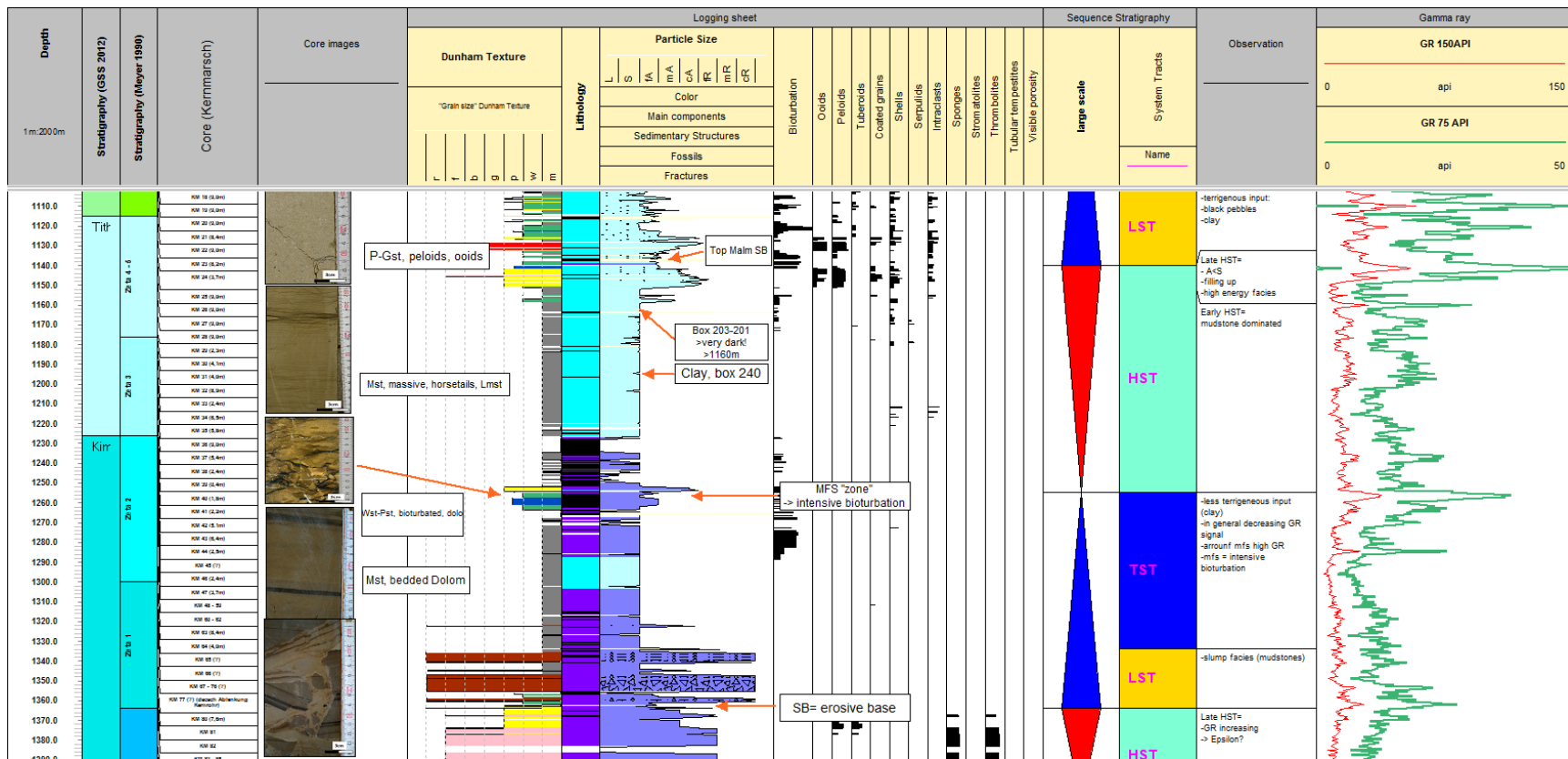


Figure 39: Sequence 3, comprising the Malm zeta intervals.

The lower sequence boundary of S 3 shows two pronounced gamma-ray peaks (Platynota and Crussoliensis marls). The maximum flooding zone is intensively bioturbated and dolomitized. The upper sequence boundary shows a very high gamma-ray peak, which is caused by the storey bioturbation, dolomitization and possible exposure. Above the sequence boundary, the gamma-ray signal stays significantly higher than and shows a serrated pattern.

Sequence 4 (S 4) from 1140.10m – 983.00m

Observations

The sequence boundary (SB) described in Figure 42 is the base of S 4. A succession of very dark, intensively bioturbated wackestone dominates up to 1101.30 m (Figure 40; (1) and (2)). The GR log shows high values and peaks associated with bioturbated wacke- and mudstones. An almost 4m thick cross-bedded peloidal-oolithic grainstone interval is present from 1132 m – 1128m (Figure 39; (3)). An 8 m thick bioturbated mudstone interval is present from 1098 m – 1090 m with the highest GR values observed in the Moosburg SC4 well. This zone of intensive bioturbation is very dark in color and might contain organic remains causing the high GR peak. A succession of 1-3 m thick cycles comprised of laminated mudstone, (often) bioturbated wackestone, and oolithic grainstone follow. The top of the only dm-thick oolithic grainstone beds is a reworking or exposure surface (Figure 40, (8)). These cycle motives repeat up to 1045 m. Algal boundstone, black pebbles, blackened ooids, multiple exposure surfaces, desiccation cracks (Figure 40; (4) – (8) and increasing clay content can be observed in the uppermost part of well Moosburg SC4, with the presence of clay-silt and fine sandstone at the top of core box 1.

Interpretation

Above the SB described in Figure 42, bioturbated wackestone, and a 4 m thick cross-bedded peloidal-oolithic grainstone interval is present. The following interval up to 1101.3 m contains intensively bioturbated, very dark mud and wackestone. This succession is interpreted as low stand system tract (LST). Up to 1045 m, a high-frequency cyclicity can be observed comprising 1-3m thick shallowing upward cycles. The cycle motif starts with laminated mudstone, (often) bioturbated wackestone and oolithic grainstone with an erosive top (exposure surface). This succession is interpreted as a transgressive system tract (TST) associated with shallowing upward cycles motif. From 1033m onwards, exposure and reworking horizons become more frequent, also brecciated zones and black pebbles. Oolithic packstone and grainstone beds are less frequent and often blackened (Figure 40; (4)). The black color of the ooids might be of similar origin like the development of black pebbles (Miller et al., 2013). Algal boundstone, flat pebble conglomerate, and massive dolomites can be observed as well, indicating a very shallow environment of

1D Analysis

deposition with frequent phases of exposure. Hence, this succession is interpreted as high stand system tract (HST) with a gradual filling up of accommodation space and change from a marine setting to a terrestrial environment (sandstone of the Lower Cretaceous, core box 1, (Meyer, 1994b)).

1D Analysis

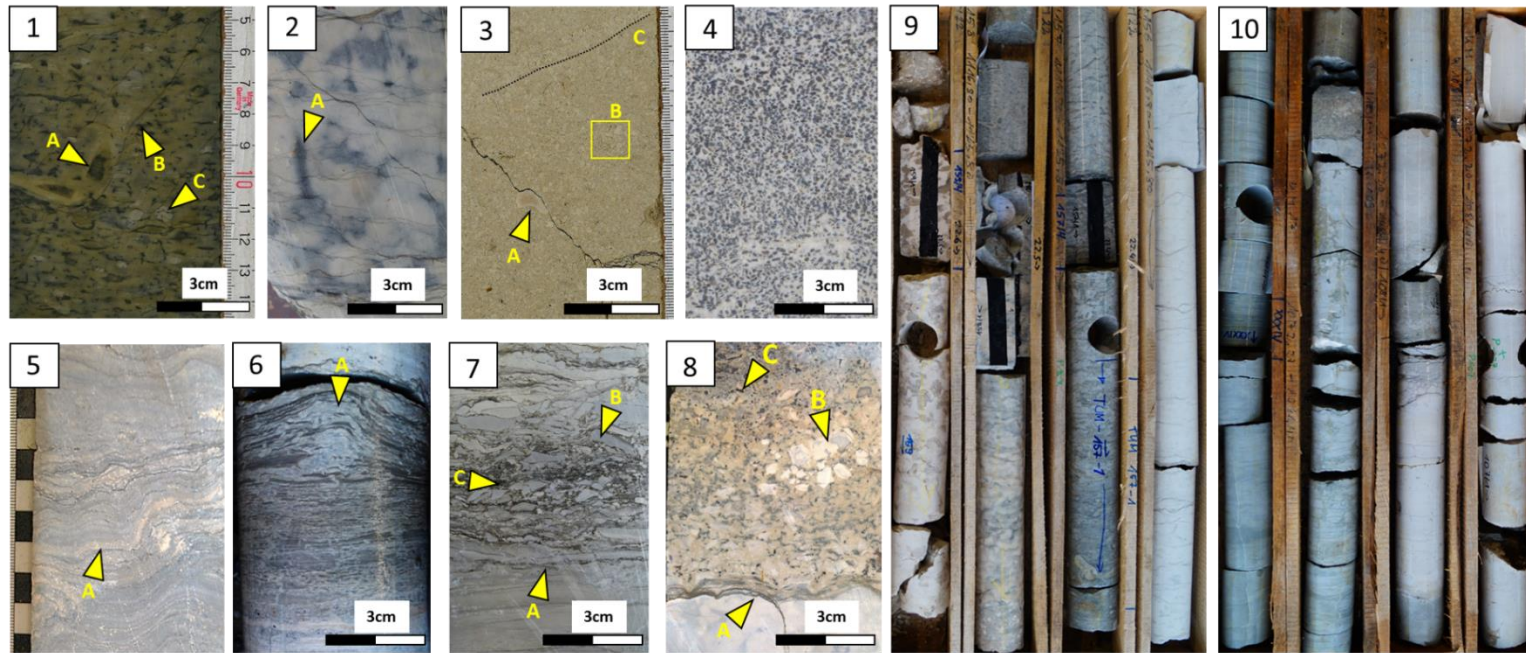


Figure 40: Sedimentological characteristics of S 4 (Malm Zeta to Purbeck interval).

(1): Slab 158: Intensively bioturbated mudstone. Occasional burrow traces are still visible (A) and also intraclasts up to 1cm (B). The main diagnostic feature is the dark, black color caused by abundant black pebbles and/or organic remains (B). (2): Slab 133 shows a bioturbated mudstone, with very dark burrow traces (A). These mudstones (slab 158 and 133) have remarkably high GR values and show a characteristic well log signal, commonly referred to as “Purbeck-peak”. (3): Example of cross-bedded (C) peloidal-oolitic (B) grainstone (slab 167) with intraclasts (A). (4): Slab 16 contains abundant peloids, occasional ooids and they are all blackened. This black peloidal packstone is only present at the uppermost section of the Purbeck. The black color might be associated with exposure, similar to the formation of black pebbles (Miller et al., 2013). (5): Slab 10 shows a wavy, laminated texture (A) and is interpreted as algal boundstone. (6) shows an example of a desiccation crack (A). (7): A chaotic, brecciated and reworked surface is visible in slab 40. The bedding is undisrupted (A) followed by a sharp erosive contact and abundant mudstone clasts (B). Between the clasts, clay-rich mud is present. This is interpreted as a reworking surface, also known as flat pebble conglomerate indicating very shallow to exposure conditions. (8): Slab 109 shows a reworked surface again, with a sharp erosive contact (A) and abundant clast (B) and black pebbles (C). These reworked surfaces have very high GR values, causing a major peak in the well log signal.

1D Analysis

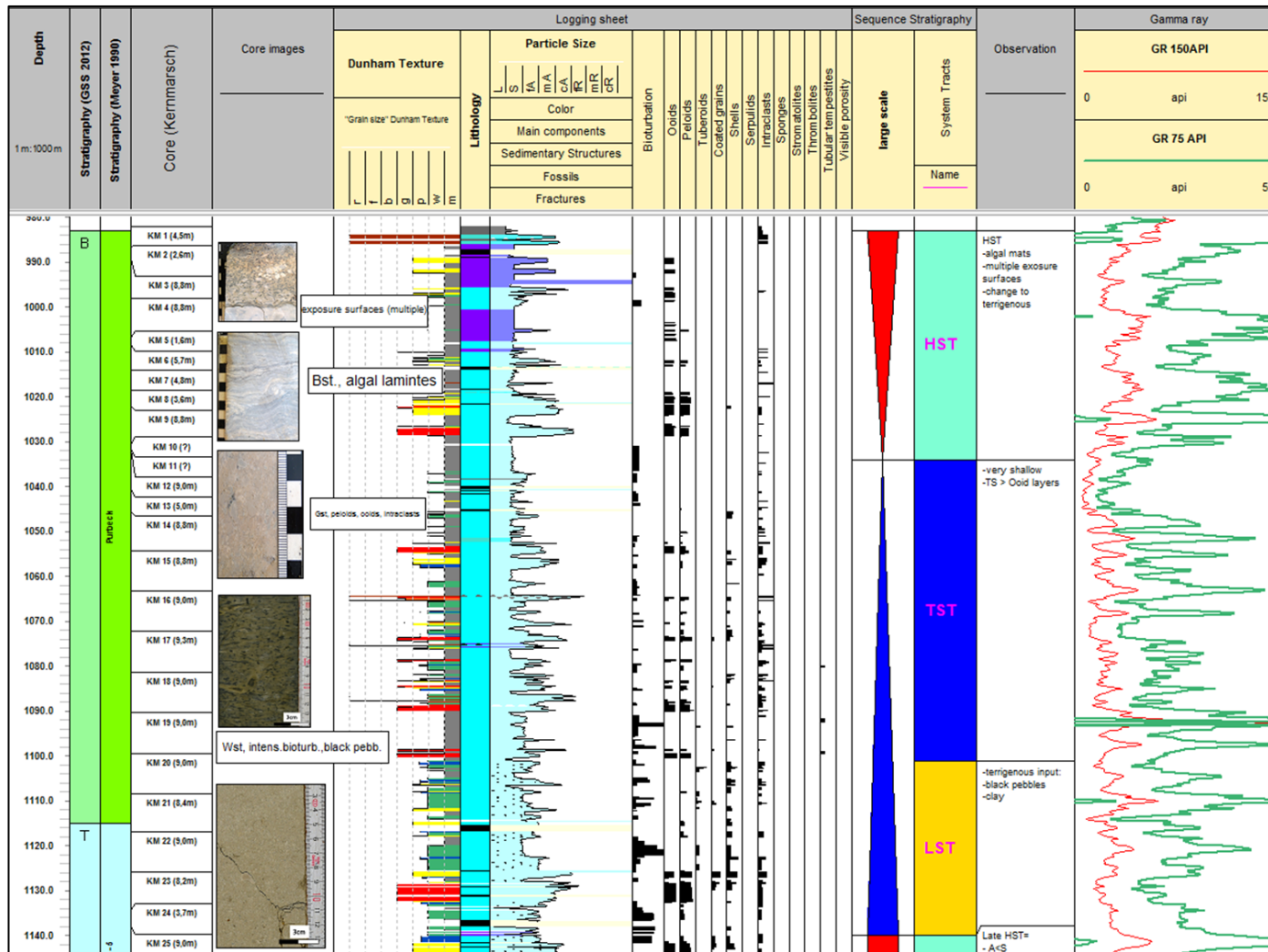


Figure 41: Sequence 4, comprising the Malm Zeta to Purbeck interval.

The gamma-ray pattern for the Purbeck Formation has a different character compared to the Upper Jurassic Malm and can be described as serrated. The gamma-ray pattern is caused by a frequently changing lithofacies.

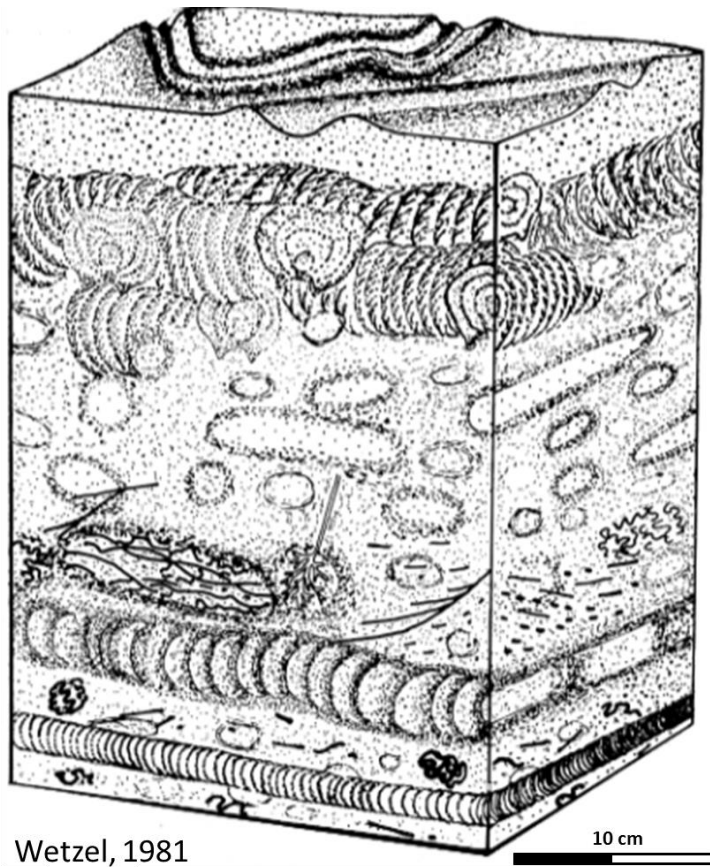
3.3.2 Observations Core-to-Log Calibration

Sequence 3: Top Malm Sequence Boundary

As discussed in chapter 3.1 and shown in Figure 7, the Top Malm sequence boundary has not consistently been interpreted from wireline logs in the subsurface. Increased gamma-ray peaks at the top of the Upper Jurassic are observed, but its origin is unknown. Therefore, the top Malm of research well Moosburg SC 4 is investigated and compared to the gamma-ray log.

Towards the top of S3, in core box 179, 178, and 177 an important change of bioturbation can be observed (Figure 42, Figure 43 marked in orange color). In core box 179 sparse bioturbation occurs, the individual burrow traces are visible with a diameter < 2cm (Figure 42, A). At the base of core box 178 the bioturbation intensity increases, but also the diameter of the T-branched burrow traces (Figure 42, B). Towards the middle of core box 178 the burrows are very thick, almost half the diameter of the core (Figure 42, C). They are interpreted as shrimp burrows, possibly *Thalassinoides*, which corresponds to the *Cruziana* facies (Seilacher, 2007)

All burrows are filled with coarse-grained dolomite (Meyer, 1994b). The top of box 178 and the base of box 177 is a massive dolomite with abundant moldic porosity. This succession of bioturbation is interpreted as “story bioturbation” caused by a break in sedimentation and preservation of the original ichnofacies composition of the burrowing organisms (Werner and Wetzel, 1982). This interval shows a distinct gamma-ray peak and is interpreted as Top Malm sequence boundary.



Wetzel, 1981

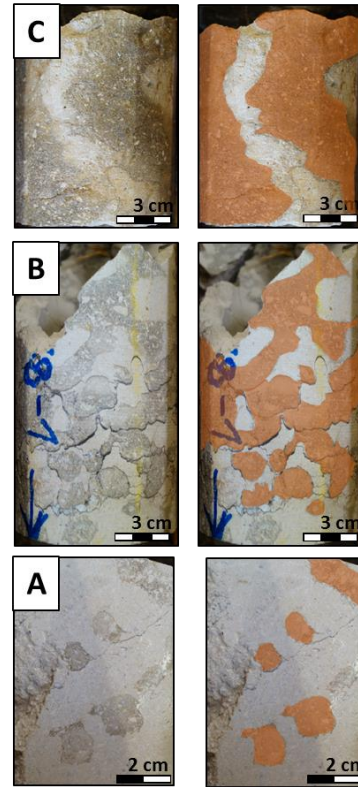


Figure 42: Storey bioturbation after Wetzel (1981) compared to the Top Upper Jurassic Sequence Boundary observed in research well Moosburg SC 4.

1D Analysis

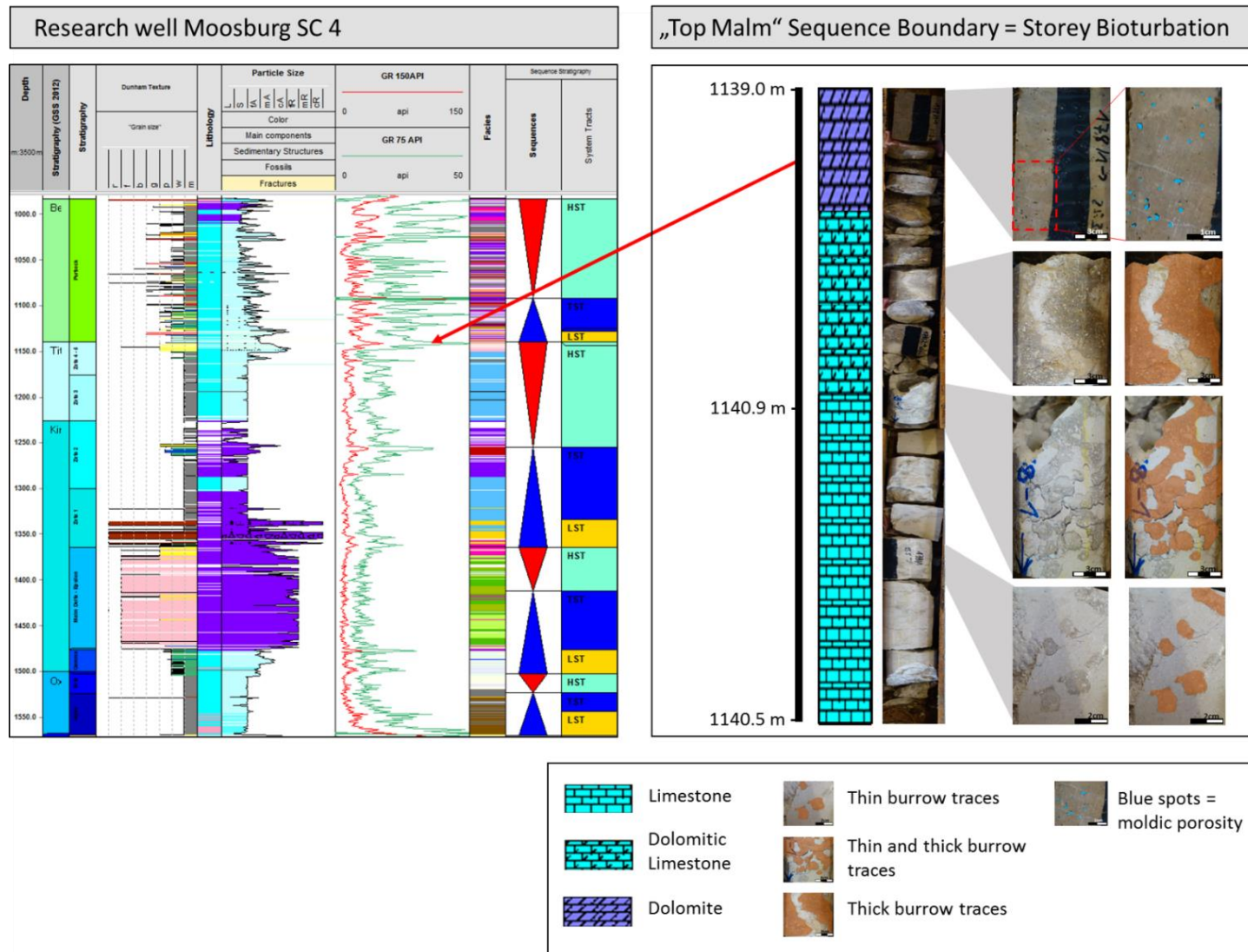


Figure 43: Top Malm sequence boundary interpreted from research well Moosburg SC4.

Sequence 3: Maximum flooding zone

A bioturbated interval is interpreted as a maximum flooding zone. From base to top: the bioturbation sets in gradually and becomes more frequent and intense, until the well-bedded mudstones are completely de-stratified. Along with the bioturbation, the dolomitization is increasing as well. Above the de-stratified zone, the bioturbation is decreasing gradually until the mudstones are well-bedded again. The gamma-ray reflects this trend as a bell shape pattern followed by a funnel shape pattern. This maximum flooding zone can be interpreted in several geothermal wells in the greater Munich area via gamma-ray and borehole image logs, and is, therefore, a potential datum for the 2D correlation (chapter 4).

Sequence 4: Serrated gamma-ray pattern

Core analysis of the Purbeck succession showed that the lithofacies types alternate very frequently on a dm- to m scale. Frequent small-scale cyclicity (approximately 1m) can be observed and are the main reason for the pronounced gamma-ray peaks (Lesić, 2019). Most gamma-ray peaks correlate to exposure surfaces (Figure 40; (8)) or dark, bioturbated mudstones (Figure 40; (1) and (2)). The low gamma-ray values correspond to oolitic grainstones and packstones. The small scale cyclicity represented by frequently alternating lithofacies types and sharp erosive exposure surfaces can be recognized very well by borehole image logs from the geothermal wells. This provides consistent diagnostic criteria to define the Purbeck Formation and the Top Malm sequence boundary.

Summary of Sequence Stratigraphy

Research well Moosburg SC4

1. Sequence 1: During the LST, terrigenous material (clay, silt) was transported into the basin, and very dark mudstones were deposited. The TST shows a gradual decrease in clay content. The carbonates of the HST are very pure and white, with occasional crinoids indicating open marine conditions.
2. Sequence 2: The LST is rich in clay again, containing two marker beds (Platynota- and Crussoliensis marls (Meyer, 1994)). The TST is comprised of dolomitic sponge-thrombolite floatstone. These floatstones dominate the HST as well, and a gradual increase of massive dolomites is observed for the late HST.
3. Sequence 3: A 30m brecciated slump/debris flow interval characterizes the LST. During the TST dolomitic, well-bedded mudstones were deposited. The zone of maximum flooding is intensively bioturbated. Well-bedded lime mudstone represents the HST. During the late HST, shallow water and partly high-energy facies is observed (e.g., ooids, peloids, and corals). Bioherm/reef debris wedges, extending several 100's m into the basin, are frequently observed on the 3D seismic and interpreted as highstand shedding (Schlager et al., 1994). The Top Malm SB is characterized by bioturbation and a change in lithology from limestone to dolostone.
4. Sequence 4: During the LST increased clay input is observed as well as the presence of black pebbles (Strasser, 1983, 1986; Meyer, 1994). The TST consists of dark, bioturbated mudstones interbedded with numerous cm to dm-thin oolitic grainstone layers. Algal boundstone and multiple exposure surfaces and dolomitic intervals characterize the late HST. The late HST marks a gradual change into a terrestrial system with the presence of silt and sandstone.

1D Analysis

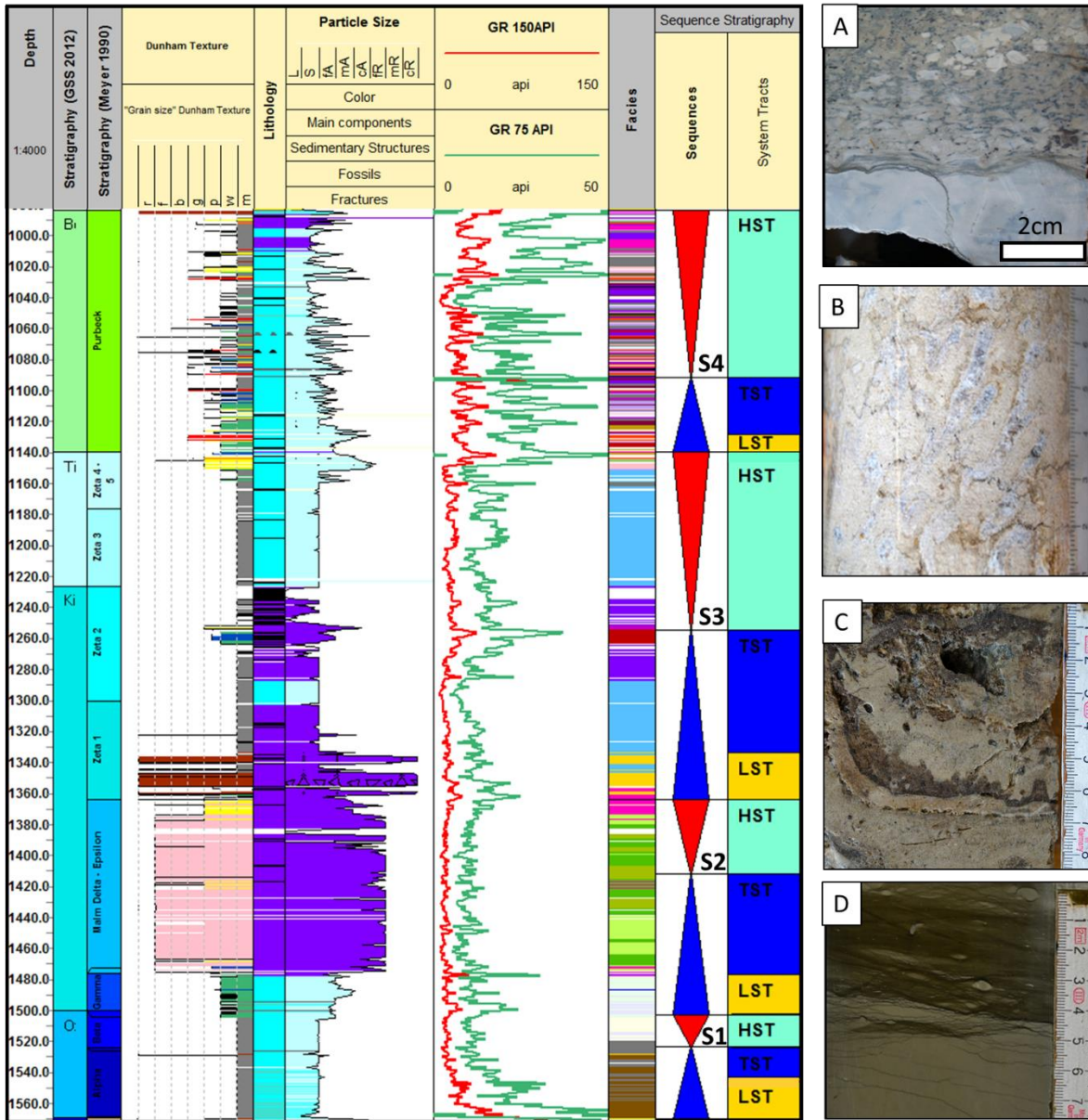


Figure 44: Overview of the well Moosburg SC4 and the interpreted large scale sequences.

(A) Erosive exposure surface (TST, S4); (B) oolitic-peloidal shallow-water facies with corals (late HST, S3); (C) dolomitized sponge floatstones (TST, early HST, S2); (D) dark, marl-rich mudstones (LST, S1).

1D Analysis

The aim of the sequence stratigraphic analysis of research well Moosburg SC 4 is to transfer the interpretation into the surrounding (un-cored) geothermal wells and establish a stratigraphic framework for the Upper Jurassic of the Molasse Basin. Figure 45 shows the spreading of sponge facies in relationship with the global sea-level curve and the content of clay input (Leinfelder, R. R., Nose, M. et al., 1993). Leinfelder et al. (1993,1994) showed that the maximum spreading of the sponge dominated bioherms occurs during times of high sea levels. Because sponges are filtering organisms and very sensitive to murky water (=clay input), they thrive best during times of a high sea level as the terrestrial influence is kept to a minimum. Further studies from (Pross et al., 2006b; Ruf et al., 2005a; Ruf et al., 2005b) that combine sedimentology, chemostratigraphy and palynofacies data support this interpretation. The source of terrigenous input is from the Rhenish land in the NW (Meyer, R. K. F. and Schmidt-Kaler, H., 1990). During times of relatively low sea level, more of the hinterland was exposed. Due to the monsoon-like rain pattern during the Upper Jurassic (Weissert and Mohr, 1996), more terrestrial material was transported into the system resulting in increased clay and marl deposits. Similar observations have been made by (Tinker et al., 2004) for the South Dagger Field, New Mexico, where during relative sea-level low stands, terrigenous material (clay, silt, organic matter) were transported across the carbonate ramp into the basin.

For the Upper Jurassic of South Germany, the clay-rich intervals are, therefore, related to sea-level low stands and the spread-out of the sponge-dominated bioherms to relative sea-level high stands.

The observed large scale sequences (S 1-3) from research well Moosburg SC4 are shown in Figure 45 and correlate with the global sea level curve (Ponsot and Vail, 1991b) and the spreading of sponge facies and clay input (Leinfelder, Krautter et al., 1994).

1D Analysis

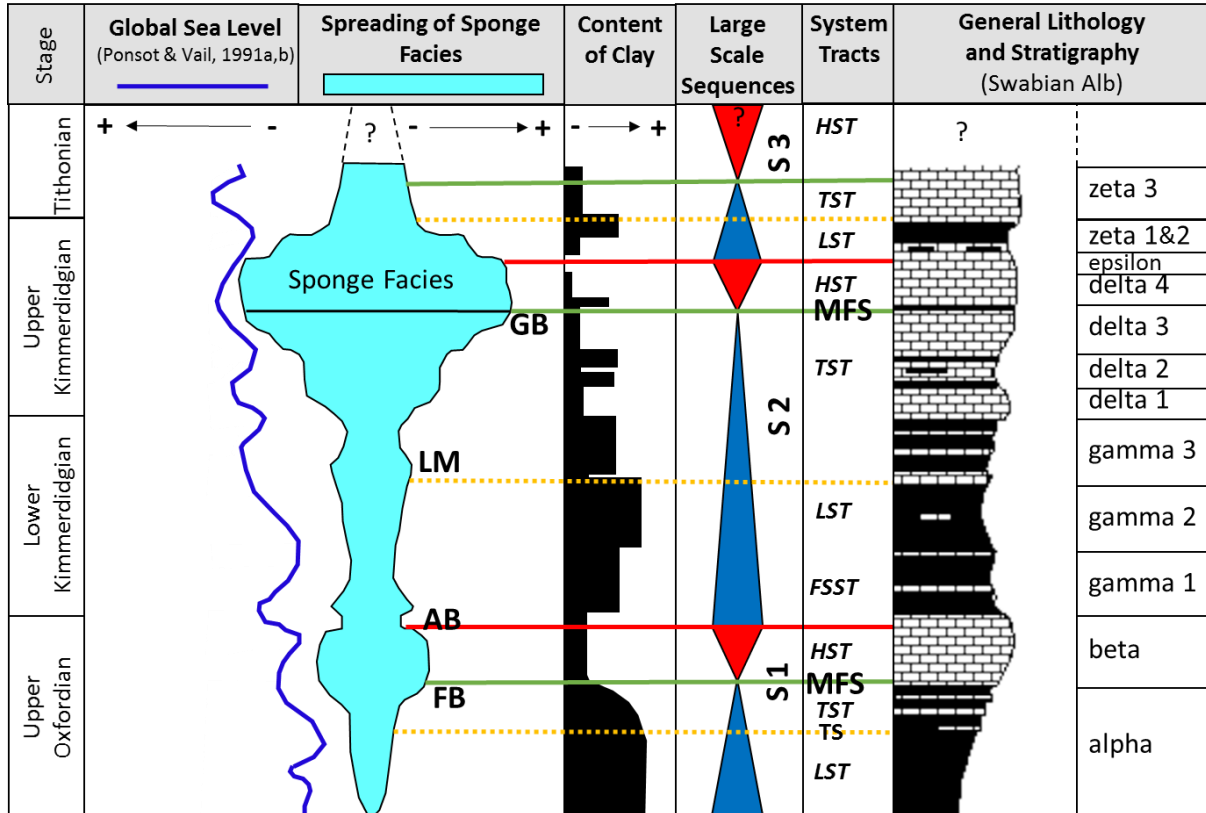


Figure 45: General sequence stratigraphic interpretation for the Upper Jurassic (modified after Leinfelder et al., 1994).

3.4 Borehole-Image Interpretation

Borehole images are micro-resistivity measurements along the borehole wall. These logs detect the micro-resistivity contrast, which is then visualized as a false-color borehole image (Pöppelreiter, Garcia-Carbadillo, Kraaijveld, 2010; Serra, 1989). Originally, dip meter and borehole image logs were acquired to measure the dip angle of strata or fractures. Due to improving technology and resolution, the applications of borehole image logs are much broader now, and they are an established part of the reservoir characterization tool kit (Duhon and Topping, 2017; Pöppelreiter, García-Carballido, Kraaijveld, 2010a; Prenskey, 1999).

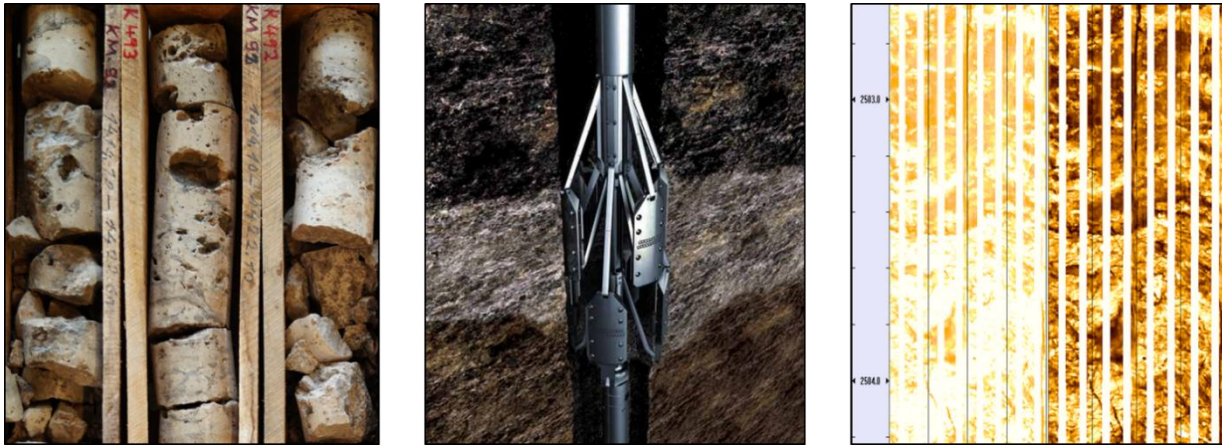


Figure 46: Linking core-based facies with the borehole image facies

However, borehole image interpretation in carbonate reservoirs is still very challenging. While fractures, faults, and karst can often be recognized very well (especially if filled with conductive drilling mud) the internal limestone texture is more subtle and difficult to identify (Akbar et al., 1995; Chitale et al., 2010; Steiner and Böhm, 2011; Wolpert and Pöppelreiter, 2019). Diagnostic features like fossils or other components commonly provide not enough resistivity contrast and, therefore, cannot be detected by the borehole image tool. In some cases, diagenesis can significantly enhance such features and highlight details of the internal composition of carbonate rocks (Lucia, 2007; Nian et al., 2018; Purwanto, 2002; Wolpert et al., 2019).

1D Analysis

In most of the geothermal wells in the greater Munich, borehole image logs were acquired and interpreted in terms of structural geology (faults/fractures) and present-day stress (Seithel et al., 2018). However, the value of information of the borehole image logs is only partly used, as shown by (Steiner and Böhm, 2011). The interpretation of basic lithofacies types or units is possible in Upper Jurassic carbonates and helps to reduce uncertainty in reservoir characterization

The vertical stacking of borehole image facies, important stratigraphic marker beds, and stratal surfaces reveal the sequence stratigraphic architecture and help to delineate genetically linked depositional units (potential flow units which often found at sequence boundaries).

Therefore, one of the aims of this study is to link the established core-based lithofacies atlas from chapter 3.2.1 with the borehole image facies (Figure 46). Prior to interpreting the borehole image facies, thorough quality control of borehole image log data was conducted for each well, following a standardized workflow (Garcia-Carbadillo et al., 2010; Trice, 1999).

3.4.1 Borehole Image Facies

The following Figure 47 to Figure 55 are CMI Logs (dynamic image) acquired in freshwater mud and conventionally color-scaled (dark colors = conductive). They show examples of borehole image facies types that are linked with the core-based lithofacies from research well Moosburg SC4.

1) Well-bedded limestone

Observation: Frequent alternations of parallel-bedded conductive (dark) and resistive layers (bright) are characteristic of this borehole image facies. The dark, conductive layers are typically 1-5 cm thick and the bright, resistive layers 10 to 18 cm. True dip angles are less than 10° and very consistent in dip azimuth.

Interpretation: The dark, conductive layers on the borehole image correspond to the marly layers observed in the core. The bright layers represent the limestone beds. The vertical thickness of this facies type is several m to 10's of m. This facies type corresponds to the distal well-bedded basin facies.

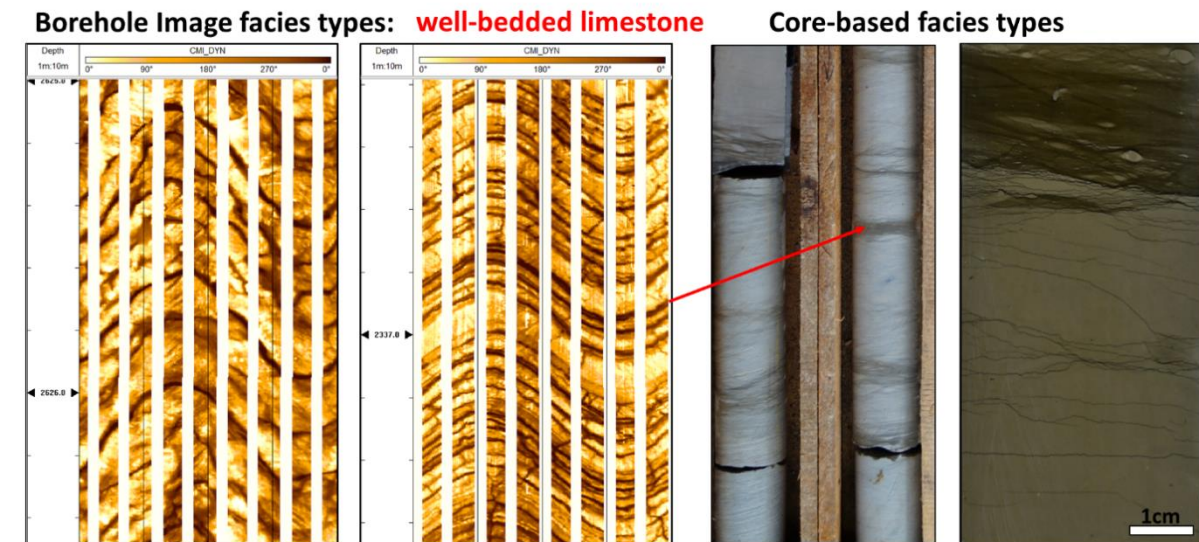


Figure 47: Borehole image facies type: Well-bedded limestone

2) Clasts and debris

Observation: The diagnostic features for this borehole image facies type is the mottled texture, which is composed of irregular shaped and poorly sorted, resistive components (1-5 cm). The components are surrounded by a conductive matrix. Several dm to several m of vertical thickness has been observed on borehole image logs from the study area.

Interpretation. The core shows that limestone clasts and debris are often embedded into a marly, mud-dominated matrix. Outcrop analog studies (Chiracal, 2019) and Eigler 2018, as well as interpretation from 3D seismic (chapter 5.1), show that bioherm debris wedges can be significantly thicker (30-50 m) as interpreted from borehole image logs. A reason for the difference in thickness is that the geothermal wells usually target the top of the bioherms rather than the flanks where the bioherm debris wedges are thickest.

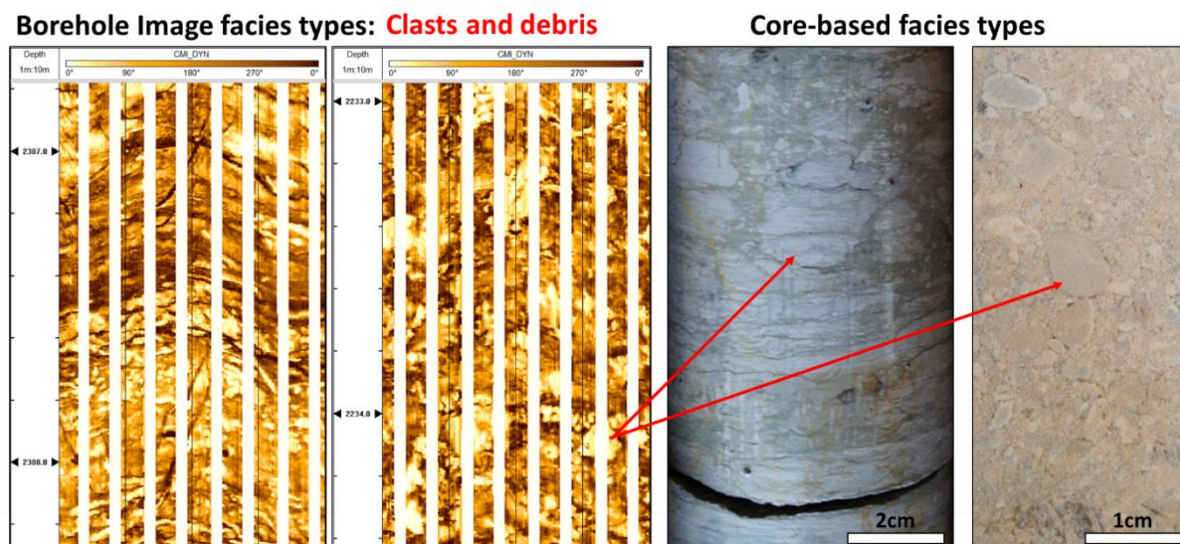


Figure 48: Borehole image facies type: Clasts and debris

3) Bioclast debris

Observation: Thin, elongated and very resistive components (up to 5 cm long) are visible on the borehole image log, together with smaller, resistive subangular features (1-2 cm). They are often concentrated in discrete beds, that are usually 10-15 cm in thickness but can occasionally reach up to 80 cm. Most of the elongated features are subparallel to the normal bedding planes.

Interpretation: This borehole image facies is interpreted as bioclast debris. The elongated, very resistive features correspond to large (1-5cm), disarticulated shells, as observed in the core. Smaller shells are also frequently observed in the core, as well as a fining-up trend in component size. The orientation of the shells is mostly parallel to bedding. The resistive subangular features (1-2 cm) are interpreted to correspond to reworked intraclasts. Based on the core description, these layers are interpreted as bioclast event beds. They are usually sandwiched between the well-bedded mudstones (distal facies) and indicate certain proximity to a bioherm/reef.

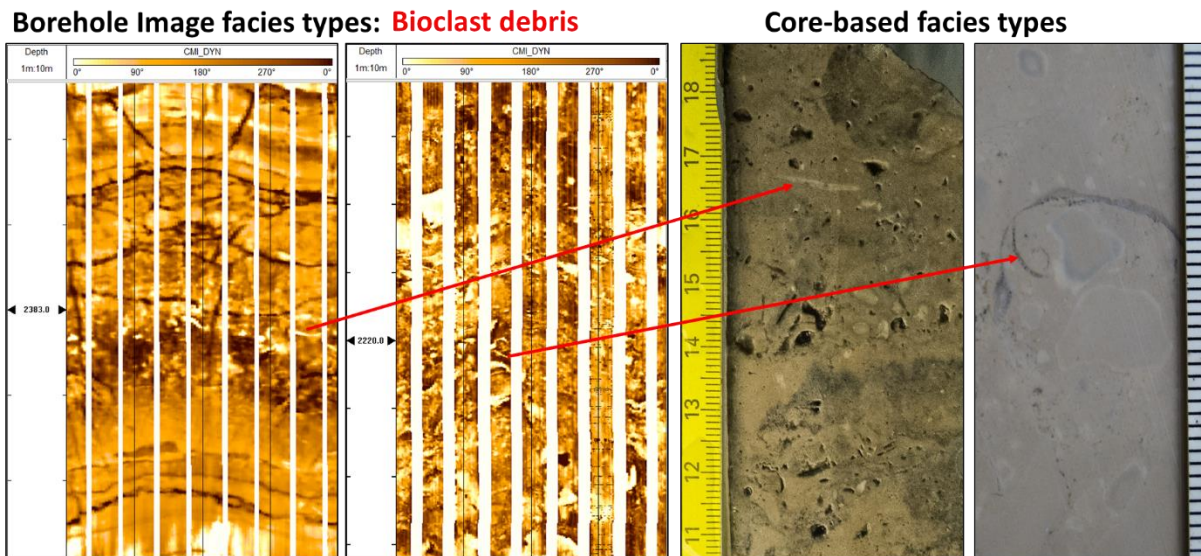


Figure 49: Borehole image facies type: Bioclast debris

4) Bioturbation

Observation: A dark, conductive mottled texture is typical for this borehole image facies. A closer inspection of the conductive spots shows that there are frequently conductive, sub-vertical, and branched traces. Often the mottled texture sets in gradually, become more intensive, and comes to an abrupt end, followed by conductive layers with a massive texture. Typically the vertical thickness ranges from several dm to m, but can occasionally exceed 10's of meters.

Interpretation: The conductive, mottled texture with the sub-vertical branched traces is interpreted as bioturbation. The core description reveals that the burrow traces often have a coarse-grained fill. In research well Moosburg SC4, similar traces are dolomitized (Meyer, 1994) and have higher porosity than the surrounding tight limestone. Considering a conventional color-scaled borehole image log acquired in freshwater mud, the burrow traces are conductive and appear as dark and mottled texture. A gradual increase/decrease of bioturbation intensity has been observed in core and borehole image but also an abrupt end of bioturbation, which can be a potential stratal surface.

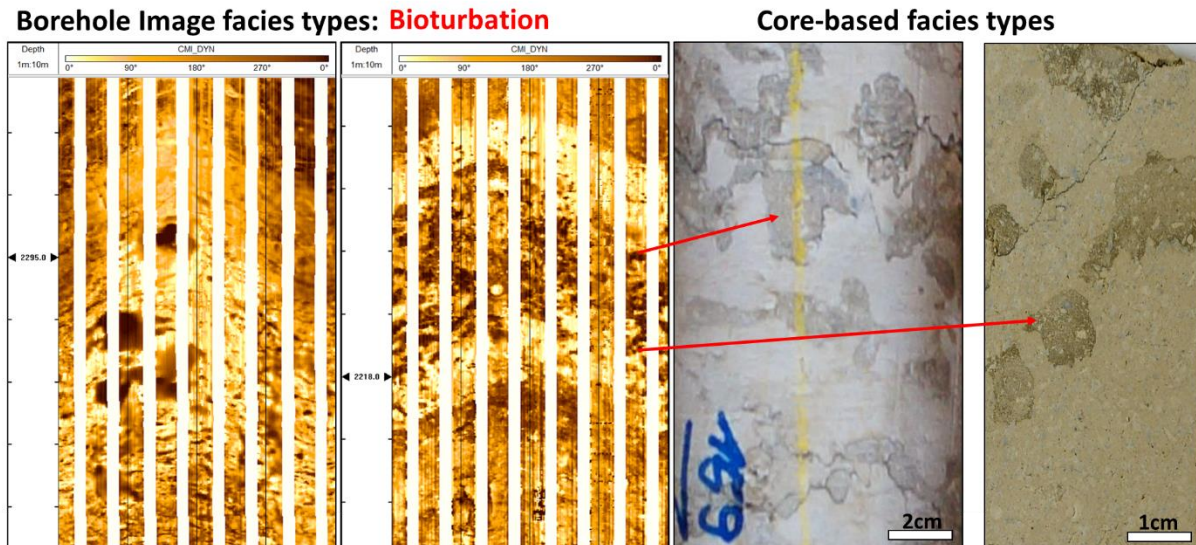


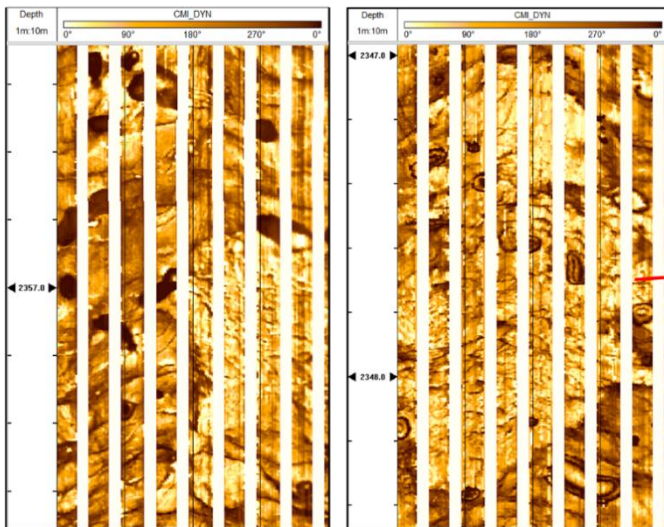
Figure 50: Borehole image facies type: Bioturbation

5) Olistolith (allochthonous bioherm blocks)

Observation: The dynamic borehole image logs show resistive, roundish features with a massive texture. They are several dm to 2 m in vertical thickness and are surrounded by more conductive layers with sub-parallel or deformed bedding. These resistive, angular features contain ring-shaped or elongated conductive components (up to 12 cm in size). An important observation is that the orientation of the conductive components shows a great variation (including vertical), whereas the same conductive components in the strata below and above are oriented approximately sub-parallel to bedding.

Interpretation: The resistive, roundish features with a massive texture are interpreted as olistoliths, possible reworked bioherm blocks. The ring-shaped or elongated conductive components are interpreted as sponges (see Figure 52). Supporting evidence for the interpretation as olistoliths is also the orientation of the sponges, which is not parallel or sub-parallel to the normal bedding (sponge living-position) compared to the bioherm. Bold (2010) made detailed observations and measurements of sponge orientation during outcrop work which further supports this interpretation. Larger olistoliths (several m to 10s of m) are present in outcrop but very challenging to recognize in subsurface due to their large size and similarity to the actual bioherm.

Borehole Image facies types: Olistolith



Outcrop-based facies types

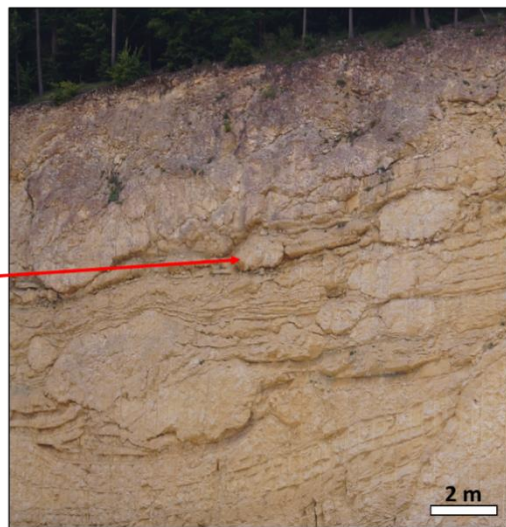


Figure 51: Borehole image facies type: Olistolith

6) Sponge bioherm

Observation: Ring-shaped or elongated very conductive components (up to 12 cm in size) surrounded by a more resistive matrix are the diagnostic features for this borehole image facies type. The conductive rings/ovals are often separated, but occasionally touching resulting in enhanced conductive areas.

Interpretation: The elongated, ring-shaped conductive features are interpreted as sponges. They are very common in the Upper Jurassic of South Germany and are major bioherm building organisms (Leinfelder, Krautter et al., 1994; Leinfelder, R. R., Nose, M. et al., 1993; Meyer, R. K. F. and Schmidt-Kaler, H., 1990). Observations from research well Moosburg SC4 show that due to dolomitization and diagenesis, the rims of the sponges and/or the complete sponges are frequently dissolved. While logging, the conductive drilling mud fills out the created pore space. Therefore, the sponges appear as dark, conductive features on the borehole image log. This facies type is considered an important geothermal reservoir type as it can provide a significant amount of porosity and permeability.

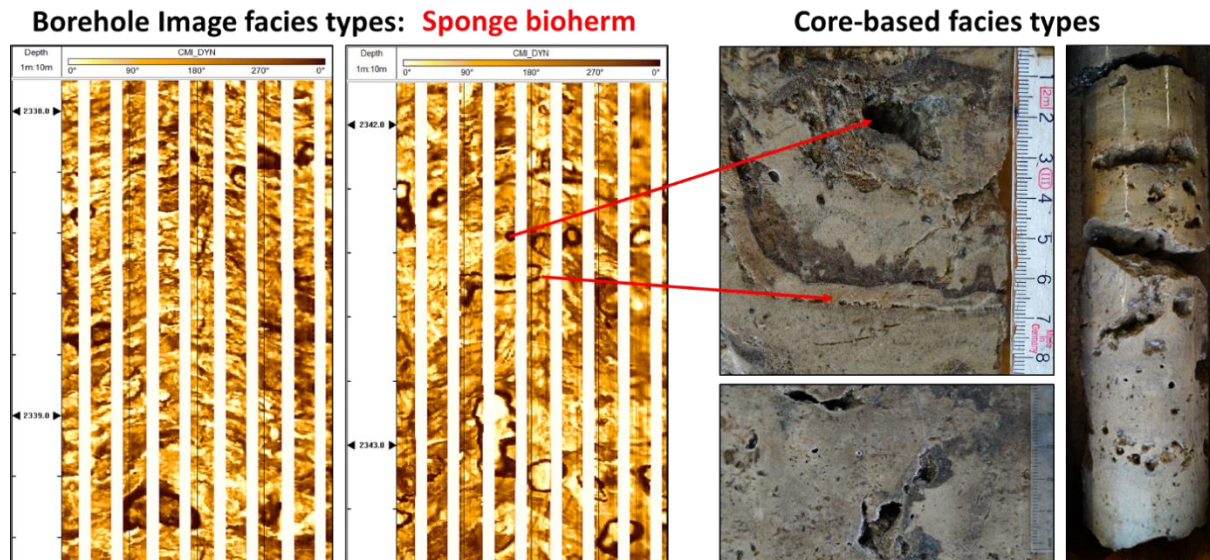


Figure 52: Borehole image facies type: Sponge bioherm

7) Corals

Observation: Intensively branched, very resistive features are visible on the borehole image logs. The individual branches are approximately 1-2 cm thick. The complete features have a vertical thickness of 30 to 80 cm. A more conductive matrix usually surrounds them.

Interpretation: The resistive and branched features are interpreted as corals in living position. Comparison with core showed that the corals are frequently calcified and completely tight which might explain the resistive character. Porous oolitic-peloidal packstones and grainstones surround the corals, which explains the resistivity contrast and the detailed resolution of the borehole image log. The presence of corals was only observed in the uppermost part of the Upper Jurassic (Meyer, 1994a) which corresponds to the late HST of depositional sequence 3 from well Moosburg SC4 (see chapter 3.3.1). The presence of corals in image logs indicates a shallower depositional environment as the sponges as main bioherm building organisms are gradually replaced by corals.

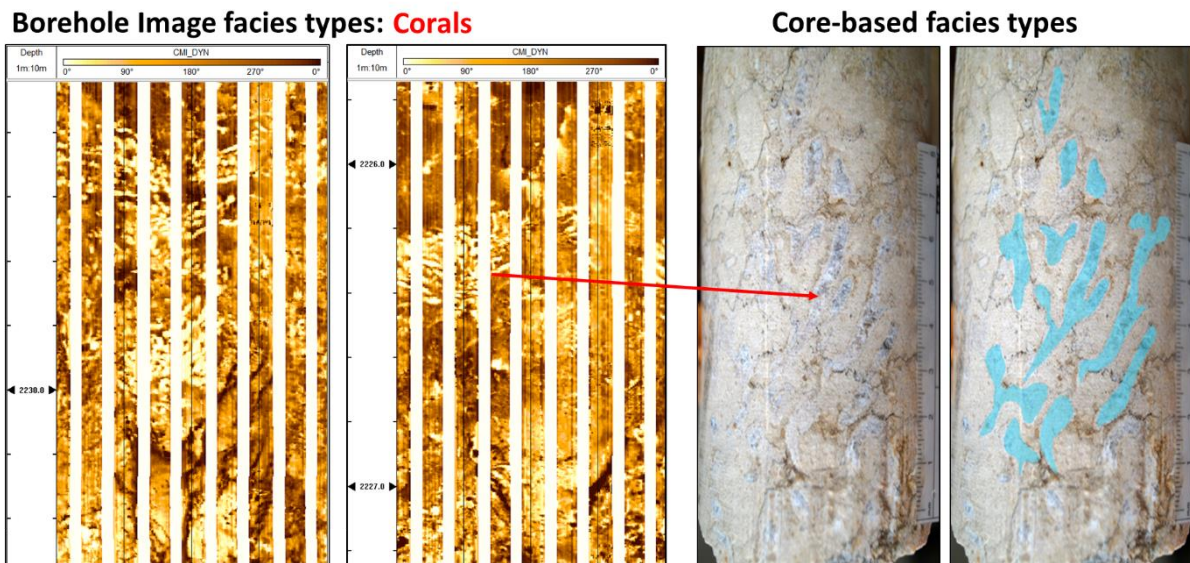


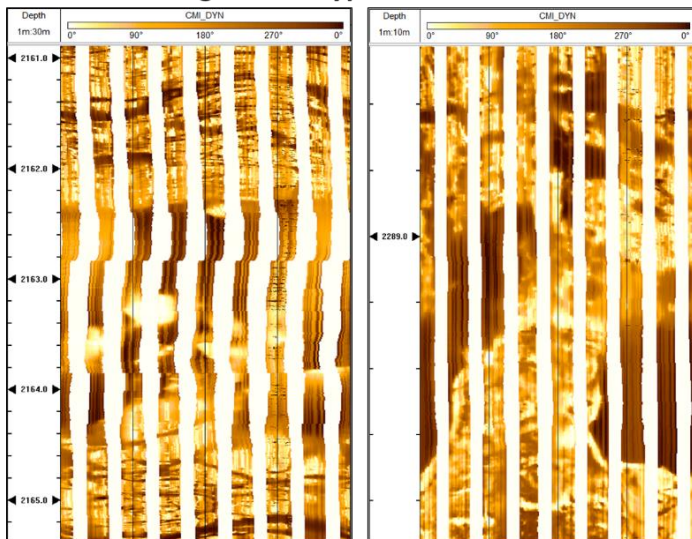
Figure 53: Borehole image facies type: Corals

8) Karst

Observation: This borehole image facies type shows no borehole image as such. It is completely dark or blurred without internal features. The arms of the BHI tool loose contact with the borehole wall. Occasionally, an indented, irregular surface at the base can be observed. The vertical thickness can reach from 20 cm up to 1.8 m.

Interpretation: The interpretation as Karst is not based on the borehole image log alone. Caliper data and dynamic data like fluid losses while drilling or production tests confirm the interpretation as Karst. This borehole image facies type can be one of the most prolific geothermal reservoir types in the greater Munich area.

Borehole Image facies types: Karst



Core-based facies types



Figure 54: Borehole image facies type: Karst

9) Vuggy macropores

Observation: This facies type shows a mottled texture with very dark, conductive spots. They vary very much in size and form (1cm to 10 cm) and are, in contrast to the mottled texture interpreted as bioturbation, not branched. Furthermore, their increase/decrease in intensity is also more gradual and not sharp, as the stratal surfaces associated with bioturbation.

Interpretation: The dark, conductive spots are interpreted as vuggy porosity because their borehole image character is different from the mottled texture interpreted as bioturbation. This borehole image facies type is associated with the sponge dominated bioherms. Borehole cuttings from these intervals are often dolomitic. Production tests from several geothermal wells confirm this facies type as a potential geothermal reservoir type.

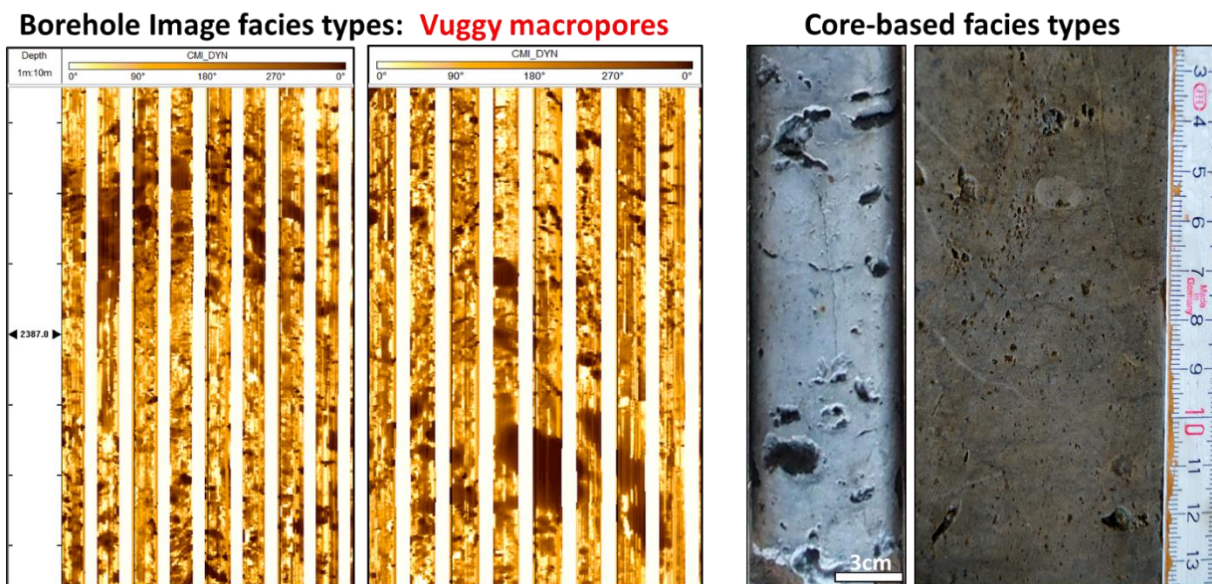


Figure 55: Borehole image facies type: Vuggy macropores

10) Undefined borehole image facies

Although the quality of the borehole image logs and the resolution is very good for most of the geothermal wells, there are also image facies types that are ambiguous. Figure 56 shows an example where no components, textures (other than “massive”) or sedimentary

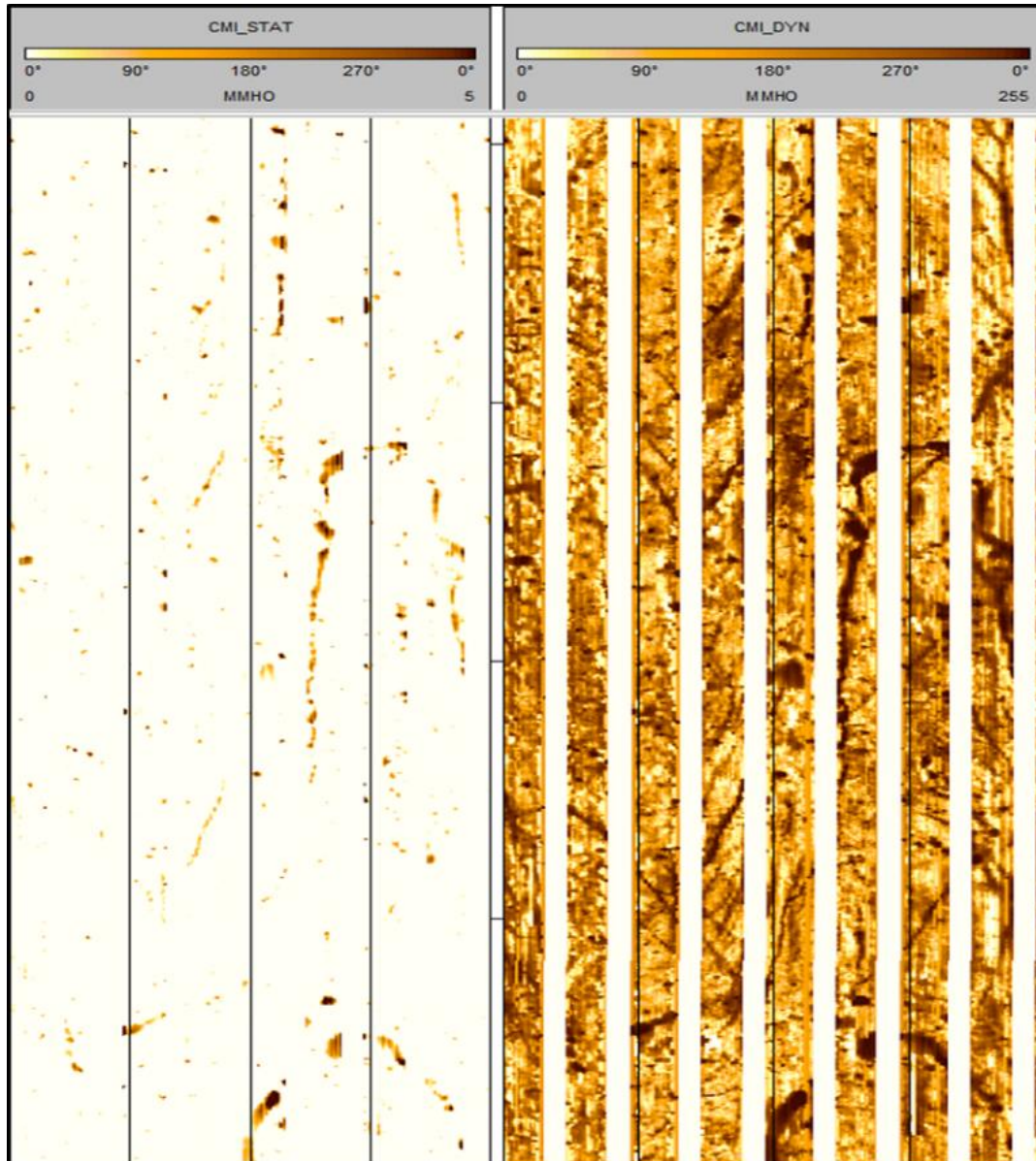


Figure 56: Undefined borehole image facies

structures can be identified. This problem is frequently encountered in carbonate rocks (Akbar et al., 1995), as diagenesis can reduce the porosity dramatically until the rock is basically tight. Because a borehole image logs is a visualization of micro-resistivity

1D Analysis

measurements, the tool can not detect any internal features of such tight rock units. The undefined borehole image facies accounts for approximately 20-35% of the geothermal wells in the study area, leaving gaps in the interpretation.

Table 3: Summary BHI Facies Types

Code	Name	Diagnostic criteria
1	Well-bedded mudstone	Well-bedded alternations of resistive and (thin) conductive layers. Low angle dip, consistent azimuth.
2	Bioturbation	Conductive mottled texture with branched traces. Sharp surfaces often terminate the mottled texture.
3	Bioclast	Elongated, very resistive features and clasts, oriented sub-parallel to the normal bedding. Confined in discrete layers, usually 10-15 cm in thickness.
4	BHI Debris	Mottled texture, which is composed of irregular shaped and poorly sorted, resistive components (1-5 cm). Increasing and decreasing trends in clast size.
5	Sponge bioherm	Ring-shaped or elongated very conductive components (up to 12 cm in size) surrounded by a more resistive matrix
6	Olistolith	Resistive, roundish features with a massive texture, several dm to 2 m in vertical thickness and surrounded by more conductive layers with sub-parallel or deformed bedding; ring-shaped or elongated conductive components with a great variation in orientation (including vertical).
7	BHI Corals	Intensively branched, very resistive features surrounded by a more conductive matrix. Branches are 1-2 cm thick; the succession of 30 to 80 cm.
8	Vuggy macropores	Mottled texture with very dark, conductive spots. They vary very much in size and form (1cm to 10 cm), no branched traces are observed.
9	Karst	Completely dark or blurred borehole image without internal features. Additional data needed (caliper, PLT).

3.4.2 Stratal Surfaces Interpreted from Borehole-Image Logs

Although the borehole image facies is calibrated to the core, there are still gaps in the interpretation due to the tight character, which makes borehole image facies classification very challenging. Therefore, other additional observations are needed to support the borehole image facies interpretation and to close gaps in the tight intervals.

The interpretation and importance of stratal surfaces is a widely applied concept in geology, especially in seismic sequence stratigraphy (van Wagoner et al., 1988; van Wagoner et al., 1990). It is usually applied to define the system tracts, which are separated by important surfaces like sequence boundaries or maximum flooding surfaces (Catuneanu et al., 2011). This concept can be applied to a variety of scales, down to the borehole image and core scale. Stratal surfaces can be erosional, depositional or non-depositional (Miall, 1985) and are usually documented during standard core description.

These stratal surfaces can, as shown here, also be interpreted from borehole image logs and provide important information about genetically related sedimentary facies, which are also fundamental to establish a 2D well-correlations (Durkin et al., 2017; Keeton et al., 2015).

The following section describes characteristic surfaces from the geothermal wells, that are interpreted as stratal surfaces. They are used as additional criteria to improve borehole image interpretation in carbonates and to close the gaps where no borehole image facies can be assigned due to the lack of diagnostic criteria.

1) Highly indented surfaces

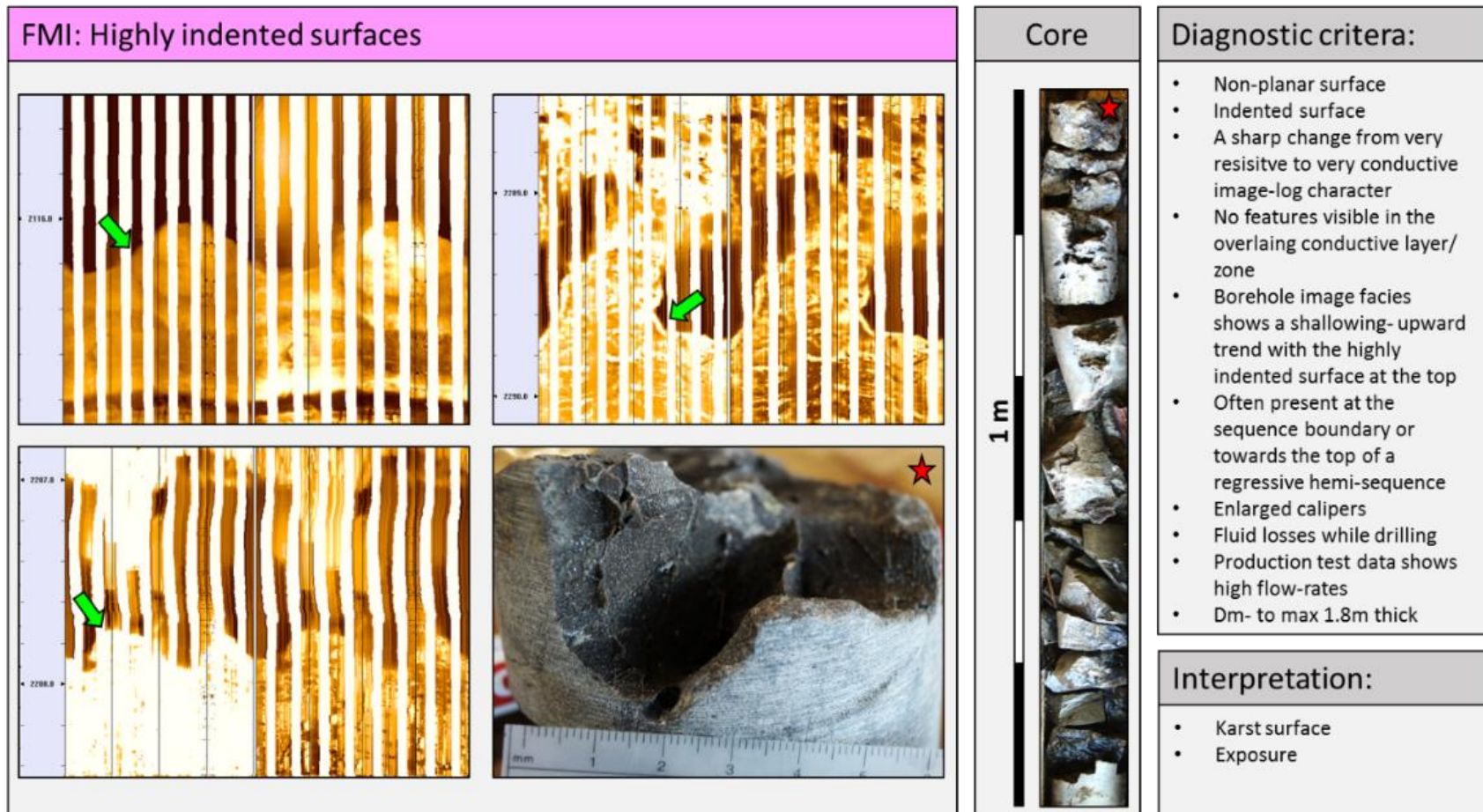


Figure 57: Stratal surfaces from image logs: Highly indented surfaces

2) Truncated surfaces

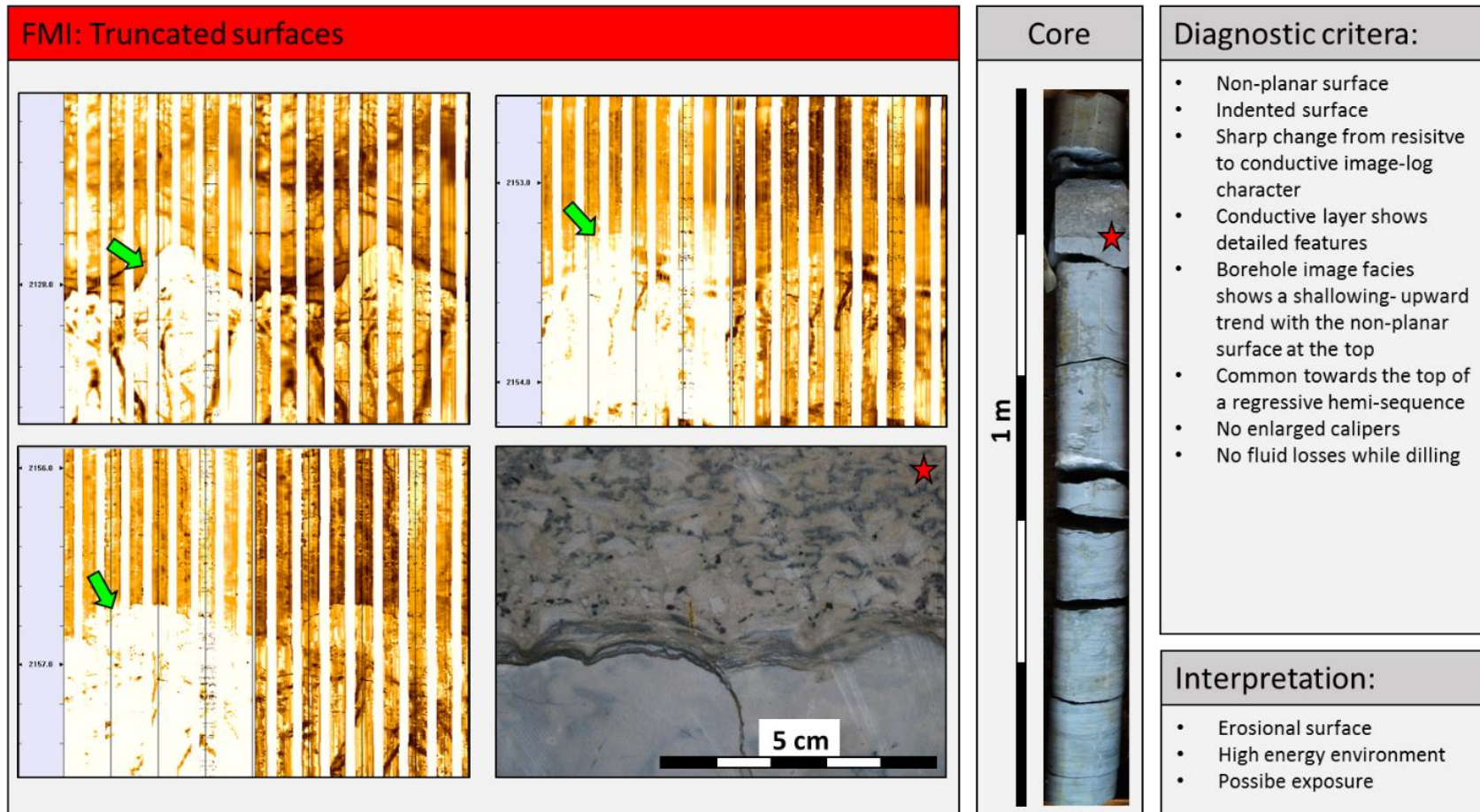


Figure 58: Stratal surfaces from image logs: Truncation surfaces

3) Concordant surfaces

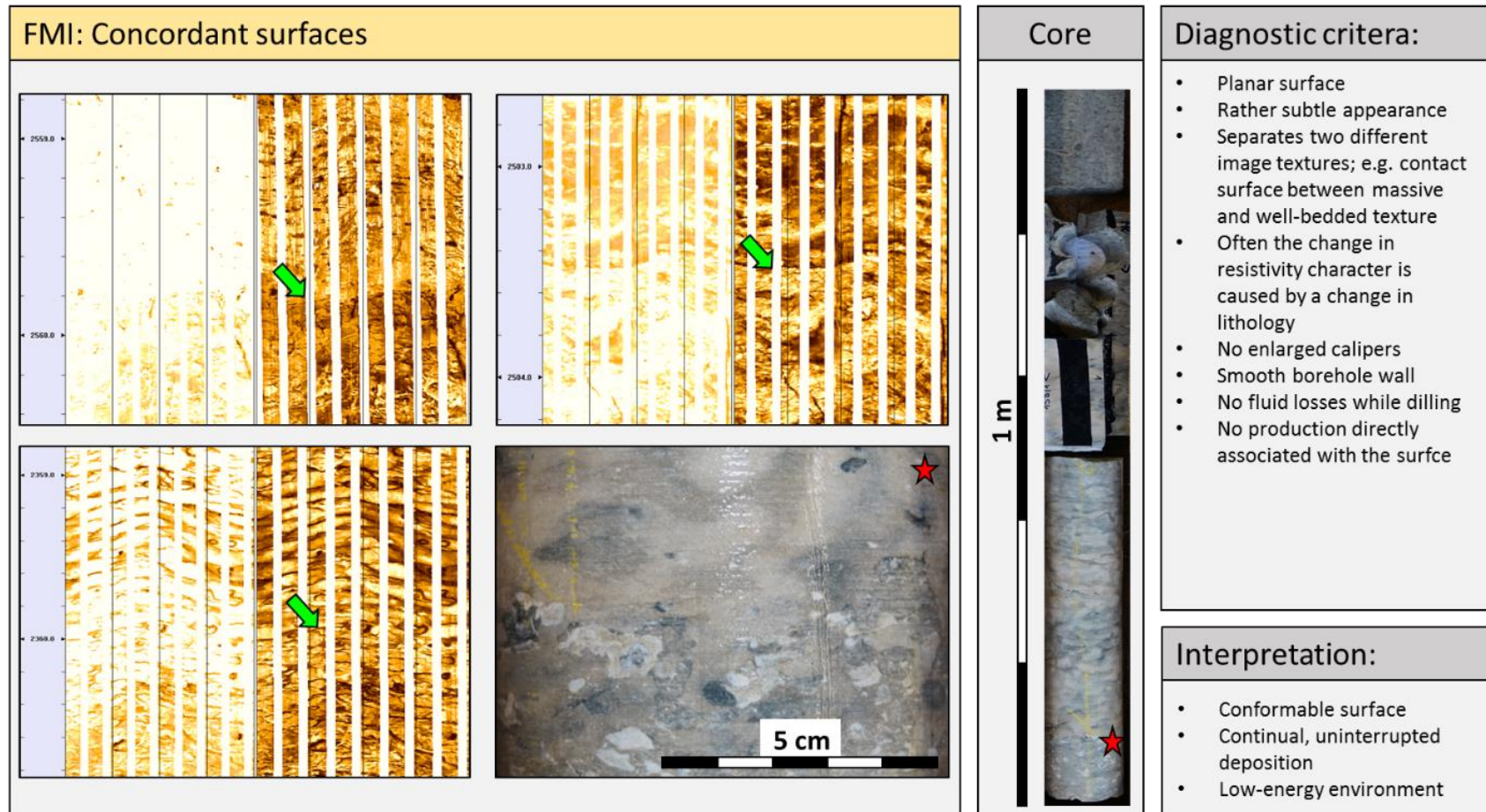


Figure 59: Stratal surfaces from image logs: Concordat surfaces

1D Analysis

The four types of stratal surfaces (Figure 57- Figure 60) are interpreted in terms of depositional energy. A simplified depositional model (Figure 61) shows the position of the stratal surfaces in relation to the sea-level and water energy.

- (1) Highly indented surfaces are interpreted as Karst (together with dynamic data) and represent the shallowest part of the depositional model (exposure).
- (2) Truncated surfaces are interpreted as erosive surfaces. They are associated with increased water energy in a relatively shallow, proximal setting.
- (3) Concordant surfaces represent normal, un-disrupted depositional conditions and are interpreted to form in a quiet, lower water energy setting.
- (4) Draping surfaces are interpreted as potential maximum flooding surfaces, associated with deposition in a distal, very low energy, deeper-water setting.

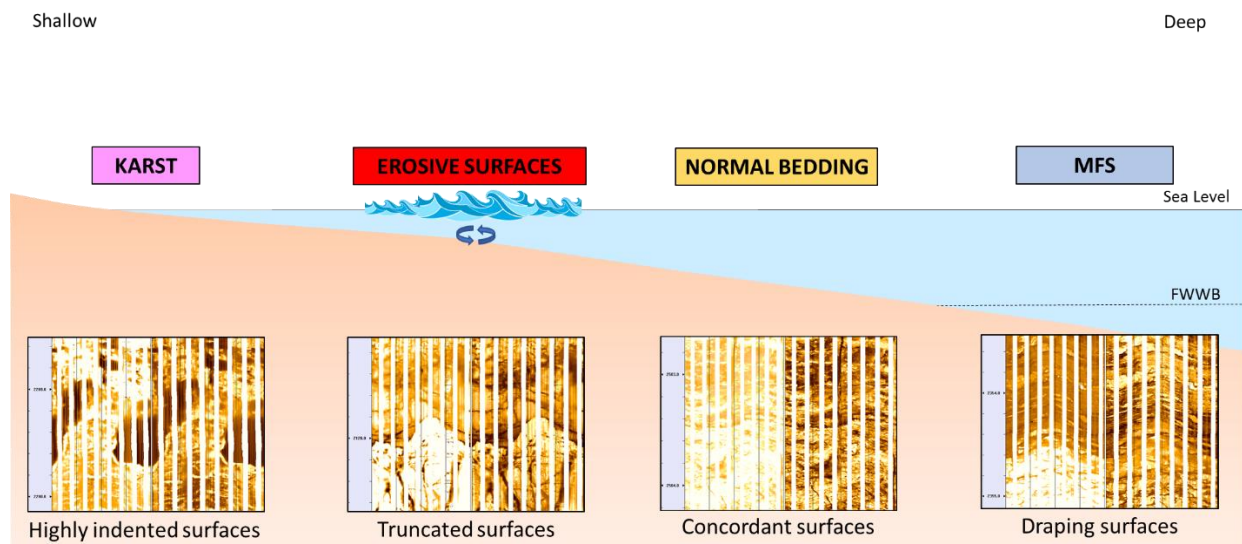


Figure 61: Statal surfaces as proximal-distal indicators

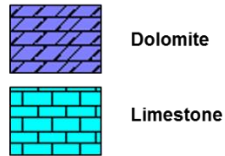
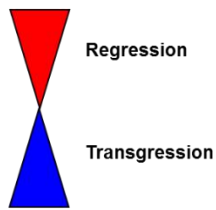
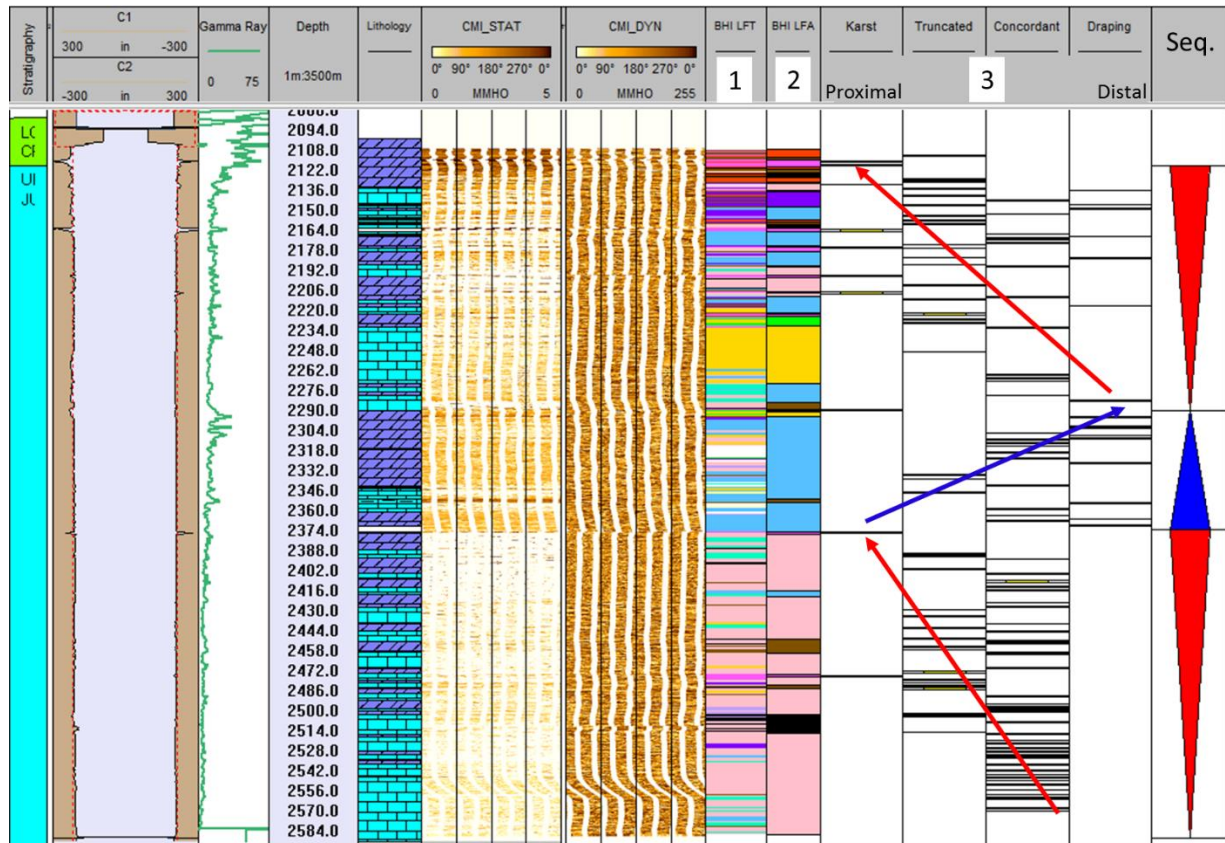
1D Analysis

These stratal surfaces can be identified very well on the borehole image log because they are often associated with a change of sedimentary texture, structures, mineral composition or lithology. All of those features represent a more or less pronounced change of resistivity, which can, therefore, be captured and visualized by the borehole image log. This allows the interpretation of stratal surfaces from borehole image logs to be independent of the borehole image facies interpretation. Stratal surfaces provide additional information of proximal-distal trends on multiple hierarchies and can be used to close the gap, where the resolution of the borehole image logs inhibits the classification of borehole image facies.

Charting of stratal surfaces

Figure 62 shows the BHI template used in the WellDAD software. The left borehole image is the static image and the right the dynamic image. Track 1 shows the lithofacies (chapter 3.2.1), and track 2 shows the facies association (chapter 3.2.2). Track 3 represents the stratal surface type. They are arranged in the same proximal-distal configuration, as shown in Figure 61. This allows recognizing depositional trends, similar to the vertical stacking of facies. This novel approach of charting stratal surfaces reveals several levels of cycle hierarchy that help to delineate genetically linked depositional units. This improves the borehole image facies interpretation in tight intervals, where it is challenging to assign the correct image facies. With the additional knowledge of the depositional trends and units, the ambiguous image facies can be interpreted with more confidence and in context with the overall trends.

1D Analysis



Code	Color	BHI Facies
1	Light Blue	Well-bedded mudstone
2	Purple	Bioturbation
3	Light Purple	Bioclast debris
4	Yellow	Debris
5	Pink	Sponge bioherm
6	Light Yellow	Olistolith
7	Green	Corals
8	Black	Vuggy macro-pores
9	Magenta	Karst

Figure 62: Multi-proxy BHI workflow to identify large scale sequences

3.4.3 Borehole-Image Cycles, Cycle-Sets, and Sequences

Sequences

As shown in chapter 3.3, three large scale sequences were identified for the Upper Jurassic in research well Moosburg SC4 and one for the Purbeck Fm. The sequence boundaries are characterized by truncated or karstified surfaces, a sudden change in mineral composition and lithology or a change of sedimentary structures. All of these features provide resistivity contrast that can be detected by the borehole image log as shown in Figure 63.

To recognize the three large scale sequences, it is important to distinguish the correct level of the cycle hierarchy. The quantitative charting of stratal surfaces is a vital part of this interpretation, additional to the classical interpretation of gamma-ray log patterns (Emery and Myers, 1996). The borehole image is used to investigate the gamma-ray log patterns, especially the top and base boundaries, and verify the interpretation. It is important to work on a very large scale first, to find the large scale depositional changes as shown in Figure 63, and then to zoom in more details with the borehole image log.

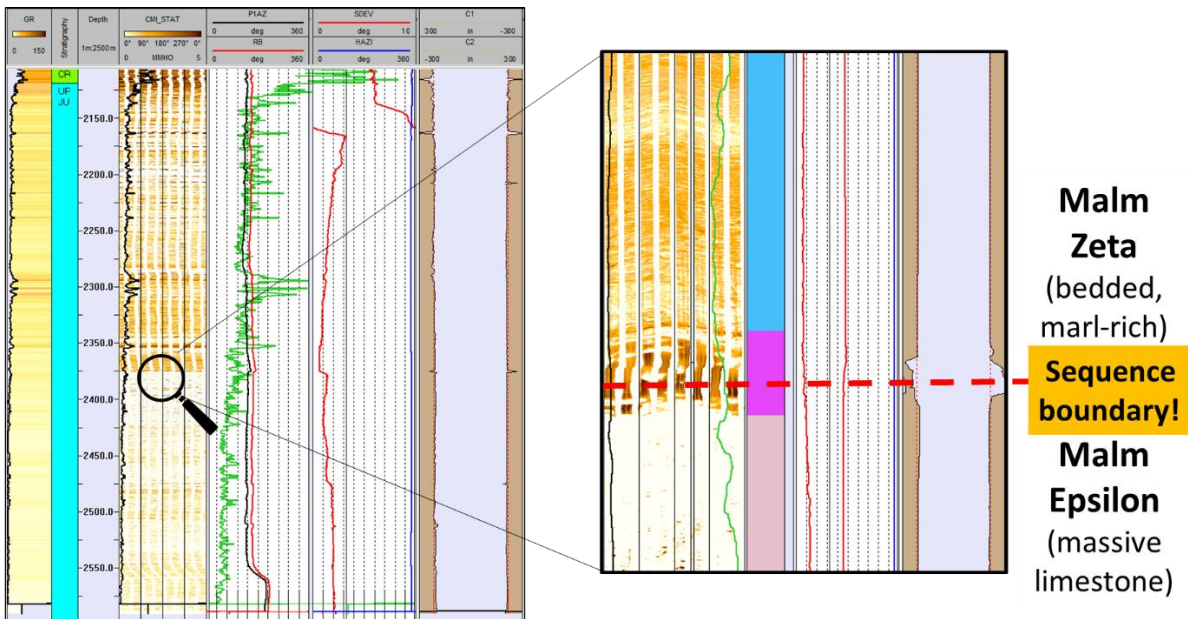


Figure 63: Sequence boundaries identified from borehole image logs.

Cycles and Cycle-Sets

The recognition of cycles and cycle sets for the Upper Jurassic carbonates in South Germany is challenging. The classical sequence stratigraphic approach (Pomar, 2001; Reid and Dorobek, 1993) can only partly be transferred in this relatively deep depositional environment (below fair-weather wave base) because it is hindered by the lack of diagnostic sedimentological criteria. However, (Pawellek and Aigner, 2003a, 2003b) showed that a sequence stratigraphic interpretation is still possible by focusing on “facies turnarounds” rather than discontinuity surfaces and by integrating palynofacies data (Pross et al., 2006b) and chemostratigraphy (Ruf et al., 2005a; Ruf et al., 2005b). This approach works very well with core data but is below the resolution of the borehole image tool. Additionally, dolomitization in the subsurface of the greater Munich area can inhibit the recognition of sedimentary texture and components. However, a high-frequency cyclicity is observed for the Purbeck Fm (Lesić, 2019) (Strasser, 1986; Strasser and Davaud, 1983), as shown in Figure 64, composed of small scale cycles with a thickness of approximately 1 m.

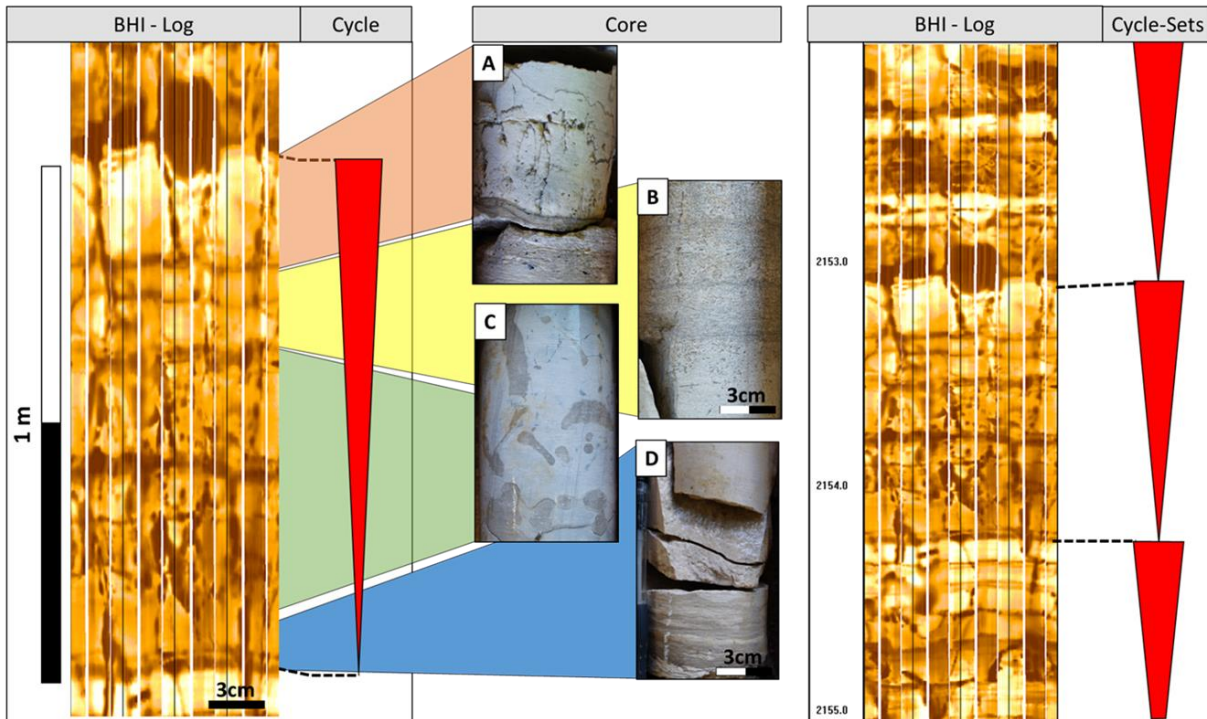


Figure 64: Cycles and cycle sets

1D Analysis

Figure 64 shows a cycle (left) observed on the borehole image logs compared to the core from Moosburgs SC 4.

Core description and BHI Interpretation (from bottom to top):

(D) **Core:** Laminated or massive texture, usually clay-rich, dark mudstones.

BHI: Dark lamination at the base followed by a massive texture.

(C) **Core:** Bioturbated wackestone with cm-thick burrows. The traces are often filled with coarse grained bioclastic packstones. Possibly *Thalassinoides* ichnofacies.

BHI: Mottled texture, individual dark spots and vertical traces are clearly visible. Occasionally branched burrow traces can be observed.

(B) **Core:** Cross-bedded oolitic-peloidal grainstones. High-energy facies, dm-thick beds.

BHI: Very bright, resistive beds. Bed thickness and resistivity increasing towards top. The cross-bedding is not visible on the BHI.

(A) **Core:** Abundant stylolites and irregular bedding planes. Frequent vertical cracks.

BHI: Non-planar bedding plan (top of bright, resistive unit) with three vertical fractures. These fractures are NOT drilling-induced as they occur in the compressive and tensile region. More likely associated with exposure and karstification. The large irregular shaped vugs are interpreted as karst. The interpretation of karst is supported through significant inflow from this zone.

This cycle type is interpreted as a shallowing upward sequence, in a relatively shallow depositional environment. Similar observations were made from (Lesić, 2019; Strasser, 1986). Several of these small-scale cycles compose a cycle set. As the borehole images from the geothermal wells in the subsurface of Munich cover only short sections (10s m) no other cycle motive has been observed.

3.4.4 Summary of BHI Interpretation

- Nine borehole image facies types can be identified unambiguously. The borehole image logs reveal much detail, including rock-forming components like sponges and corals, sedimentary structures and texture.
- However, tight interval and diagnostic features below resolution (e.g., rock color, microfossils) did not allow the recognition of all 22 lithofacies types with the borehole image log.
- As a completely novel approach, four types of stratal surfaces were classified and interpreted according to their depositional setting (proximal-distal). The interpretation of stratal surfaces is independent of the borehole image facies and allows, therefore, interpreting intervals, where recognition of image facies is not possible. The stratal surfaces are charted during borehole image interpretation, providing additional information to recognize large scale depositional trends.
- Basic interpretation of gamma-ray log patterns on a 1:1000 scale shows potential large scale depositional sequences. The borehole image log is then used to verify the first-pass interpretation and to “zoom-in” to investigate the sequence boundaries
- The vertical stacking of borehole image facies can be interpreted in terms of a transgressive and regressive sequence. Small scale cycles and cycle sets were only observed for the late HST of large-scale sequence 3 and the Purbeck Fm.

The above-mentioned observations show that borehole imaging, even in carbonates, has a much wider variety of applications than geomechanics and fracture/fault interpretation. The value of information of such logs can significantly be enhanced if the hierarchical multi-proxy workflow is applied. This illustrates that borehole image logs may provide a real treasure for subsurface sequence stratigraphy and for applied reservoir characterization.

3.5 Geothermal Reservoir Types

The most important geothermal reservoir types observed in core and borehole images are summarized in Figure 65 to Figure 71.

A) Karstification: This reservoir type is very important because it is often associated with high-flow rates. Karst zones from the study area are usually several dm-thick but can occasionally reach up to 1.8 m in thickness. To produce consistently high flow-rates, the Karst needs a large-scale lateral extent and connectivity with a prolific aquifer. These are also the main uncertainties associated with this reservoir type.

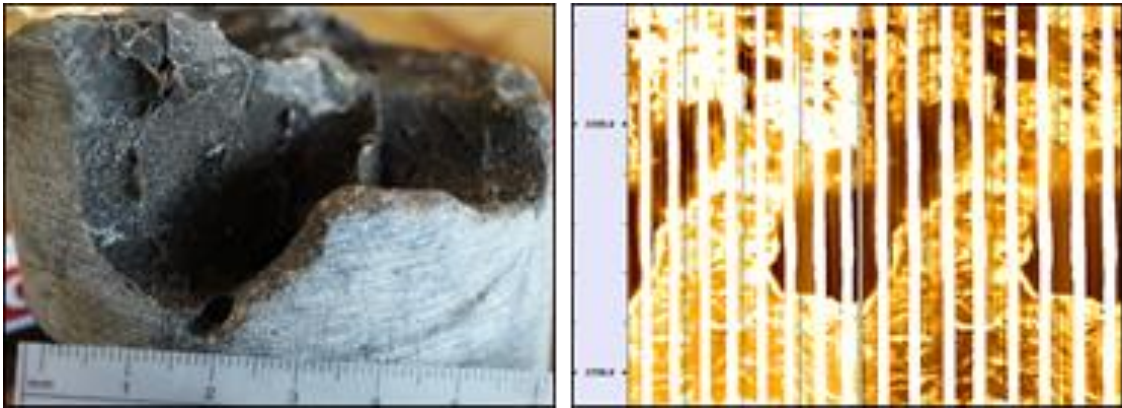


Figure 65: Reservoir Type: Karst

B) Vuggy porosity: Single vugs can reach several centimeters in size and are often very concentrated in specific zones. Observations from core showed that these vuggy zones are 1 m to 10 m thick and usually associated with dolomitization. If the vugs are separated, these zones have relatively high porosity, but almost no permeability. Only touching vugs can create high-K zones. The difference between separated and touching vuggy porosity is the main uncertainty with this reservoir type (Lucia, 2007).



Figure 66: Reservoir Type: Vuggy porosity

C) Dolomitization: Dolomitization plays a fundamental role to potentially improve matrix porosity and permeability for the Upper Jurassic in South Germany (Böhm et al., 2010). It is especially important to create large volumes of reservoir rock that have storage capacity for groundwater. Flow-rates from dolomitized intervals are relatively low (from a geothermal perspective) because they usually produce via matrix permeability. However, any other reservoir type (e.g. fractures, faults) must be connected to the dolomitized intervals, which has the main groundwater storage capacity.

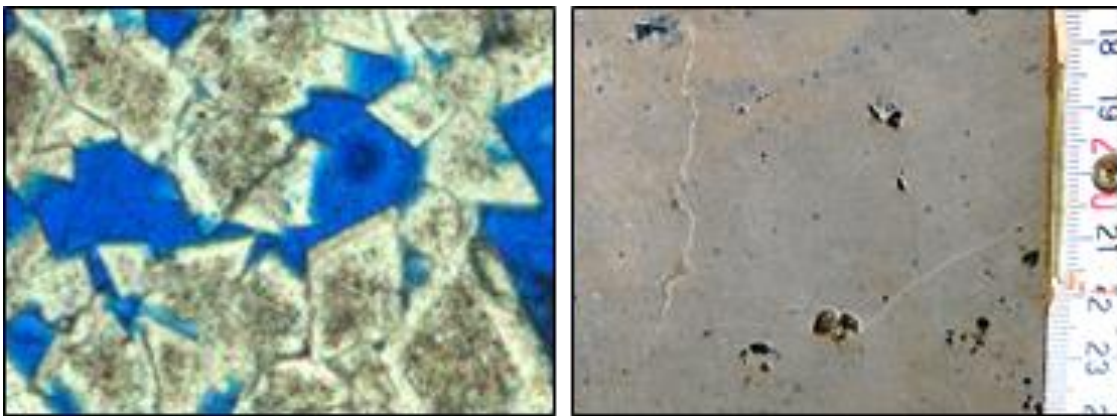


Figure 67: Reservoir Type: Dolomitization

D) Bioturbation: Towards the top of the Upper Jurassic intensively bioturbated intervals are present. These cm-thick *Thalassinoides* type burrows are filled with coarse-grained bioclast debris and usually dolomitized. This can enhance porosity and permeability and provide an important flow-zone.

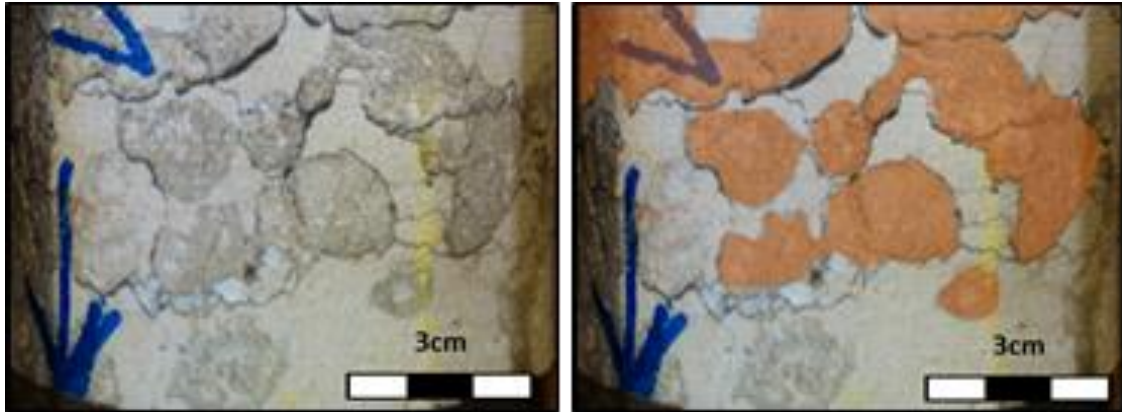


Figure 68: Reservoir Type: Bioturbation

E) Bioherm debris: The bioherm debris is composed of sponges, corals, shells, echinoderms, crinoids, peloids, ooids and lithoclasts, as shown by outcrop analog studies (Eigler, 2018). These wedge-shape reservoir types can extend several 100 m into the basins. They are component dominated and have a high diagenetic potential (dolomitization and/or leaching), especially if sandwiched between low permeable basin facies.

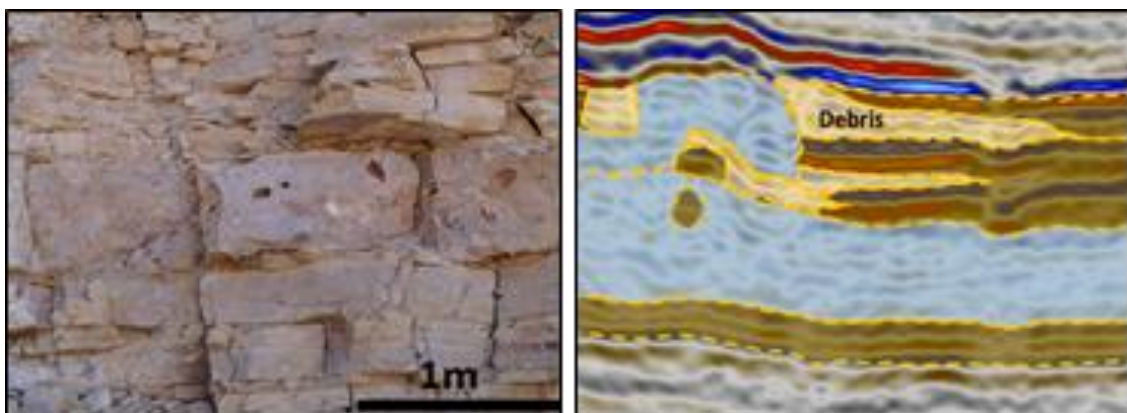


Figure 69: Reservoir Type: Bioherm debris

F) Fractures: Fractures are one of the most essential reservoir types because they can provide high flow-rates. They are more frequent in the bioherm facies, as these zones are more massive and geomechanically harder compared to the well-bedded, clay/marl-rich basin facies. However, to predict if the fractures are open, partly open or closed is a significant challenge and the main uncertainty.

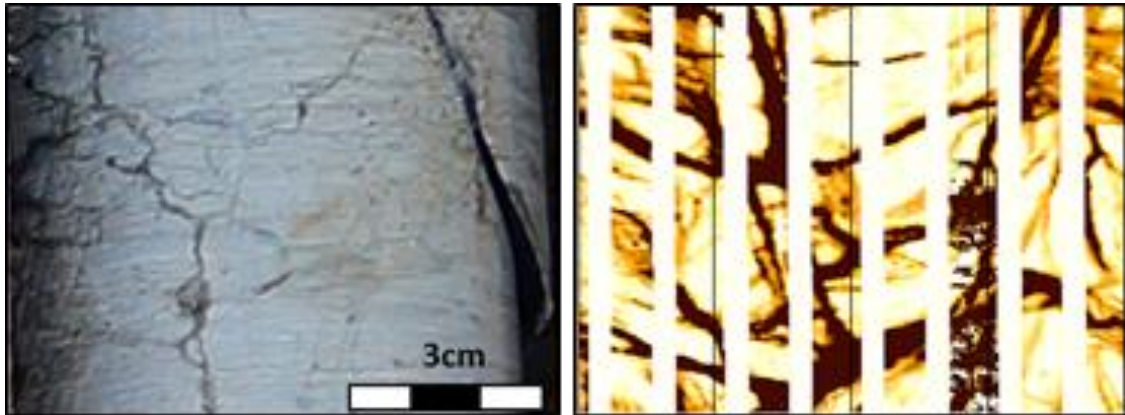


Figure 70: Reservoir Type: Fractures

G) Faults: In geothermal exploration, faults are often assumed to be high-K zones (Dussel et al., 2018), however similar to fractures, faults can be open, partly open or closed. If the fault is cutting through the well-bedded basin facies (marl/clay-rich), they are often severely affected by clay smear and, therefore, tight. Within the more massive bioherm facies, faults are more likely to be open, although calcite cementation needs to be considered as well. Another risk associated with faults is the reactivation potential. Induced seismicity can be a serious problem especially in urbanized areas (Seithel et al., 2018).

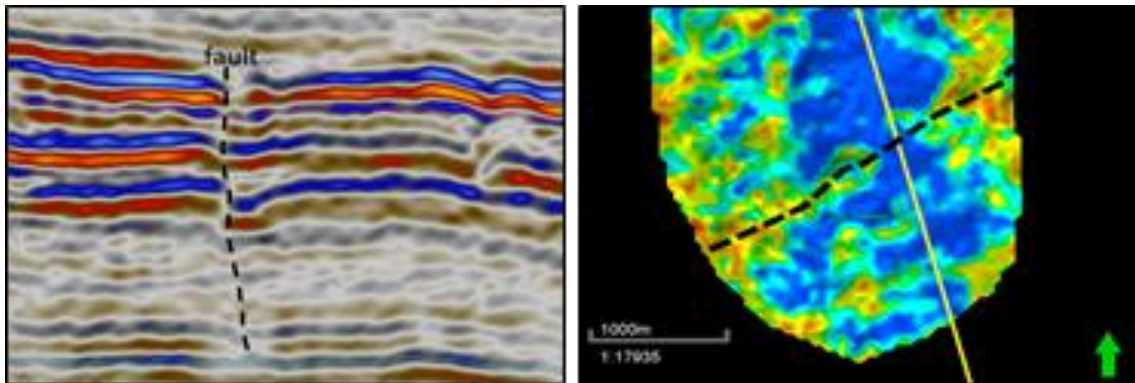


Figure 71: Reservoir Type: Faults

4. 2D ANALYSIS

4.1 Sequence Stratigraphic Well-Log Correlation

The aim of the sequence stratigraphic well-log correlation is to establish 2-D cross-sections that allow reconstructing the geometry and facies distribution of the original strata prior to compaction or tectonic deformation (Kearns and Tinker, 1997).

Because no core data is available from the geothermal wells in the study area, a sequence stratigraphic well-log correlation is established on a local (20 km), regional (70 km), and basin-wide scale (150 km), as shown in detail in section 4.1.1 to 4.1.3. The large scale sequences (S1-3) described in section 3.3.1 are chosen as the level of hierarchy for the well-log correlation because they can be interpreted consistently with the existing database (gamma-ray and borehole image logs). This approach allows establishing a sequence stratigraphic framework and transferring observations from the research well Moosburg SC4 and outcrop analogs into the subsurface of the Molasse Basin.

Datum selection

The selection of the datum is a fundamental part of the well-log correlation and an iterative process. Usually, any stratigraphic marker bed that was deposited more or less “flat” can be used as a potential datum for the first-pass interpretation (Kearns and Tinker, 1997).

For the Upper Jurassic of South Germany three datums were identified:

(1) Top Malm Sequence Boundary:

This sequence boundary (see chapter 3.3) can be recognized very well with the gamma-ray log. The Upper Jurassic carbonates usually have low gamma-ray values and consist of a blocky, funnel or bell-shaped gamma-ray patterns at a 1:1000 scale. The Top Malm sequence boundary shows abrupt and pronounced high gamma-ray peaks (>60 API), followed by consistently higher gamma-ray values and a serrated log (Emery and Myers, 1996). This sequence boundary is chosen as a datum for the correlations shown in Figure 72 to Figure 74

2D Analysis

(2) Maximum Flooding Zone Sequence 3:

The bioturbation sets in gradually and is constantly increasing. Very intensive bioturbation, destratification, and dolomitization characterize the maximum flooding zone from large scale sequence 3 (observed at research well Moosburg SC 4). This trend is followed by decreasing bioturbation until the strata are un-disrupted again. The core to log calibration shows that the gamma-ray reflects this trend very well, which results in a bell and funnel-shaped log-pattern (Emery and Myers, 1996) (see chapter 3.3.2). In several geothermal wells, the interpretation of borehole image logs could verify this interpretation (Wolpert et al., 2019).

(3) Malm Gamma

Two prominent marker horizons are present in the Malm Gamma interval, which are the *Platynota* and *Crusoliensis* marls (Schick, 2004). The fossil content (e.g., type of ammonites) can not be recognized in the subsurface using well logs, but the marly horizons as such are well visible on the gamma-ray log. Core-to log calibration from research well Moosburg SC 4 confirms that these marly layers represent a very pronounced gamma-ray peak.

Cross-section orientation

The cross-sections are oriented parallel (strike-section) and perpendicular (dip-section) to the slope of the shelf/coast. A first-pass orientation is based on paleogeographic maps shown in section 1.3 (Meyer and Schmidt-Kaler, 1989). Multiple correlation phases were implemented between strike and dip-sections to assure consistency, as shown by (Arlat, 2020). Figure 72 to Figure 76 show the results of the correlation and are discussed in detail in the following sections 4.1.1 to 4.1.3.

4.1.1 Correlation panel: Local-scale

Observation

The local correlation panel is composed of the wells Altdorf Th2, Moosburg SC, and Erding 1 and oriented approximately NE-SW, which represents the dip section (Figure 72). The correlation is based on the gamma-ray log. The datum for the correlation is the Top Upper Jurassic sequence boundary. Large scale sequences (S1-S3) are interpreted and

2D Analysis

calibrated to the gamma-ray log from well Moosburg SC4, and can be identified in well Altdorf Th2 and Erding 1. An increase in thickness can be observed from the NE to the SW due to the Landshut-Neuöttinger High. Well Altdorf is located on this paleo-high, which results in less accommodation space (355 m). Well Moosburg is on the edge of the Landshut-Neuöttinger high (Meyer, 1994a) and shows, therefore, a greater thickness (430 m). The well Erding 1 is situated 19 km further to the SW and away from the paleo-high. Therefore, more accommodation space was available and the Upper Jurassic succession has a total thickness of 485 m, 55 m more compared to Moosburg SC4 and 130 m compared with Altdorf Th2.

Interpretation

A comparison of the individual sequences (S 1-3) shows that depositional sequences 1 and 2 have almost the same thickness, regardless of the paleo-high in the NE. The largest increase in thickness is observed in depositional sequence 3. A possible explanation could be syn-depositional tectonics, which means that the uplift of the Landshut-Neuöttinger begun already around the sequence boundary S2 – S3. Supporting evidence for this interpretation is the 30 m thick debris breccia at this sequence boundary in well Moosburg SC4, interpreted as slump/slide event caused by slope instability. This sequence boundary corresponds approximately to the Malm epsilon – zeta boundary (Quenstedt, 1858). Outcrop analog studies from the Swabian Alb (Bold, 2010) document an abrupt onset of lithified bioherm debris (olistoliths) at this boundary.

Furthermore, the maximum flooding zone of sequence S3 is very well developed in well Erding 1 and Moosburg SC4, but less pronounced in well Altdorf Th2. This might indicate uplift of the Landshut-Neuöttinger high resulting in a shallowed depositional environment for well Altdorf Th2.

2D Analysis

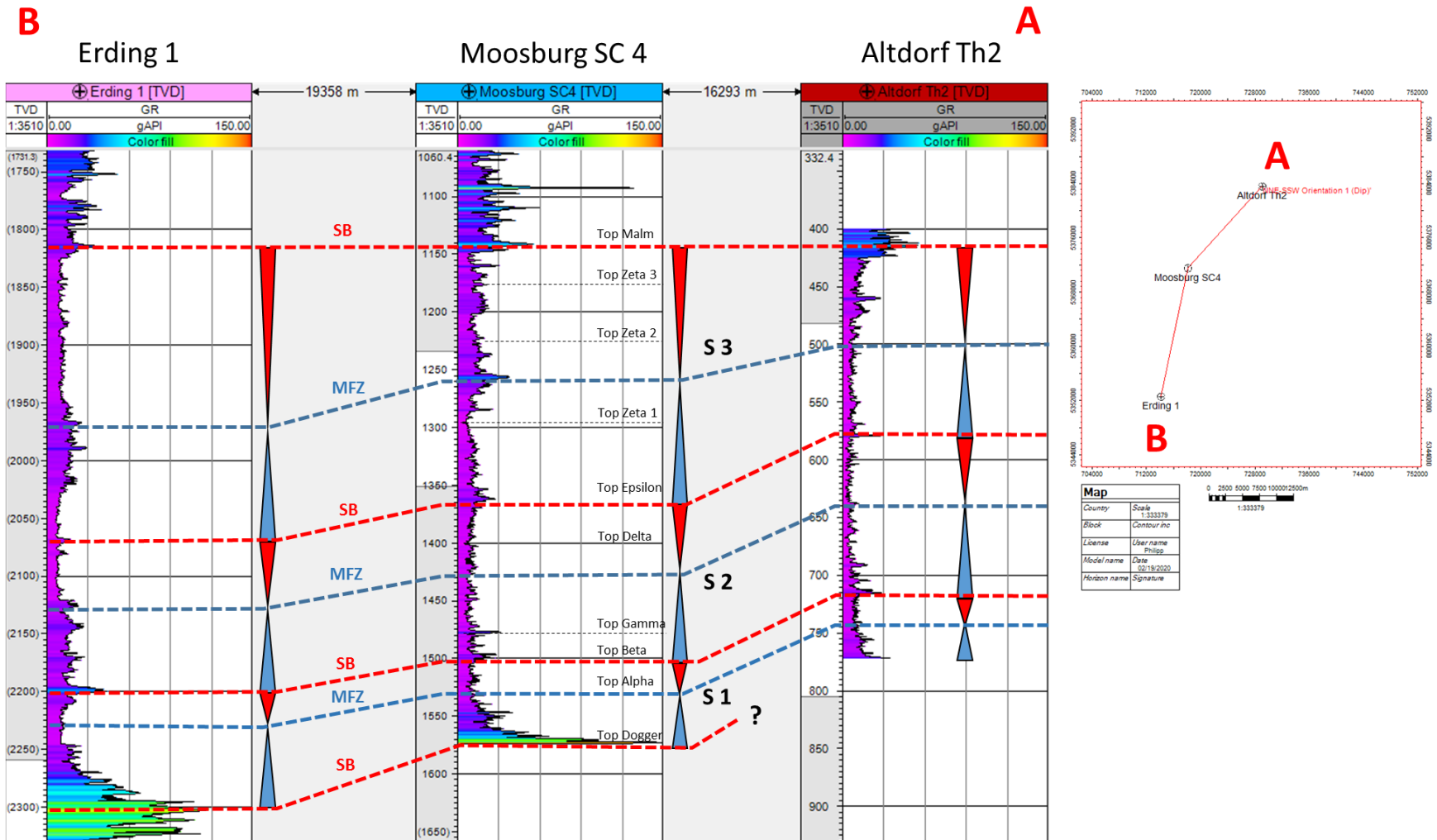


Figure 72: Local correlation in approx. dip orientation.

2D Analysis

4.1.2 Correlation panel: Regional-scale

The correlation on a regional scale aims to further establish the sequence stratigraphic framework and to transfer the observations of the reference well Moosburg SC4 into the subsurface of the greater Munich area. Figure 73 shows the location of the wells Altdorf GWM, Altdorf Th2, Moosburg SC4, Erding 1, Aschheim Th1 and Unterhaching Gt2a. A paleogeographic and basic structural context is shown in Figure 74, which is the transition from the Landshut-Neuöttinger high into the bioherm/reef platform. The correlation panel is an extension of the correlation on a local scale (Figure 72), and represents the dip section oriented approximately NE-SW. The datum for the correlation is the top Malm sequence boundary.

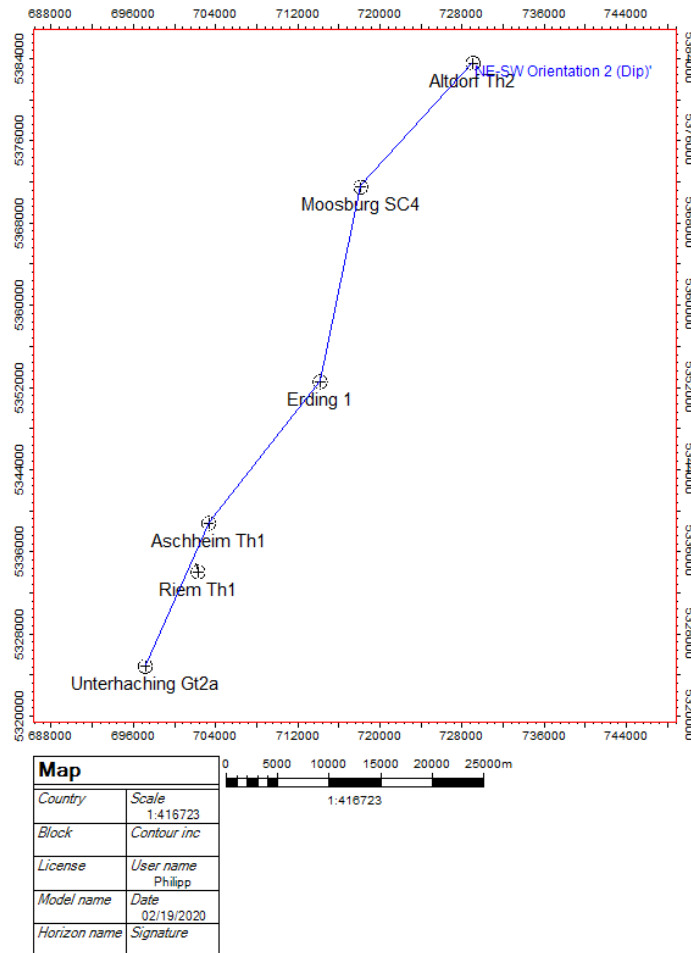


Figure 73: Orientation of dip section on a regional correlation scale.

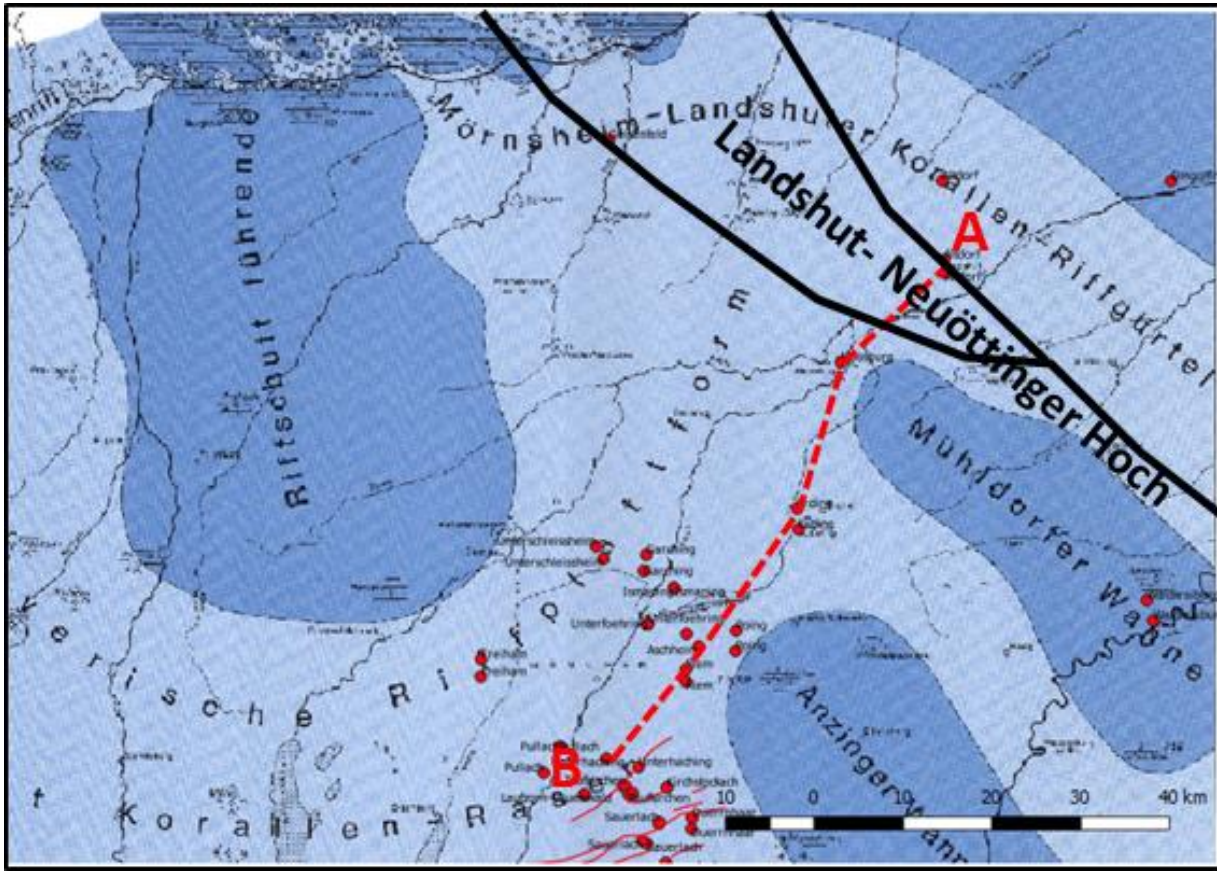


Figure 74: Orientation of dip section with paleogeography and structural elements.

Observation

Similar to the correlation panel on the local scale, the increase in thickness is observed as well for the wells Aschheim Th1 and Unterhaching Gt2a. Because both wells are geothermal wells, they did not penetrate the complete Upper Jurassic succession. Therefore the increase of thickness is mainly observed for depositional sequence S3.

Interpretation

The increase of thickness is interpreted again as an increase in available accommodation space (Schlager, 1993), from the Landshut-Neuöttinger high into the center of the bioherm/reef platform. The maximum flooding zone is not well developed in wells Unterhaching Gt2a and Aschheim Th1, which is rather an effect of the well placement. Both geothermal wells target biohermal buildups/reefs where the maximum flooding zone is only poorly developed. The wells Erding 1 and Moosburg SC4 are research or wildcat

2D Analysis

wells that also recovered sections between the biohermal buildups (intra-basins) with intensive bioturbation. However, the correlation on a regional scale confirms and extends the interpretation of the local scale, which shows increasing accommodation space and thickness towards the SW.

2D Analysis

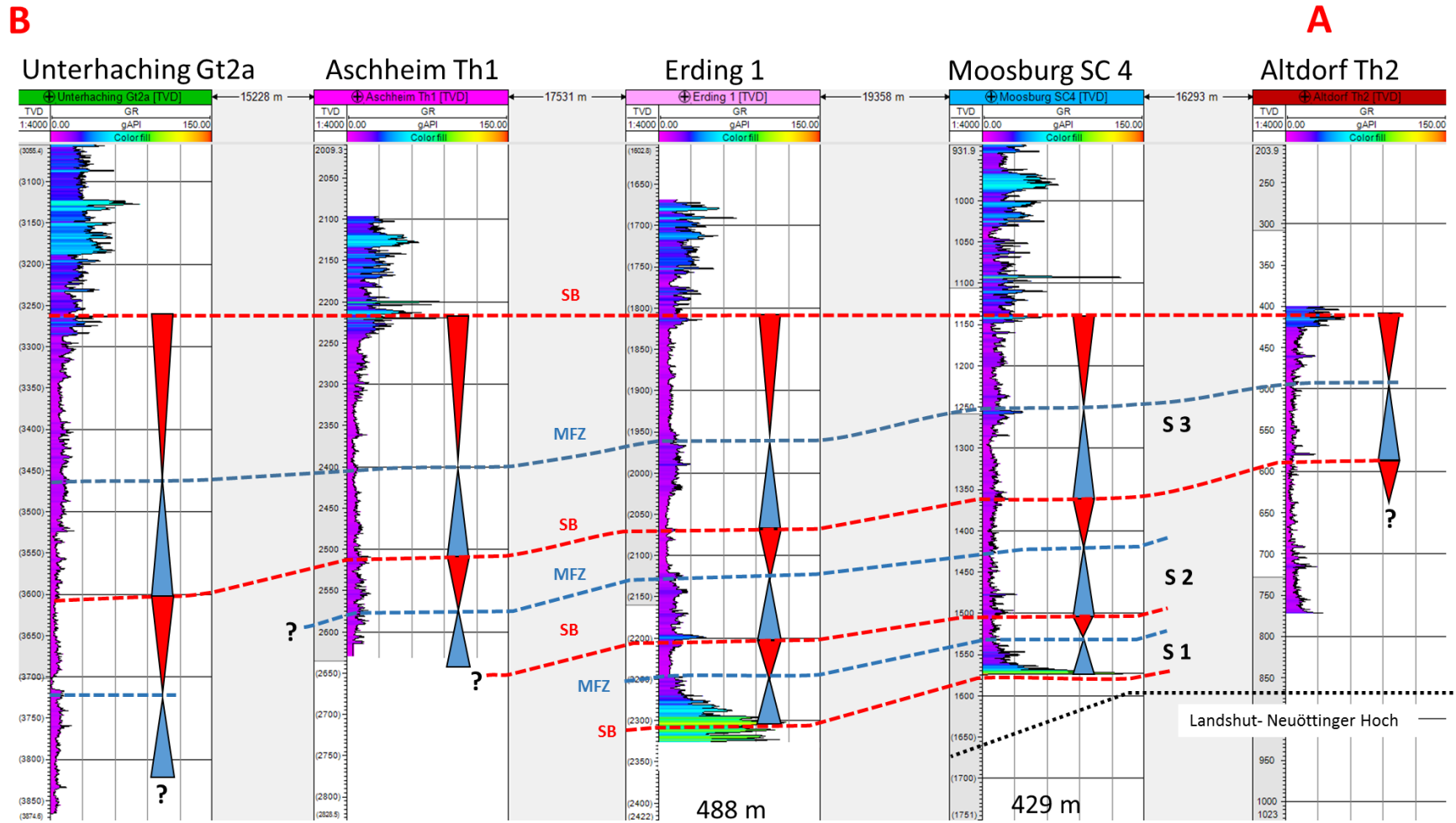


Figure 75: Regional correlation in approx. dip orientation.

4.1.3 Correlation panel: Basin-scale

The purpose of basin-wide correlation is a better understanding of the depositional system and of general geological trends. The basin-wide correlation panel extends well beyond the focus of the study area (greater Munich area). But to differentiate between allochthonous and autochthonous signals on a regional-scale, it is fundamental to consider the interpretations in context with the basin-wide development of the Upper Jurassic. For that purpose, Arlat (2020) increased the database by integrating well logs and core from numerous hydrocarbon and research wells to improve the over-regional understanding of the depositional development. Figure 76 shows the basin-wide, sequence stratigraphic correlation oriented NNE-SSW (approximate dip section). The distance between A and B is 150 km, and the datum is the Top Malm sequence boundary.

Observations

Similar to the correlation on a local- and regional-scale, an increase of thickness is observed from the NNE to the SSW. The constant and maximum thickness of approximately 620 m of Upper Jurassic strata is found in wells Grambach, Unterbrunn, and Heberthausen. The depositional sequences (S 1-3) can be identified very well on the gamma-ray logs from wells Gundelshausen, Geisenfeld, and Hebertshause. However, the identification of sequence boundary S2-S3 in wells Grambach and Unterbunn is not possible with the gamma-ray logs. Those wells also show an overall very flat, and homogeneous gamma-ray log pattern compared to the other wells.

Interpretation

A proximal-distal trend associated with increasing accommodation space is interpreted for the increasing thickness from the basin-wide correlation. The depositional setting of wells Grambach and Unterbrunn is interpreted as a distal, basinal setting. Especially well Grambach shows a very homogeneous gamma-ray pattern, which might represent the well-bedded mudstone facies. The wells Hebertshausen, Geisenfeld, and Gundelshausen show funnel, bell, and serrated shaped gamma-ray log patterns, interpreted as gradual or abrupt lithofacies changes due to a more dynamic, shallower depositional setting.

2D Analysis

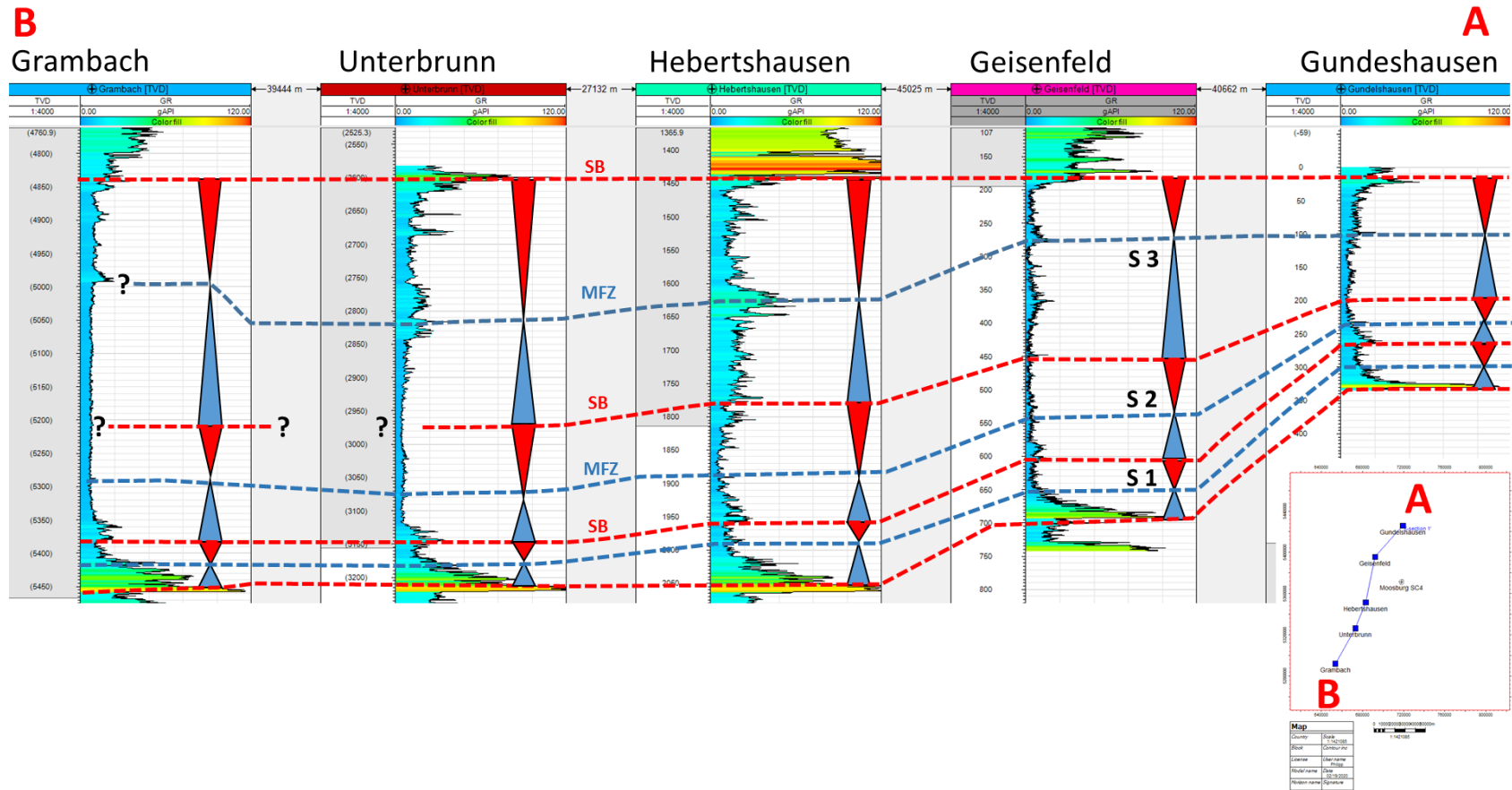


Figure 76: Basin-wide correlation in approx. dip orientation (A=proxima, B=distal)..

Conclusions: 2 D correlations on a local, regional and basin-wide scale provide basic insights such as:

- (1) Sequences, as recorded in research well Moosburg SC4, can be transferred to well log data and identified in the subsurface.
- (2) Basic paleogeographic proximal-distal trends and paleo-structural units can be recognized

5. 3D ANALYSIS

5.1 Seismic Interpretation

The chapter presents an integrated workflow of 3D seismic attribute analysis to analyze the distribution and quantification of reservoir facies (massive limestone) versus non-reservoir facies (bedded marly limestone) per time slice. Based on the vertical resolution of the Freiham 3D seismic cube, 9-time slices are used for attribute mapping using the “sum of magnitude” method. The seismic interpretation is calibrated with the two geothermal wells available within the cube: seismic facies interpretation is integrated with borehole image facies and cross-checked with cuttings. Additional observations from outcrop analogs further aid seismic interpretation and the reconstruction of the depositional development of the Upper Jurassic carbonates. Previous interpretations of seismic datasets for geothermal exploration in the Molasse basin were largely based on reprocessed 2D seismic lines from the hydrocarbon industry (Rüdiger and Schulz, 2007).

5.1.1 Reflector Termination Mapping and Seismic Facies Analysis

The first step of the workflow follows the standard seismo-stratigraphic interpretation procedure (Mitchum and Vail, 1977) and consists of: (a) seismic facies analysis and (b) reflector terminations mapping as shown in Figure 77. Three distinct seismic facies types are frequently observed in this study: (1) Parallel high amplitude (PHA), (2) chaotic (CAR), and (3) subparallel low amplitude (SR). Common reflector terminations are onlaps and downlaps.

3D Analysis

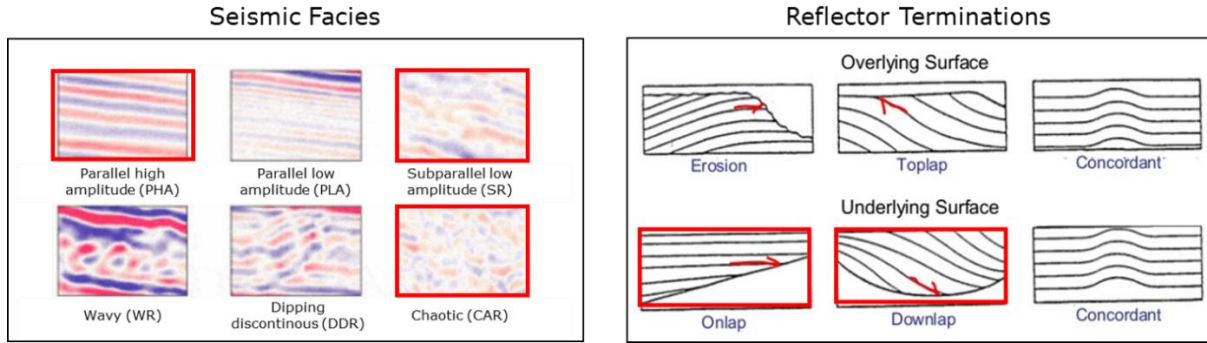


Figure 77: Seismic facies and reflector termination classification after Mitchum and Vail (1977). Marked in red are the most frequently occurring features of this study.

Figure 78 shows an example of an uninterpreted and interpreted seismic line. The parallel high amplitude seismic facies is interpreted as basin facies (well-bedded limestones) and the chaotic seismic facies as bioherm/reef. The basin facies shows onlaps with the bioherm/reef. The subparallel low amplitude (SR) seismic facies, together with wedge shape geometries, are possible bioherm/reef debris aprons. Sequence stratigraphic analysis reveals three large scale sequences (S1-S3) (Wolpert et al., 2019) Borehole image facies interpretation confirms S3 and the regressive hemi-sequence of S2. Seismic facies, reflector termination mapping, and sequence stratigraphic interpretation, reflect the large-scale depositional architecture of the Upper Jurassic (Gwinner, 1976; Geyer and Gwinner, 1979; Meyer, 1994; Meyer and Schmidt-Kaler, 1990, Böhm, 2011).

3D Analysis

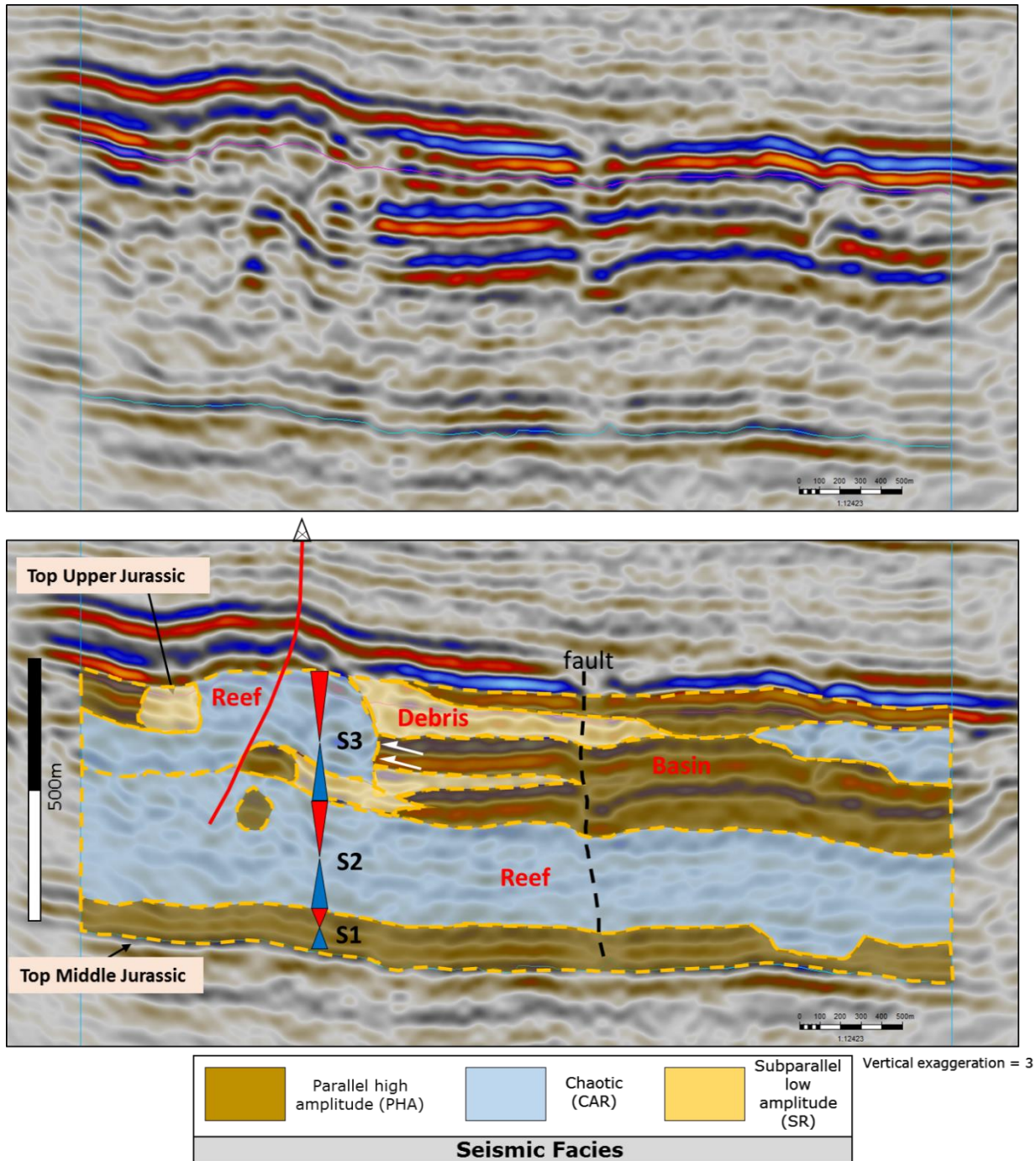


Figure 78: Seismic line showing the uninterpreted and interpreted section. Seismic facies analysis and reflector terminations show basin, reef/bioherm, and reef/bioherm debris as well as three large scale depositional sequences (S1-S3) and a fault.

5.1.2 Pseudo stratigraphic layering

A quick and elegant way to subdivide the area of interest in a 3D seismic cube is a pseudo stratigraphic layering approach (Bendias, 2017). Figure 79 A shows Top Upper Jurassic and Top Middle Jurassic, which are two interpreted seismic surfaces. The surfaces between Top Upper Jurassic and Top Middle Jurassic are calculated based on the thickness map and constrained by seismic resolution (Figure 79 B). The zone between the pseudo stratigraphic layers should resolve one peak and trough (positive and negative amplitude) of the wave.

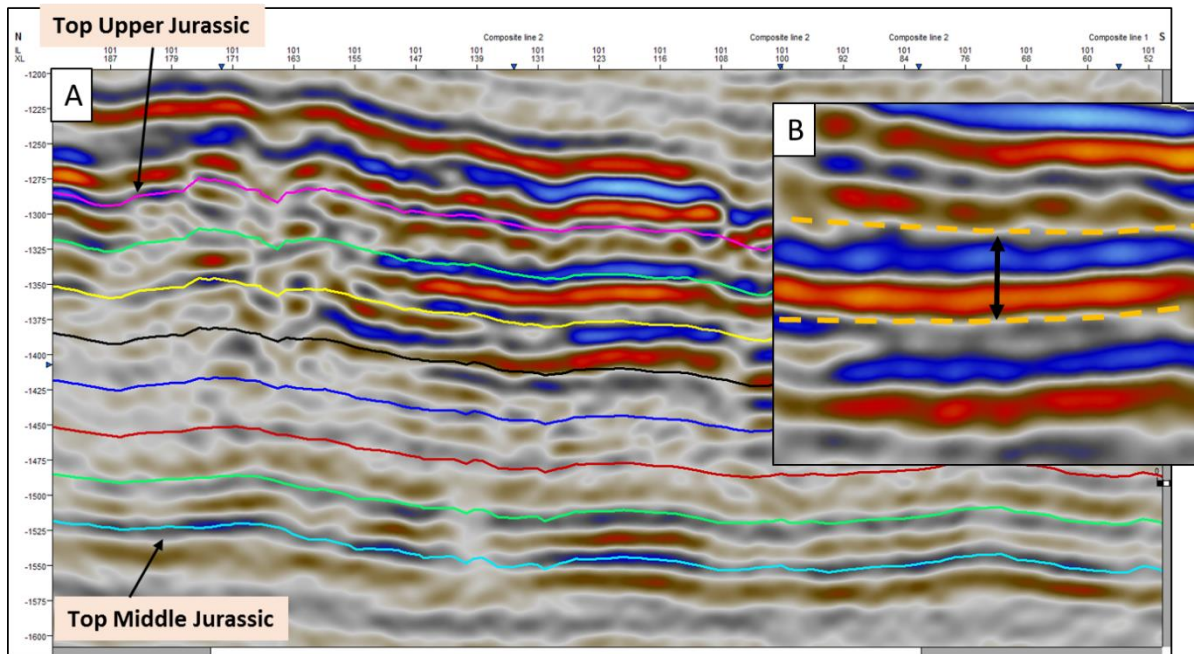


Figure 79: Pseudo-stratigraphic layering scheme. Top Upper Jurassic and Top Middle Jurassic are interpreted surfaces, whereas the layers in between are calculated based on the thickness map and seismic resolution.

5.1.3 Seismic attribute mapping per zone

Seismic attributes are specific measurements derived from the seismic data, sensitive to wave kinematics/dynamics or reservoir features. Attributes can be, e.g., amplitude, waveshape, frequency, energy, attenuation, and many more. Some attributes are better suitable to highlight certain reservoir properties (e.g., hydrocarbon indicators, subsurface anomalies, etc.) (e.g., (Brown, 1996; Chen and Sidney, 1997; Pearson and Hart, 2004). Results from the seismic facies analysis showed that the strength of the reflectors correlates very well with the seismic facies. The chaotic seismic facies has a weak reflectivity, while the parallel high amplitude facies shows a strong reflectivity. Therefore a seismic attribute that describes the strength of the amplitudes is required. The “sum of magnitude” attribute is an indicator of the reflectivity, no matter if the values are positive or negative (peak or trough). If the “sum of magnitude” attribute yields high values, a high reflectivity is present. The high reflectivity corresponds to the parallel high amplitude seismic facies, which is interpreted as basin facies. Vice versa, the low values correspond to a low reflectivity and represent the chaotic seismic facies, interpreted as reef/bioherm, which equals the potential geothermal reservoir facies.

Seismic attributes were mapped per zone, as defined by the pseudo-stratigraphic layering. Figure 80 shows the result of the “sum of magnitude” attribute for zone 1. The purple colors are areas of high reflectivity, red and yellow represents low reflectivity. The first impression of the attribute maps is very promising, as general trends and geometries can be recognized. However, the link between the values of the attribute map and the actual seismic facies still has to be established.

3D Analysis

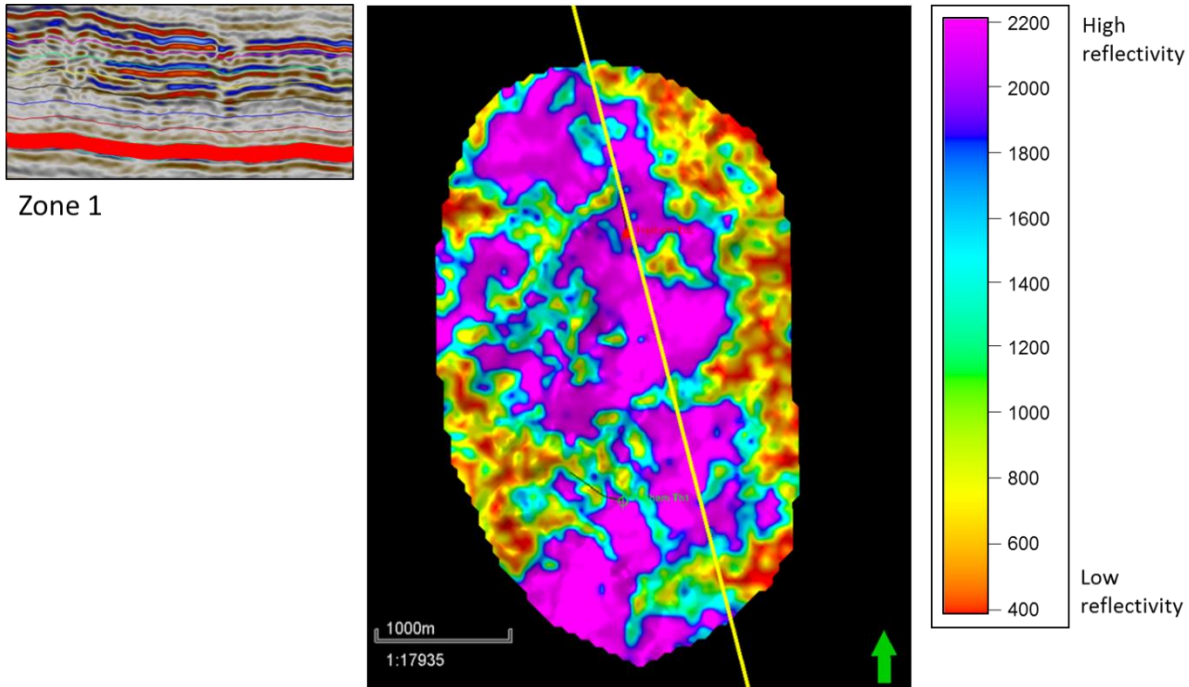


Figure 80: Seismic attribute mapping per zone. The example shows the first results for zone 1, with high reflectivity in purple and low reflectivity in yellow/red colors.

5.1.4 Cut-off definition

Defining the threshold is a critical step to convert the attribute maps into a meaningful geological tool. Hence, the cut-off definition is fundamental to differentiate between the parallel high amplitude seismic facies and the chaotic seismic facies (basin vs. bioherm/reef). The best practice is working with a split-screen mode and enable “cursor tracking mode” in Petrel (Figure 81, A and B, orange cursor). The attribute map is now compared with the seismic line. Critical features like onlaps of the parallel high amplitude facies (basin) with the chaotic seismic facies (bioherm/reef) are used to define the cut-off. Figure 9 C shows the histogram of the “sum of magnitude map” for zone 1, with the defined cut-off between bioherm/reef and basin. For this zone, every “sum of magnitude” value > 900 corresponds to the high amplitude seismic facies (basin), and ever value less 900 corresponds to the chaotic seismic facies (reef/bioherm). This process needs to be repeated for various inlines and crosslines, and then for every zone to adjust the cut-offs accordingly.

3D Analysis

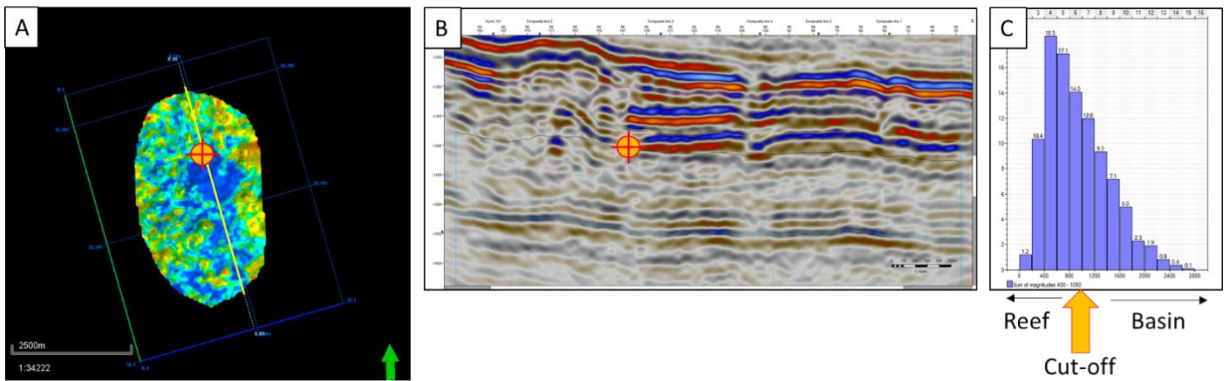


Figure 81: Cut-off definition via cursor-tracking mode. (A) Adjusted attribute map compared simultaneously with the seismic line (B) to define the threshold for basin and reef/bioherm (C).

5.1.5 Quantification of reservoir facies vs. non-reservoir facies

The following (Figure 82 - Figure 90) shows the results of the adjusted “sum of magnitude” attribute maps from bottom to top and per zone. The histogram allows quantifying the parallel high amplitude seismic facies (basin) and the chaotic seismic facies (bioherm/reef), hence provides a proxy of reservoir vs. non-reservoir distribution per zone. This approach is, however, limited to areas that are not intensively faulted because the area around the fault zones appears as chaotic seismic facies, similar to the bioherms zones (potential reservoir facies).

3D Analysis

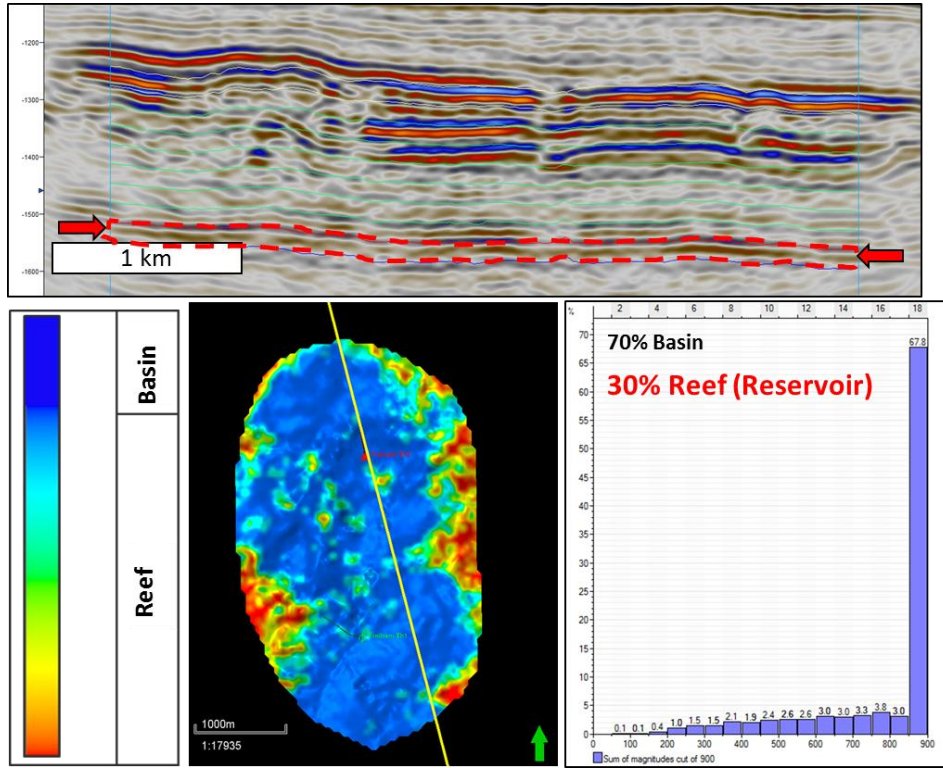


Figure 82: Sum of magnitude map for zone 1

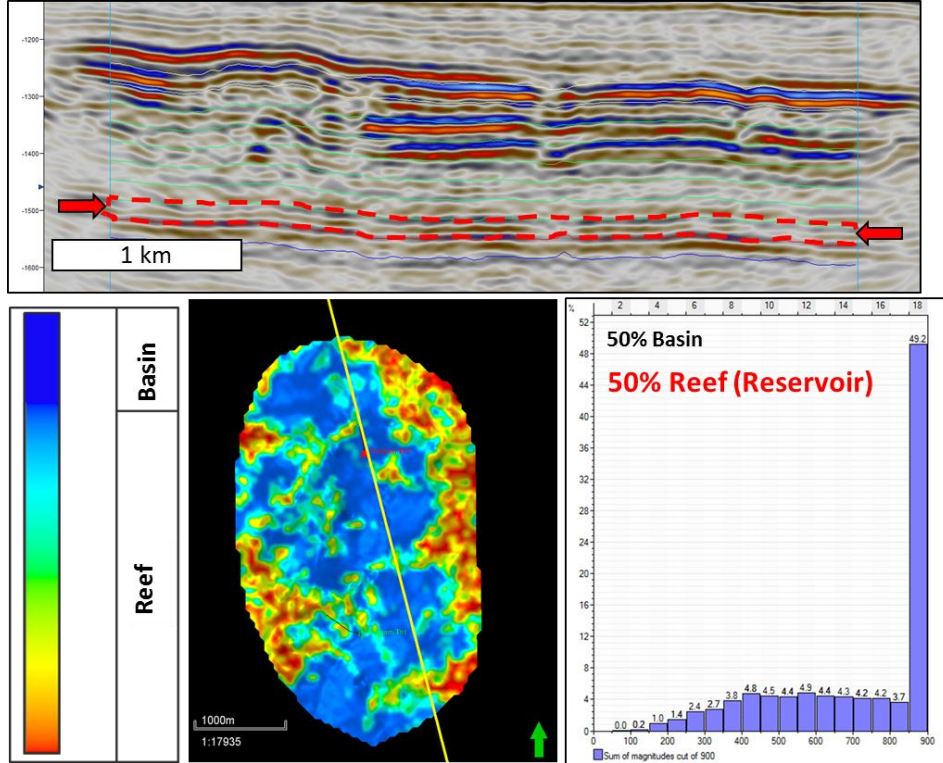


Figure 83: Sum of magnitude map for zone 2

3D Analysis

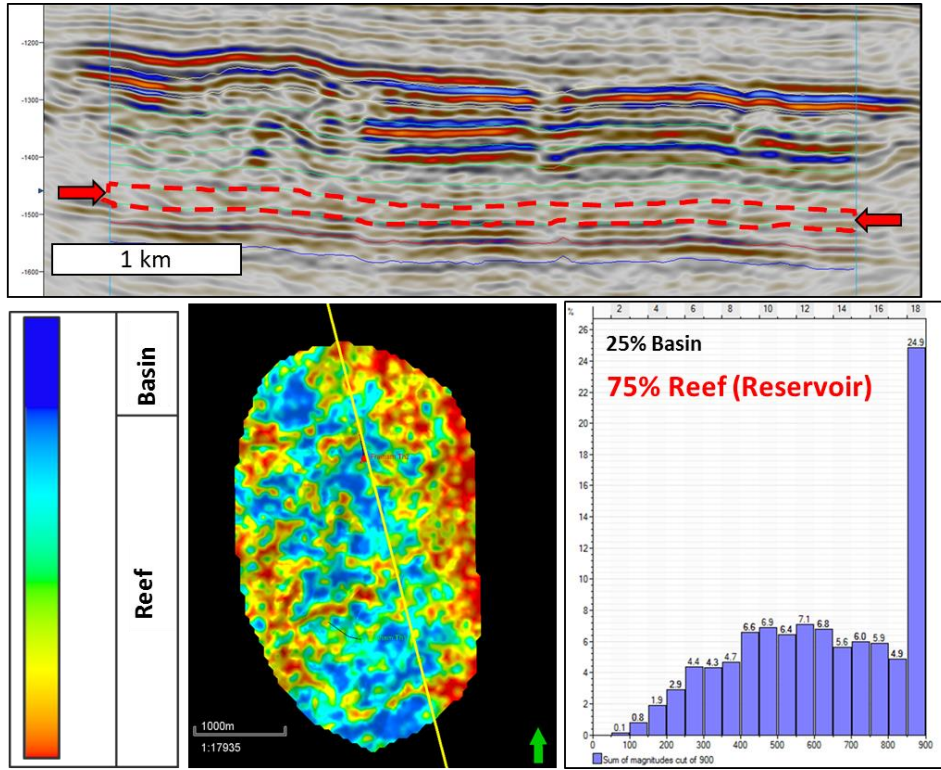


Figure 84: Sum of magnitude map for zone 3

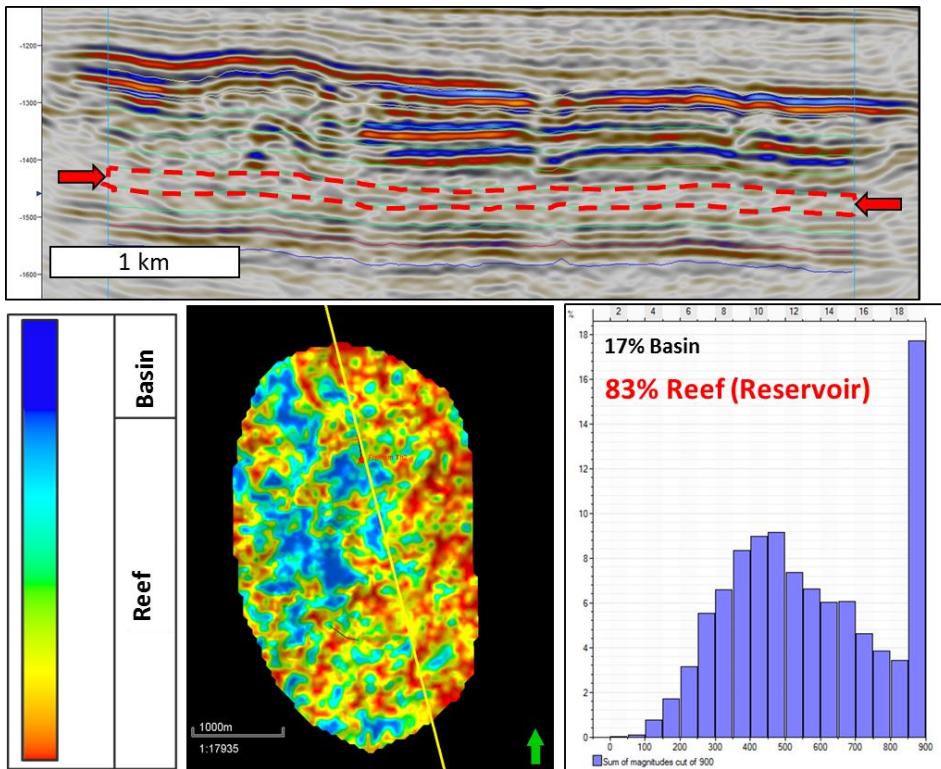


Figure 85: Sum of magnitude map for zone 3

3D Analysis

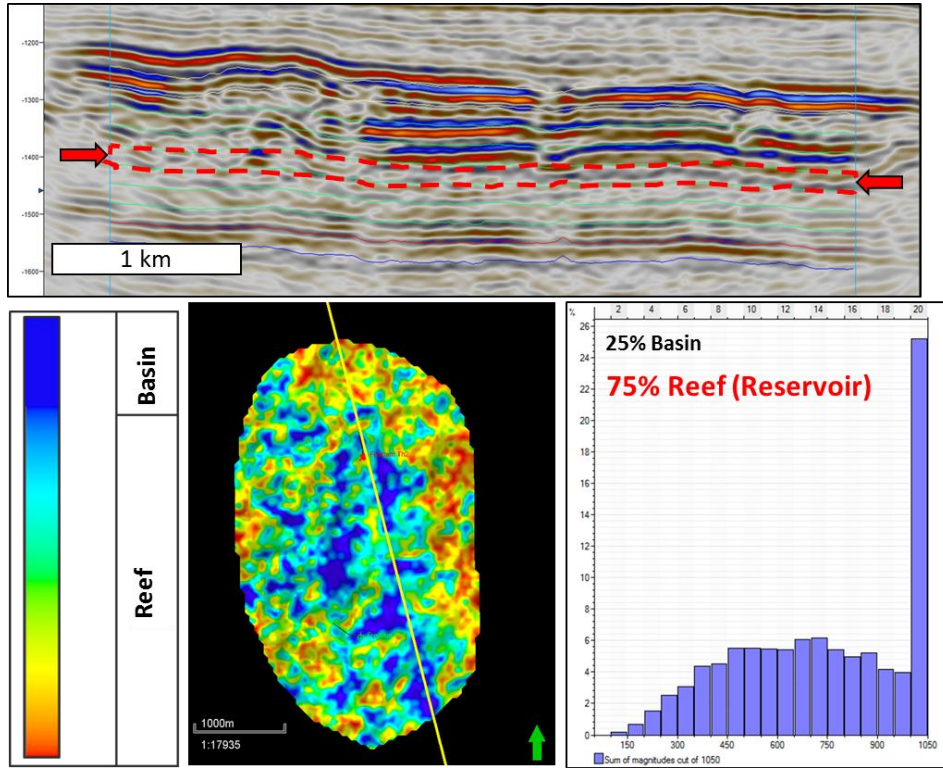


Figure 86: Sum of magnitude map for zone 4

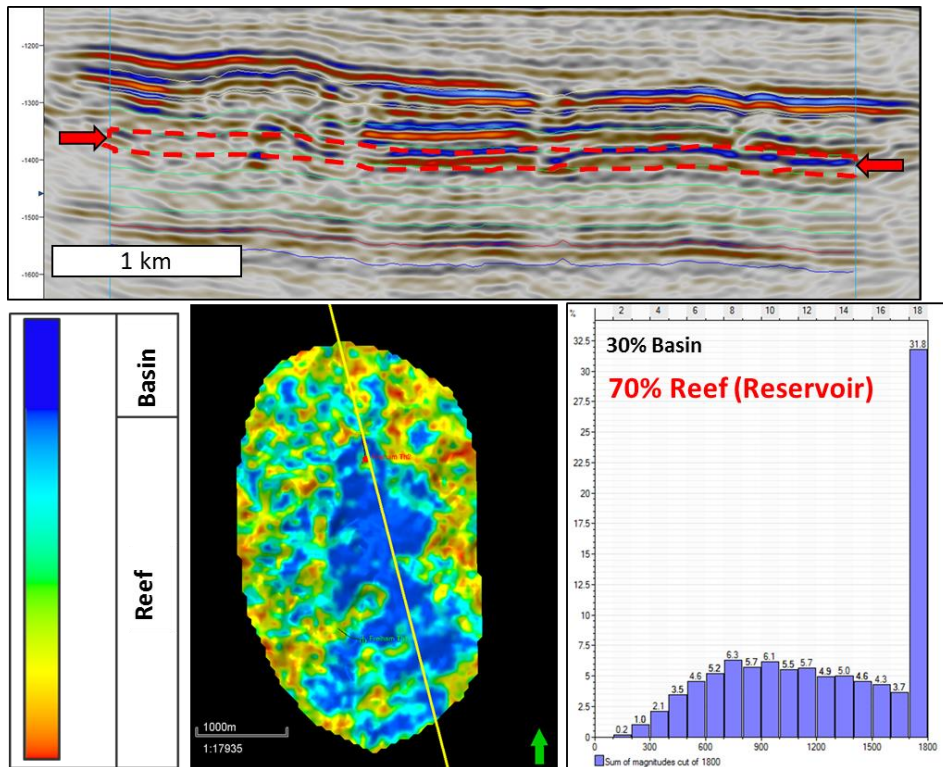


Figure 87: Sum of magnitude map for zone 5

3D Analysis

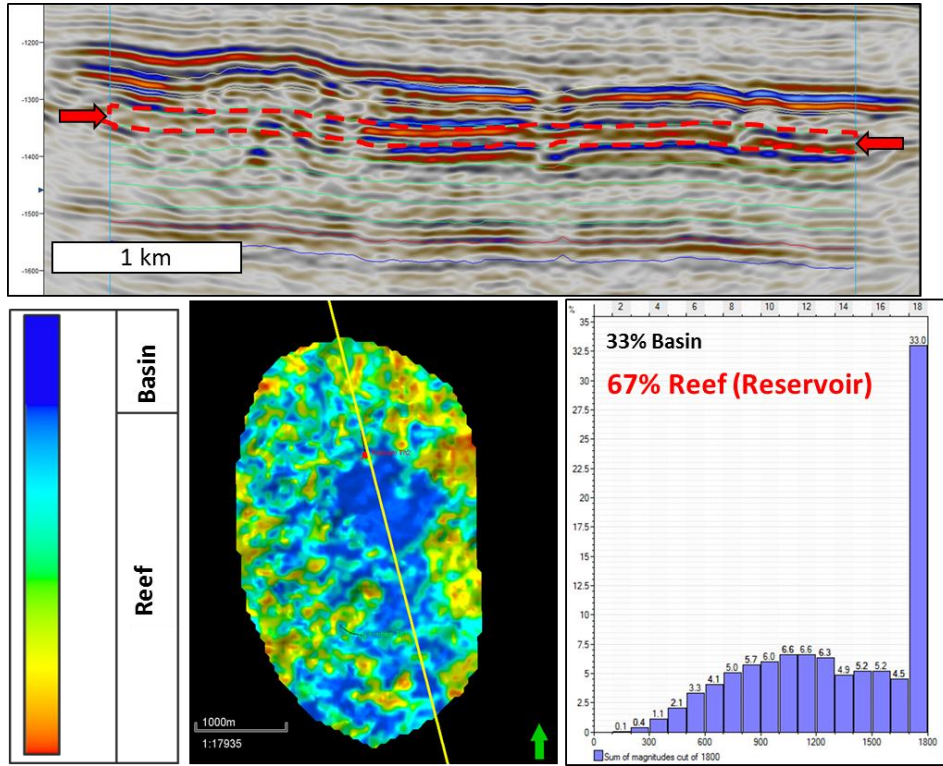


Figure 88: Sum of magnitude map for zone 5

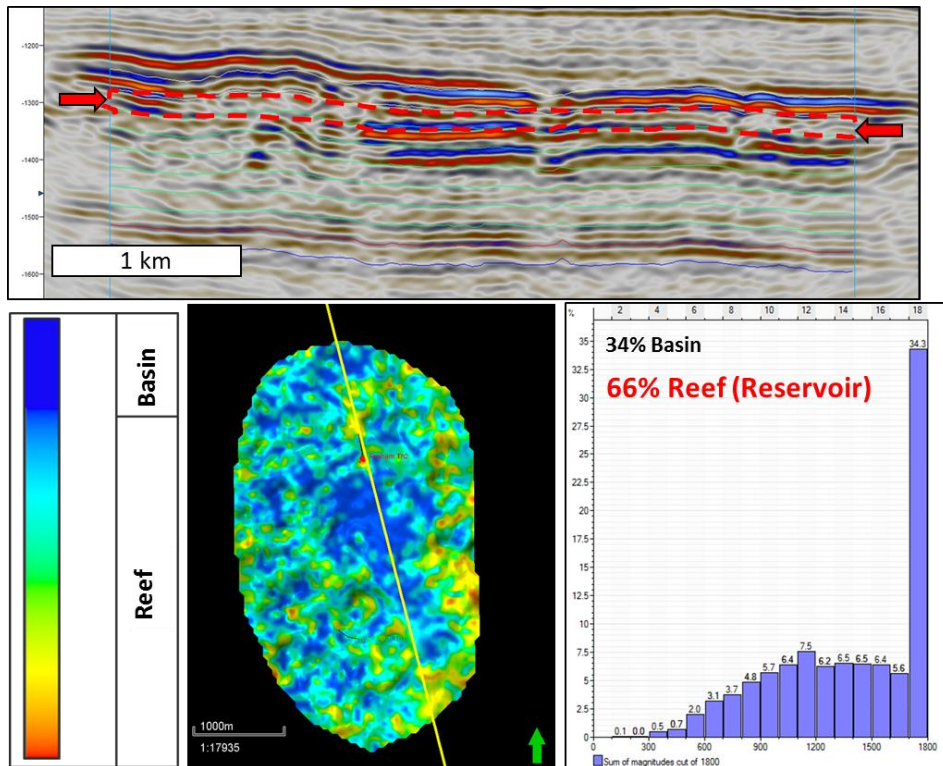


Figure 89: Sum of magnitude map for zone 6

3D Analysis

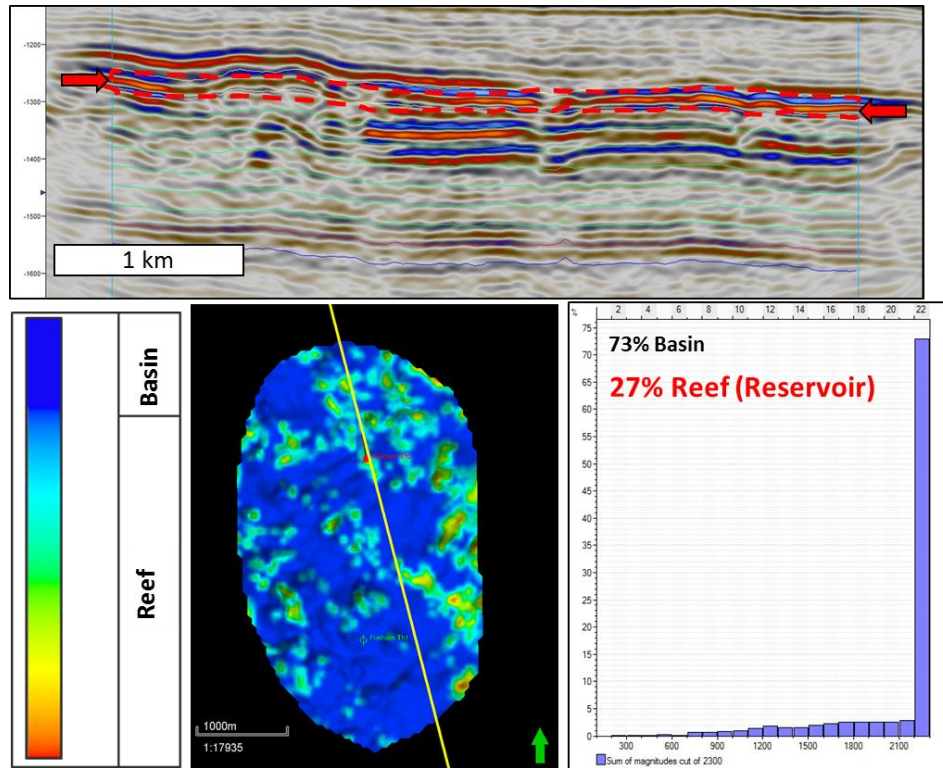


Figure 90: Sum of magnitude map for zone 7

3D Analysis

5.1.6 Summary

Fifteen million years of bioherm-growth are visualized and quantified, with their dimensions and distribution being visible on the maps Figure 91. The base of the investigated section contains only 30% of bioherm/reef and constantly increases to a maximum of 83% in zone 4, which corresponds to the maximal expansion of bioherm/reef growth as known from outcrop studies (Leinfelder, Krautter et al., 1994; Leinfelder, R. R., Nose, M. et al., 1993). From then onwards, the amount of bioherm/reef gradually decreases until only 27% of bioherm/reef is present at the top. Numerous authors like (Leinfelder (1993, 1994), Meyer, (1994); Meyer and Schmidt-Kaler, (1990, 1989), Gwinner, 1976; Geyer and Gwinner, 1979) have also documented this general trend of increasing-decreasing bioherm/reef growth of the Upper Jurassic in South Germany.

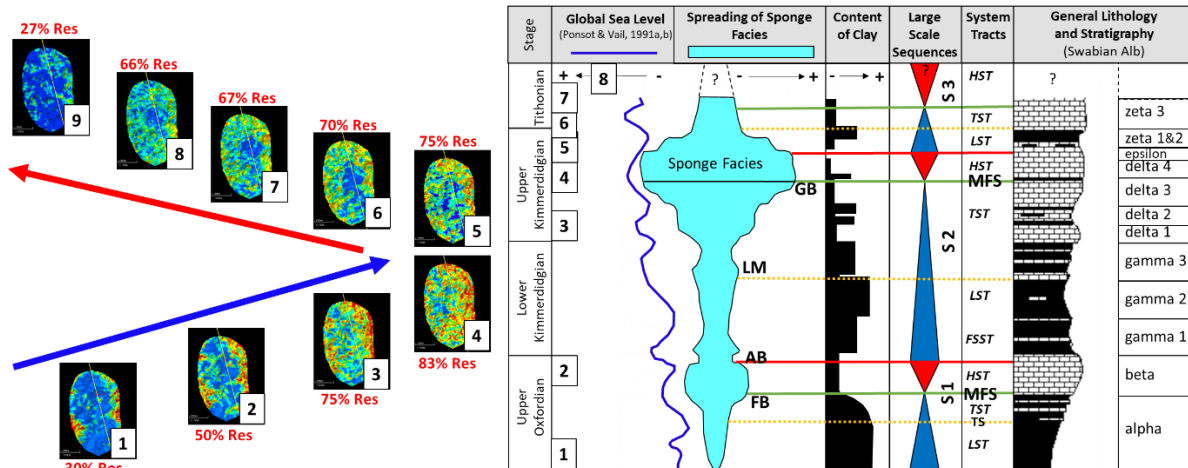


Figure 91: Summary seismic attribute maps visualizing bioherm growth during the Upper Jurassic.

5.2 Integration with BHI Logs, Cuttings and Outcrop

In most geothermal wells, borehole image logs were acquired. Although borehole image facies interpretation in carbonate reservoirs is very challenging caused by low internal resistivity contrast (e.g., Akbar et al., 1995; Chitale et al., 2010; Steiner and Böhm, 2013, Wolpert et al., 2019), an exceptional amount of detail was observed in the available dataset. It allows even to distinguish between various bio-components such as corals and sponges, reef debris, and many other distinctive features (see chapter 3.4).

3D Analysis

The borehole image facies interpretation is, therefore, used to verify the seismic facies interpretation, as shown in Figure 92. Also, the interpreted stratal surfaces are used to validate the sequence boundaries and iteratively improve the seismo-stratigraphic analysis.

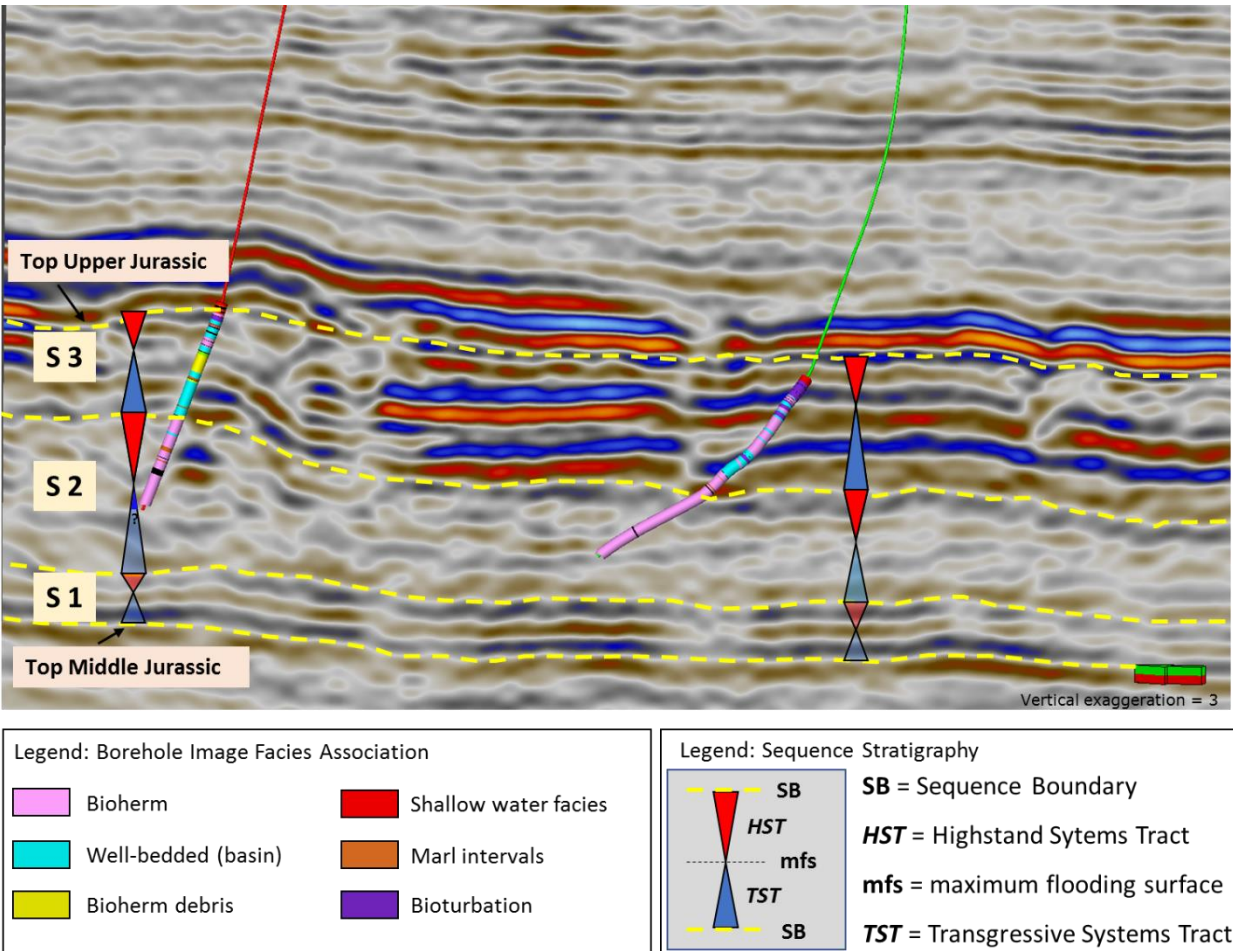


Figure 92: Integration of borehole image facies associations to validate the seismic interpretation.

3D Analysis

Borehole cuttings and thin sections were further used to calibrate and validate the borehole image facies and interpretation. Figure 93 shows an example of grainstones and mudstones identified from the borehole cutting analysis (Arlat, 2020). This additional information provides invaluable information while interpreting borehole image logs.

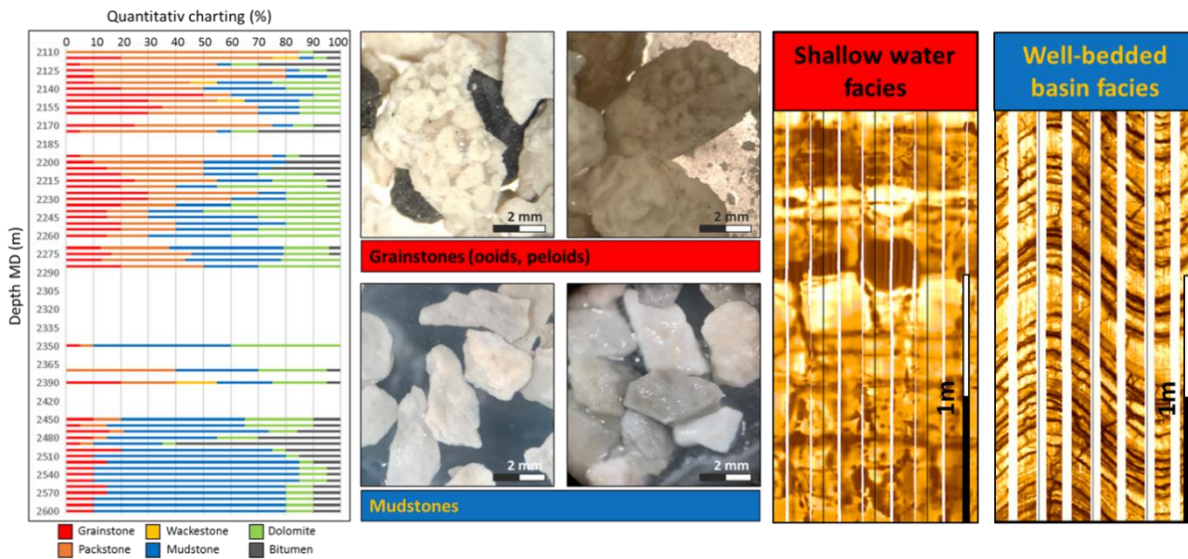


Figure 93: Borehole cuttings to validate the borehole image interpretation.

Outcrops analogs of the Swabian and Franconian Alb provide the opportunity to compare the seismic interpretation with dimensions, geometries, and characteristics of geobodies derived from field observations. Figure 94 shows an example that further supports the seismic interpretation of some key features such as onlaps of the basin facies onto the bioherm/reef, 100s of meters scale reef debris wedges and the well-bedded basin facies (e.g. Pawellek and Aigner, 2003, Ruf, 2005, Bold, 2010).

3D Analysis

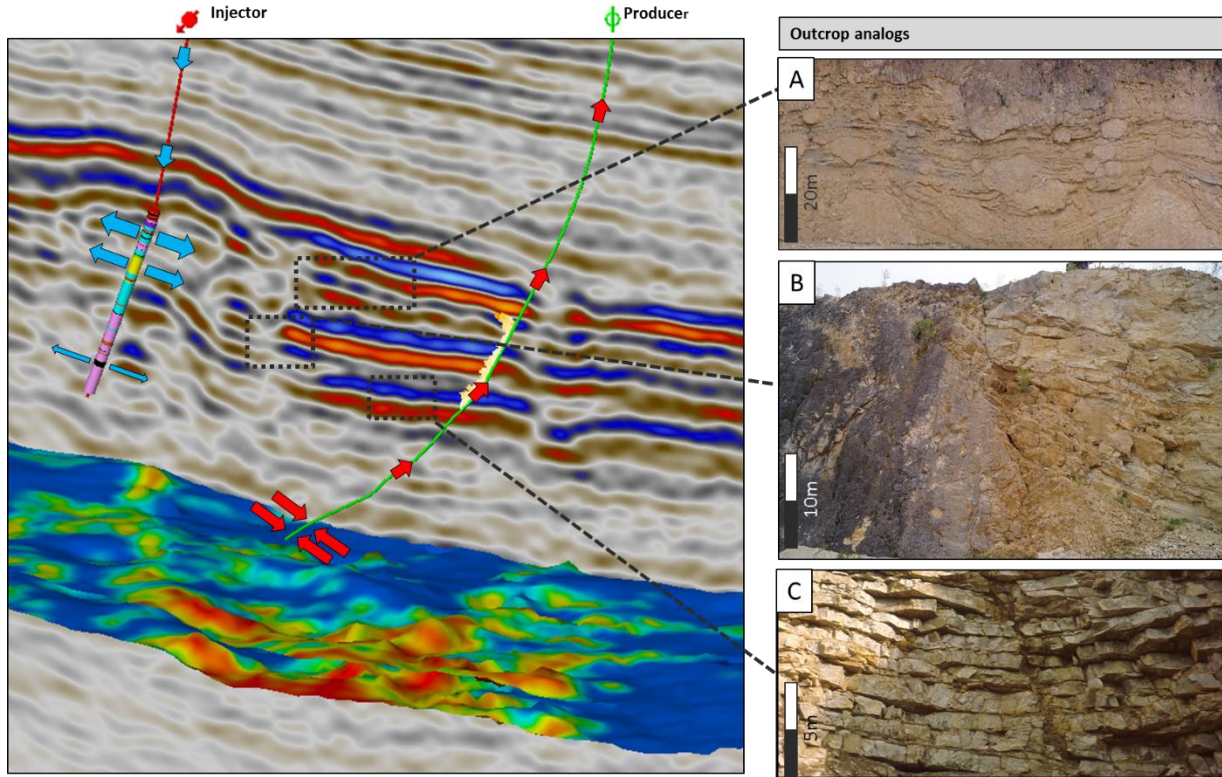


Figure 94: Key observation from the seismic interpretation compared with outcrop analogs.

The calibrated seismic attribute maps show structures and geometries that can be interpreted as biohermal build-ups or bioherm complexes (Figure 95). The „zoom-in“ shows the interpreted bioherm structures from the seismic attribute maps in detail (yellow-red colors) and the simplified subdivision (Figure 95, right) into basin facies and bioherm/reef facies (orange and blue colors).

To validate the interpretation, a field study was carried out in order to document and quantify the dimensions and orientation of bioherm build-ups located at the Swabian Alb (Chiracal, 2020). Aerial photographs and elevation profiles were used to collect quantitative data, which were compared with the seismic attribute maps.

3D Analysis

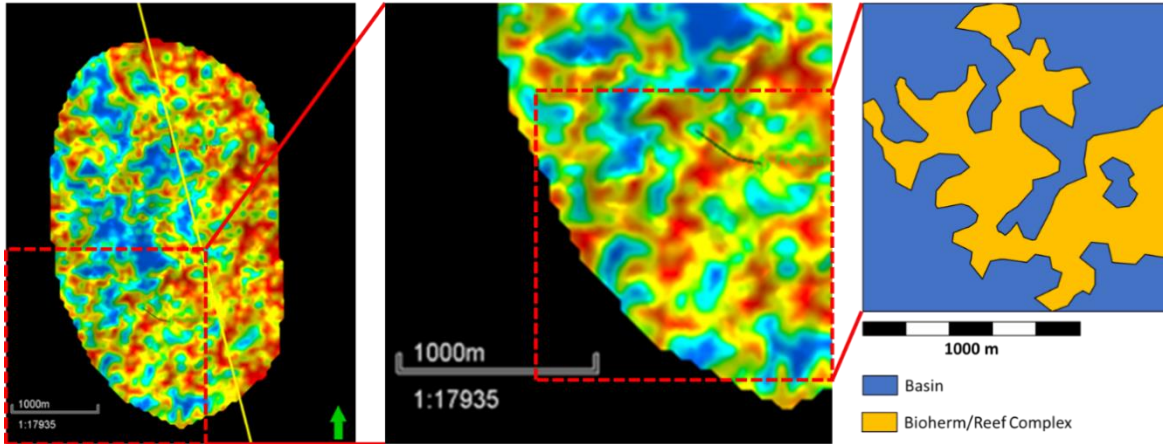


Figure 95: Size and dimensions of bioherm-complex and basins

Chiracal (2020) showed that the bioherms of the Swabian Alb (Malm Zeta) are either bioherm complexes composed of several individual bioherms with atoll-like structures (Figure 96) or that they are individual, isolated bioherm build-ups (Figure 97).

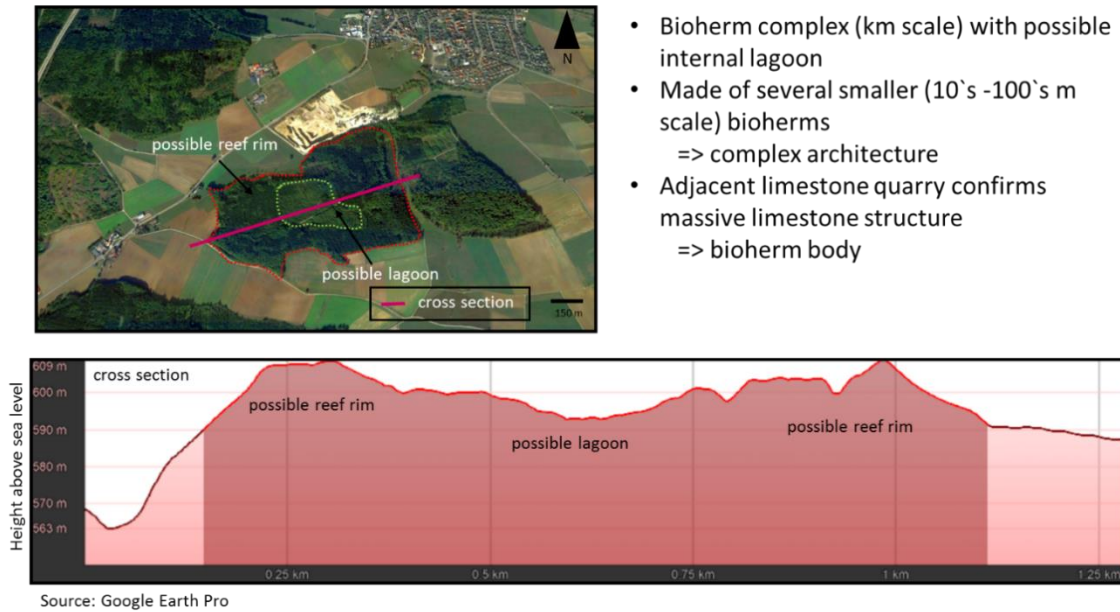
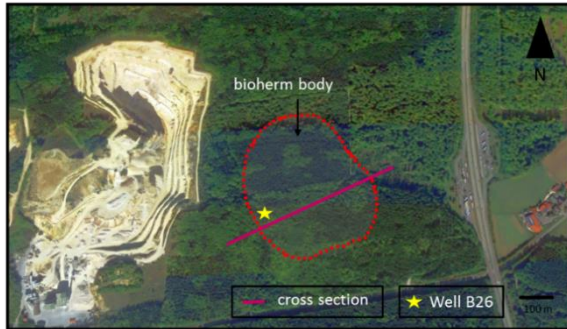
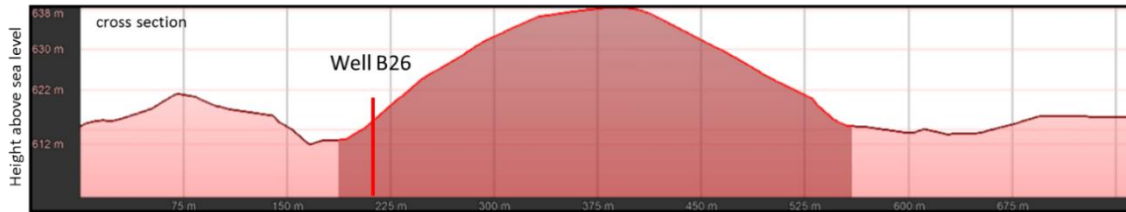


Figure 96: Bioherm complex from the Swabian Alb with an internal lagoon (from Chiracal, 2020).

3D Analysis



- Bioherm body (100's m scale)
- Probably made up of a single bioherm body
- Core analysis from well B26 confirms bioherm margin facies



Source: Google Earth Pro

Figure 97: Individual bioherm buildup (from Chiracal, 2020)

Very similar scales of sizes and geometries of the bioherms as in the outcrop can also be recognized in the seismic attribute maps and thus support the applied method and interpretation.

6. GEOLOGICAL TREND MAPPING

6.1 Thickness trends

The 2D correlation panels in section 4.1 show an increase in thickness from the NE to SW on a local, regional, and basin-wide scale. Arlat (2020) increased the database of this study with additional data from research and hydrocarbon wells to cover a larger area. Multiple 2D correlations panels (strike and dip orientation) were integrated with the sequence stratigraphic correlation of the geothermal wells from the greater Munich area ((Wolpert et al., 2019)). Based on the integrated correlations, thickness maps were created using the software Petrel. Figure 98 shows the results of the thickness map for the entire Upper Jurassic succession, comprising sequences 1-3.

The red and yellow colors represent areas where the Upper Jurassic carbonates are relatively thin (< 300 m), which corresponds to the Landshut-Neuöttinger paleo-high in the NE. The dark, blue colors show a thickness of > 550 m, which is interpreted as distal basin facies where more accommodation space was available.

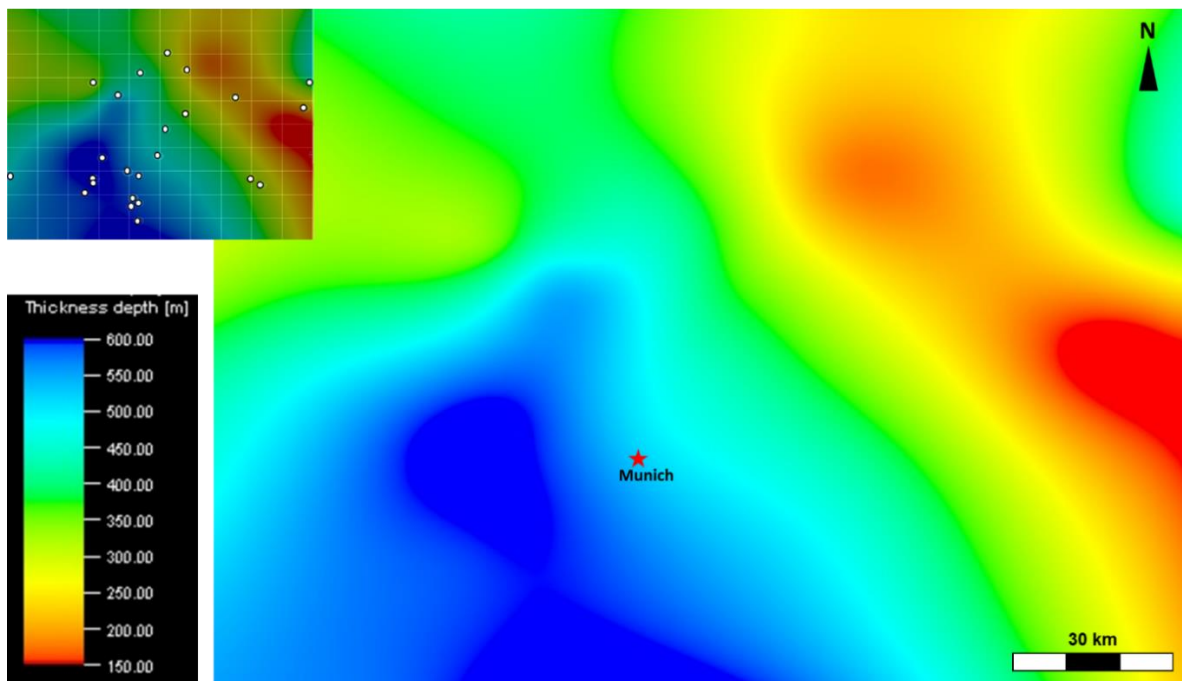


Figure 98: Thickness map of the complete Upper Jurassic Malm.

Geological Trend Mapping

Wolpert et al. (2019) showed that major karst zones of the Upper Jurassic carbonates are often found at sequence boundaries (see section 3.3.1). These observations were confirmed by borehole image logs, caliper data, and dynamic data like fluid losses while drilling or production tests. Because Upper Jurassic karstification can be one of the most important geothermal reservoir types, a potential karst map was created with the software Petrel, based on caliper data and dynamic data if available (Arlat, 2020). Figure 99 shows the potential karstification trend, which is most pronounced to the NE of Munich and oriented approximately NE-SW. The interpreted karstification trend seems to follow approximately the proximal-distal trend observed on the thickness map (Figure 99).

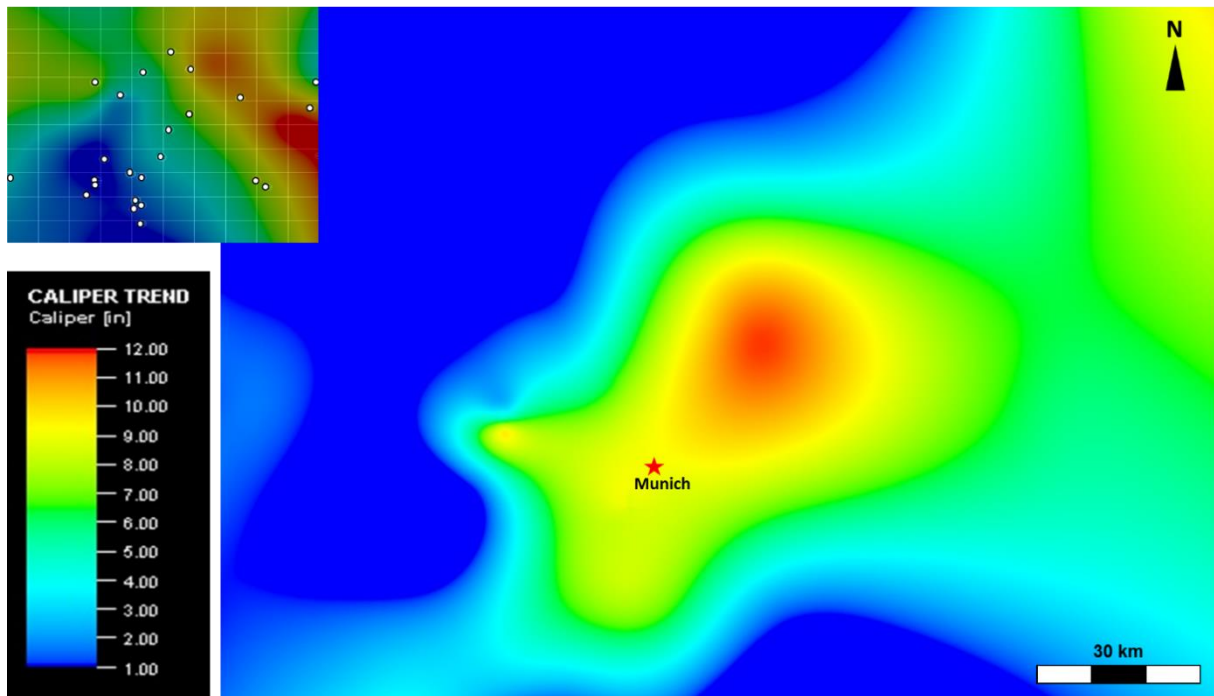


Figure 99: Potential Karst map interpreted from caliper data.

Geological Trend Mapping

6.2 Structural trends

Figure 100 shows the pre-Permian geological map of Western Europe (Ziegler, 1990). The major fault zones are related to the Variscan orogeny. The study area (greater Munich area) is located approximately 580 km south of Berlin, which is marked with the red star. As previously discussed in chapter 1.4 (basin development & tectonics), the basement of Variscan age was uplifted and eroded during the Late Carboniferous resulting in graben and trough systems (Ziegler, 1990; Ziegler and Dèzes, 2006). Three subordinated orientation trends exist for the fault systems:

- (1) NNE-SSW Fault Orientation (rheinisch)
- (2) NE-SW Fault Orientation (erzgebirgisch)
- (3) NW-SE Fault Orientation (herzynisch)

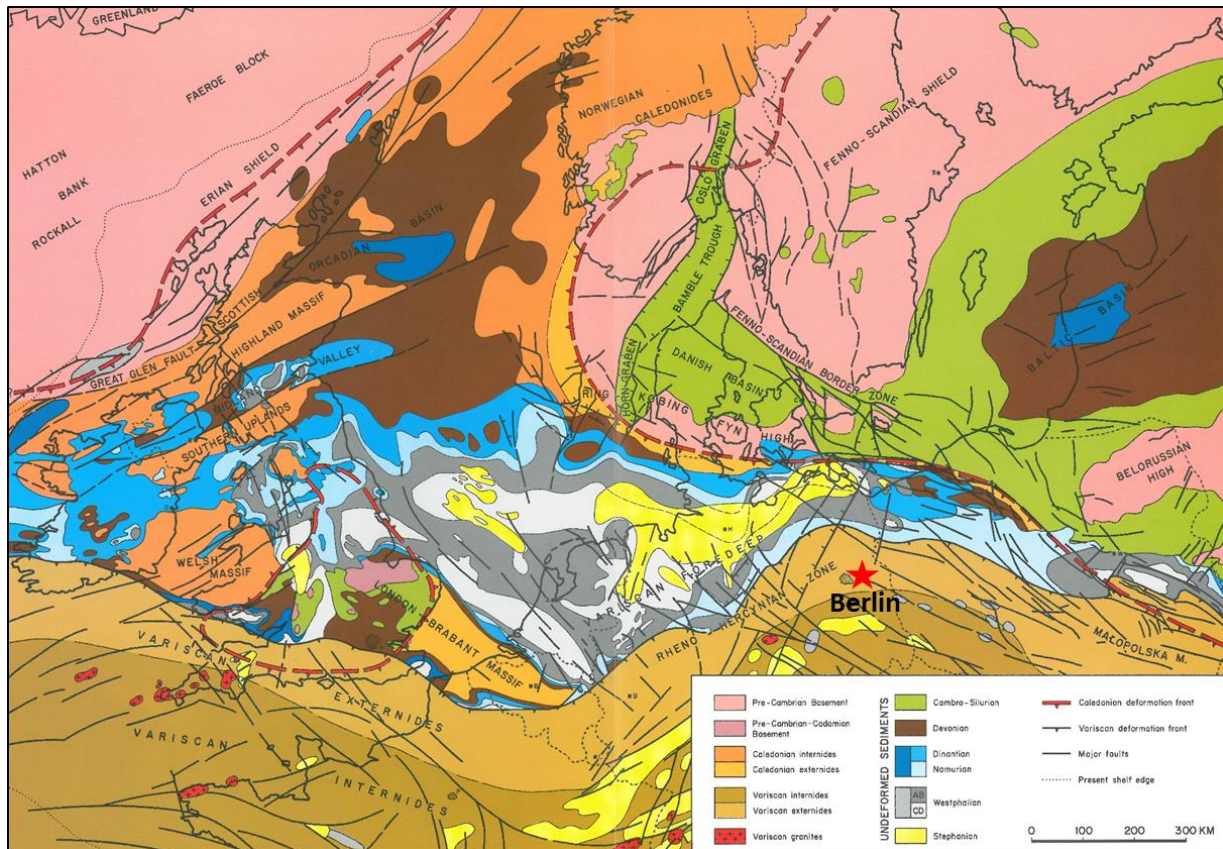


Figure 100: Pre-Permian geological map of Western Europe

Geological Trend Mapping

A “zoom-in” into the study area (Munich) is shown in Figure 101. Ziegler (1991) recognized a zone of rapid Jurassic/Cretaceous subsidence south of Munich (blue color), which is oriented approximately NE-SW. This zone seems to follow the orientation of the preexisting Variscan graben and trough systems. A possible explanation for that area might be the reactivation of preexisting basement structures causing differential subsidence rates, associated with accommodation space variations, as shown by several studies (Allenbach, 2002; Ruf et al., 2005b; Warnecke and Aigner, 2019; Wetzel et al., 2003).

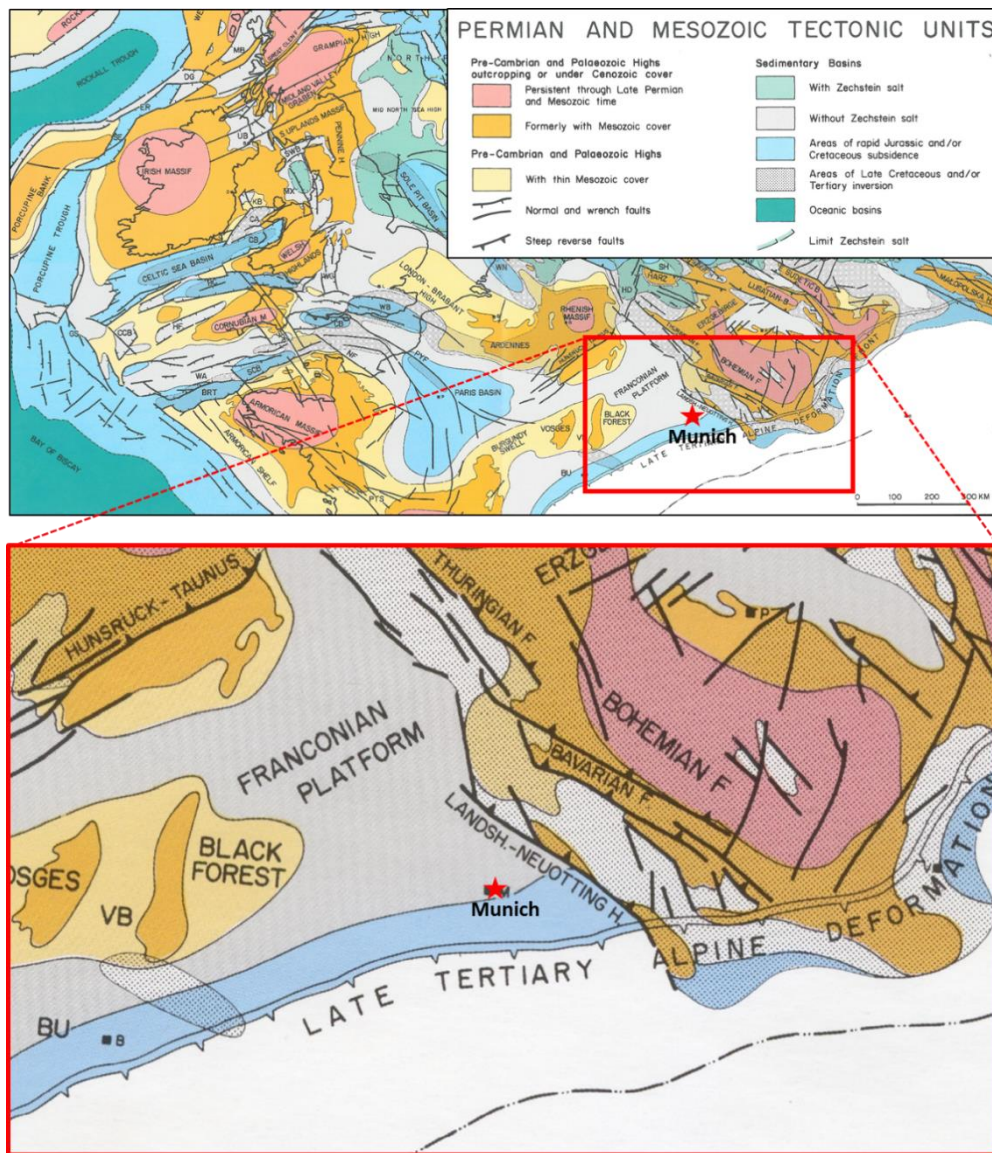


Figure 101: Permian and Mesozoic Tectonic Units

7. SYNOPSIS: GEOTHERMAL RESERVOIR TYPES AND EXPLORATION STRATEGY

7.1 Distribution of Geothermal Reservoir Types

This chapter reveals the distribution of geothermal reservoir types (described in section 3.5) in a seismo-stratigraphic context. Each scale of the systematic and hierarchical reservoir characterization workflow is integrated and validated iteratively to link and understand the distribution and properties of the geothermal reservoir types in a sequence stratigraphic context.

Geothermal reservoir types: 1) Karst (high K-streaks)

Karstification can be one of the most productive reservoir types due to the high permeability contribution. Figure 102 shows the seismo-stratigraphic interpretation in context with the borehole image log, which reveals that karstification occurs mainly at the sequence boundaries S2/S3 and Top Malm SB.

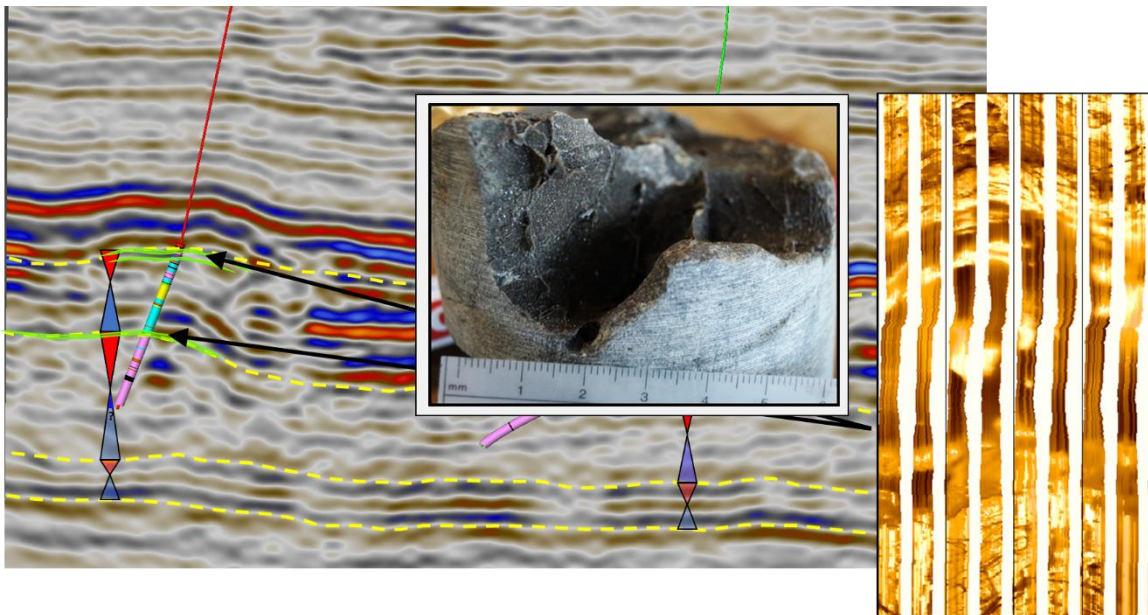


Figure 102: Geothermal reservoir type 1: Karst

Geothermal reservoir types: 2) Shallow-water facies (vuggy porosity, often touching). The shallow water facies identified from borehole image logs is characterized by frequently changing image facies types on a dm- to m scale, and by a serrated gamma-ray log pattern. The shallow water facies is present in the regressive hemi-sequence of sequence S3 (Figure 103). The vuggy porosity, however, is only present in distinct layers. Observations from the core analysis of well Moosburg SC4 suggest that these vuggy layers are present at the top of small-scale shallowing upward cycles, and are composed of oolitic-peloidal-bioclastic grainstones (see section 3.4.3).

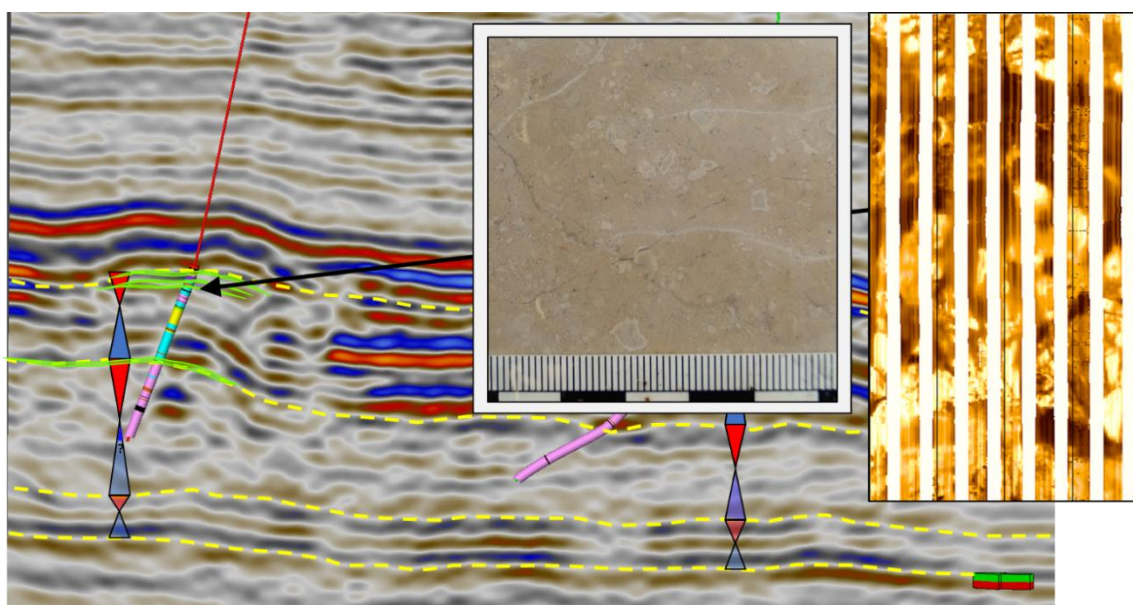


Figure 103: Geothermal reservoir type 2: Shallow water facies.

Geothermal reservoir types: 3) Bioturbation (dolomitized burrows, matrix porosity) Bioturbation with coarse-grained burrow fills show significantly enhanced porosity, especially if dolomitized. Distinct, often branched burrow traces, are characteristic of this reservoir type. Whereas bioturbation, in general, can occur in all three sequences, the dolomitized, coarse-grained burrow fills are only observed towards the Top Malm sequence boundary, similar to the observations in research well Moosburg SC4 (see chapter 3.3).

Synopsis

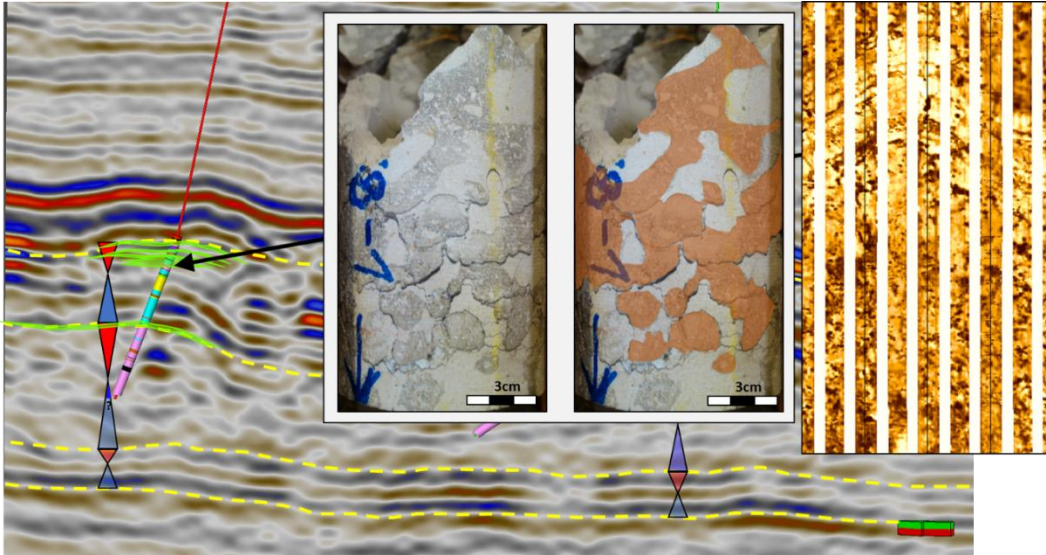


Figure 104: Geothermal reservoir type 3: Bioturbation

Geothermal reservoir types: 4) Dolomitization around clay/marl baffles (vuggy porosity, often separated vugs)

The clay/marls baffle, as such, is not the actual reservoir type, but the associated dolomitization and vuggy porosity above or below the baffle. This reservoir type is well developed in the maximum flooding zone of S3 characterized by onlaps of high reflectivity reflectors towards the bioherm buildup. Several dm thick clay/marl layers were deposited onto the bioherm buildup, compared to 10's m in the intra-basins, forming a potential aquitard to rising fluids. Below these baffles, dolomitization and the presence of vuggy porosity is frequently observed on the borehole image logs and in core (Figure 105).

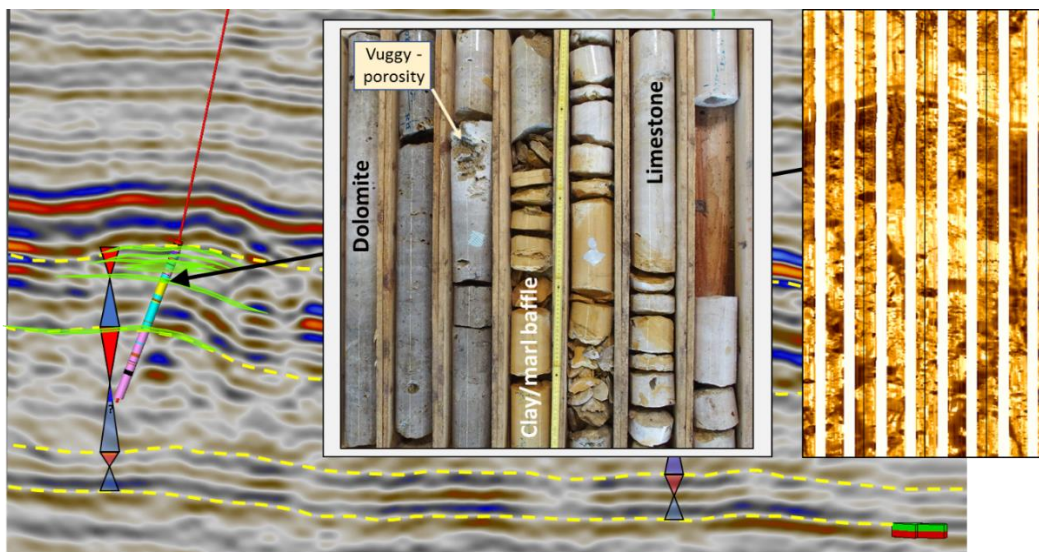


Figure 105: Geothermal reservoir type 4: Dolomite around clay/marl baffles

Geothermal reservoir types: 5) Bioherm debris (proximal: matrix and separated vuggy porosity)

Bioherm debris is mainly observed in depositional sequence S3, as interpreted from seismic (see chapter 5.1). The debris has a wedge-shaped geometry and originates at the edges of the buildup, reaching well into the intra-basin. Borehole image interpretation confirms the presence of potential bioherm debris, as large shells and subangular, resistive clasts can be observed, often associated with a component-size trend.

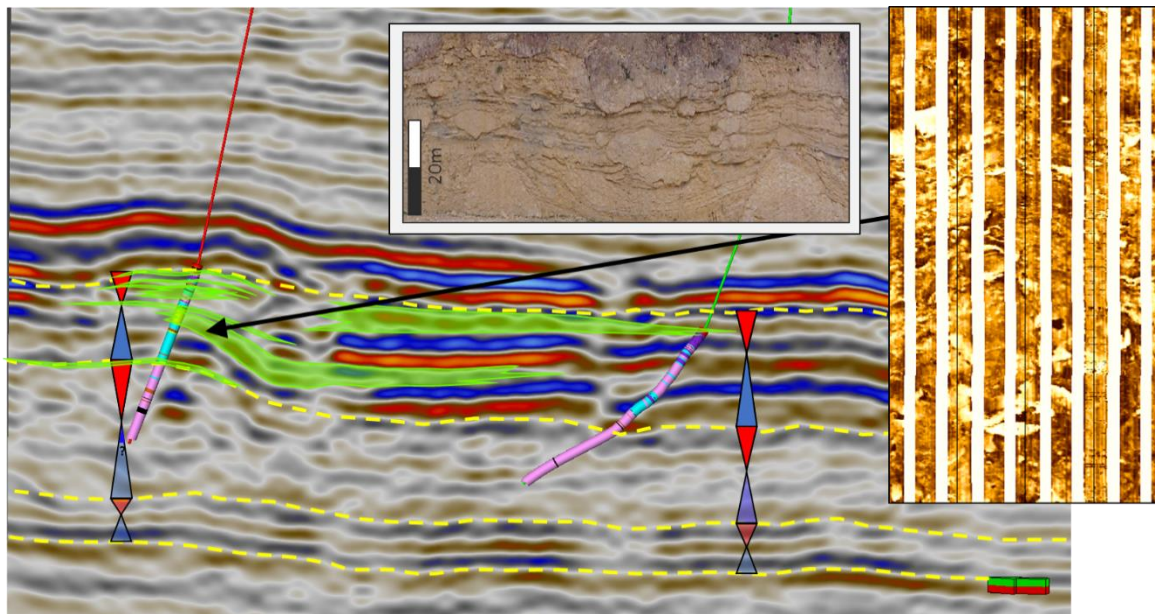


Figure 106: Geothermal reservoir type 5: Bioherm debris (proximal)

Geothermal reservoir types: 6) Fractures / Faults

Fractures and faults are one of the most important reservoir types because they can provide, similar to Karst, very productive flow rates. However, not all faults and fractures are open systems. The conductive character on the borehole image logs can also be caused by clay smear in the fracture/fault (in a water-based image log, conventional color scaled). Most production comes from the fault-zone in depositional sequence S2, whereas fractures in S3 are more affected by clay smear and therefore tight.

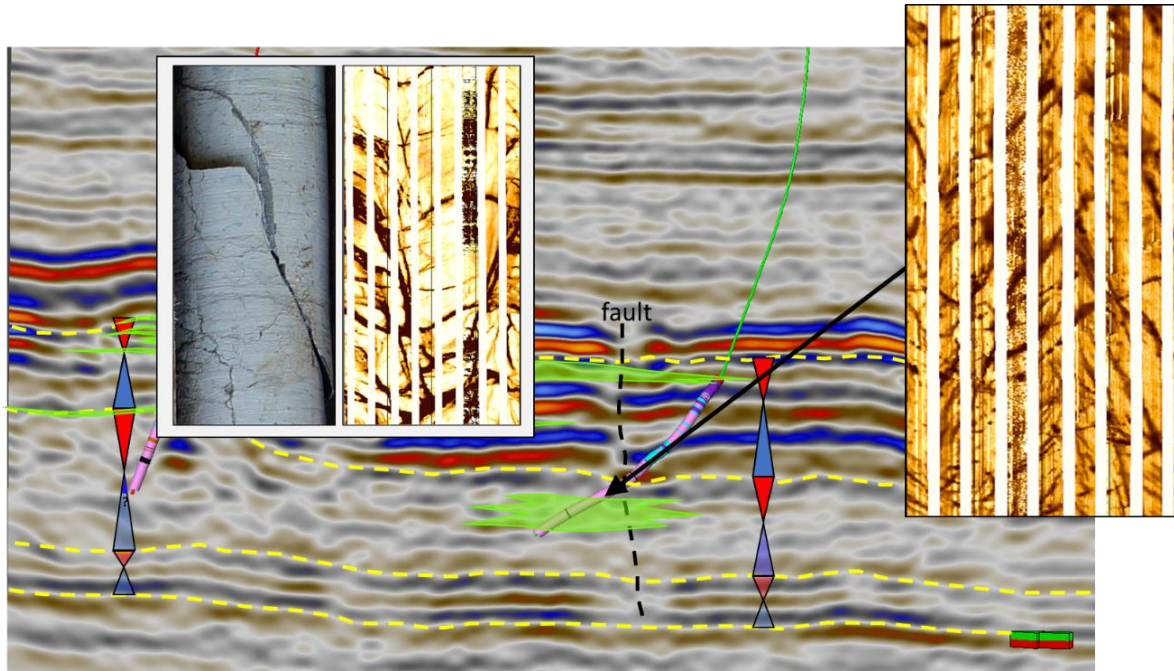


Figure 107: Geothermal reservoir type 6: Fractures and faults.

7.2 Ranking of reservoir types and integration with dynamic data

An essential part of the geothermal reservoir characterization is the integration of dynamic data (e.g., spin flowmeter test). This allows to localize the exact position of the flow zone, as well as to quantify its productivity. Table 4 shows an example where reservoir types identified from borehole image logs are linked to the spin flowmeter. The values in percentage represent the contribution of the reservoir types to the total production/injection volume. It also shows the importance of the sequence stratigraphic context.

Example 1: Karstification is often considered as a very productive high-K flow zone, and considered as the main target. The integration of dynamic data, however, reveals that there are very pronounced differences related to the stratigraphic position of the karst. The karstification at the top Malm sequence boundary S3 contributes to 47% to the total production, but the karst horizon at sequence boundary S2 only to 6%. Although both karst zones are well developed and visible on the borehole image and on caliper data, they have different dynamic properties. A possible explanation could be that the top Malm sequence boundary was longer and more intensively exposed due to a major sea-level fall at the end of the Jurassic. This exposure led to a vast karstification surface/network, which is laterally well connected and can, therefore,

Synopsis

produce high flow rates. The karst at sequence boundary S2 might be initiated by a shorter exposure time or a less pronounced sea-level fall, where only localized parts of the bioherm complex were exposed. As a result, the karst network is rather patchy and connectivity rather moderate.

Example 2: Bioturbation can be a prolific geothermal reservoir type, as observed in core and borehole image logs. The integration of dynamic data reveals, however, that the creation of porosity and permeability is only present at the late highstand of sequence S3. Other bioturbated intervals have no notable influence on the flow rates. An explanation for this observation could be that the available accommodation space was gradually filled up during the late highstand. The shallower environment is associated with higher water energy and a different ichnofauna (e.g., *Thalassinoides*) compared to bioturbated intervals related to the maximum flooding zone. The *Thalassinoides* burrow traces were filled up with coarse-grained material (peloids and ooids) that was then dolomitized. This process enhanced the creation of porosity and permeability and showed that the sequence stratigraphic context is essential to understand the processes that created the reservoir types and to predict the presence of potential geothermal reservoir types.

Furthermore, Table 4 shows the general character of the geothermal field and part of the production strategy: (1) well 1 is producing from a fault zone; (2) well 2 is injecting into multiple stratigraphic targets. This highlights how important the sequence stratigraphic framework is to understand the distribution of geothermal reservoir types. It is not enough to produce high flow rates alone but also to identify, predict, and target multiple stratigraphic targets that are capable of compensating for the capacity of the producing well.

Synopsis

Table 4: Reservoir types Integration of dynamic data.

Well 1 (Producer)		
Reservoir type	PLT (spin flowmeter)	Stratigraphic Position
Fractures/Fault	100%	Structural feature. But tendency of clay-smear in Sequence S3 (closed).

Well 2 (Injector)		
Reservoir type	PLT (spin flowmeter)	Stratigraphic Position
Shallow water facies	26 %	Highstand, regressive-hemi Sequence S3
Karst	47 % (S3) and 6 % (S2)	Sequence boundary S3 and Sequence boundary S2
Bioturbation	7 %	Highstand, regressive-hemi Sequence S3
Internal baffles	9 %	Below MFS Sequence 3
Bioherm/Reef debris	5 %	Lowstand and Highstand, Sequence S3

7.3 Inter-well connectivity via high-K streaks

Apart from high temperatures, the flow rates of the first well are an important requirement that determines the course of a geothermal project. For most of the geothermal projects in the greater Munich area, flow rates of approximately 100 L/sec are needed to produce electricity and district heating. If the flow rates of the first well are below expectations, the drilling of the second well can be in jeopardy. The production of such high flow rates is already challenging, but re-injection is often the bottleneck that impacts financial performance. If the injector well can not compensate for the high flow rates from the producer, additional drilling (e.g., sidetrack, new well) is required. It is, therefore, fundamental to understand upfront the potential fluid flow behavior and dynamics in the subsurface.

The integration of dynamic data (section 7.2) already revealed a ranking of the reservoir types. It shows furthermore that the Upper Jurassic Malm of South Germany can be classified as a dual-porosity system composed of: (1) matrix dominated and (2) high-K (high permeability) reservoir types. Dual porosity systems have been subject to numerous studies (Coats, 1989; Guo et al., 2012; Mai and Kantzas, 46; Popov et al., 2009), especially from the perspective of enhanced oil recovery and water-flooding FDP (Al-Harthy et al., 2012). Figure 108 shows the importance of understanding the double porosity system in context with the geothermal field development strategy for a closed-loop system. The re-injected, cold fluid is flowing back to the producer well,

Synopsis

absorbing the heat from the surrounding rocks. Therefore, flow velocity and time are two critical factors. If the re-injected, cold fluid flows too fast to the producer well, there is not enough time to recharge the fluid with heat, and the geothermal power plant is producing its own, cold water again. In a karstified and fractured carbonate reservoir like the Upper Jurassic Malm of South Germany, this is a critical part of the geothermal field development strategy.

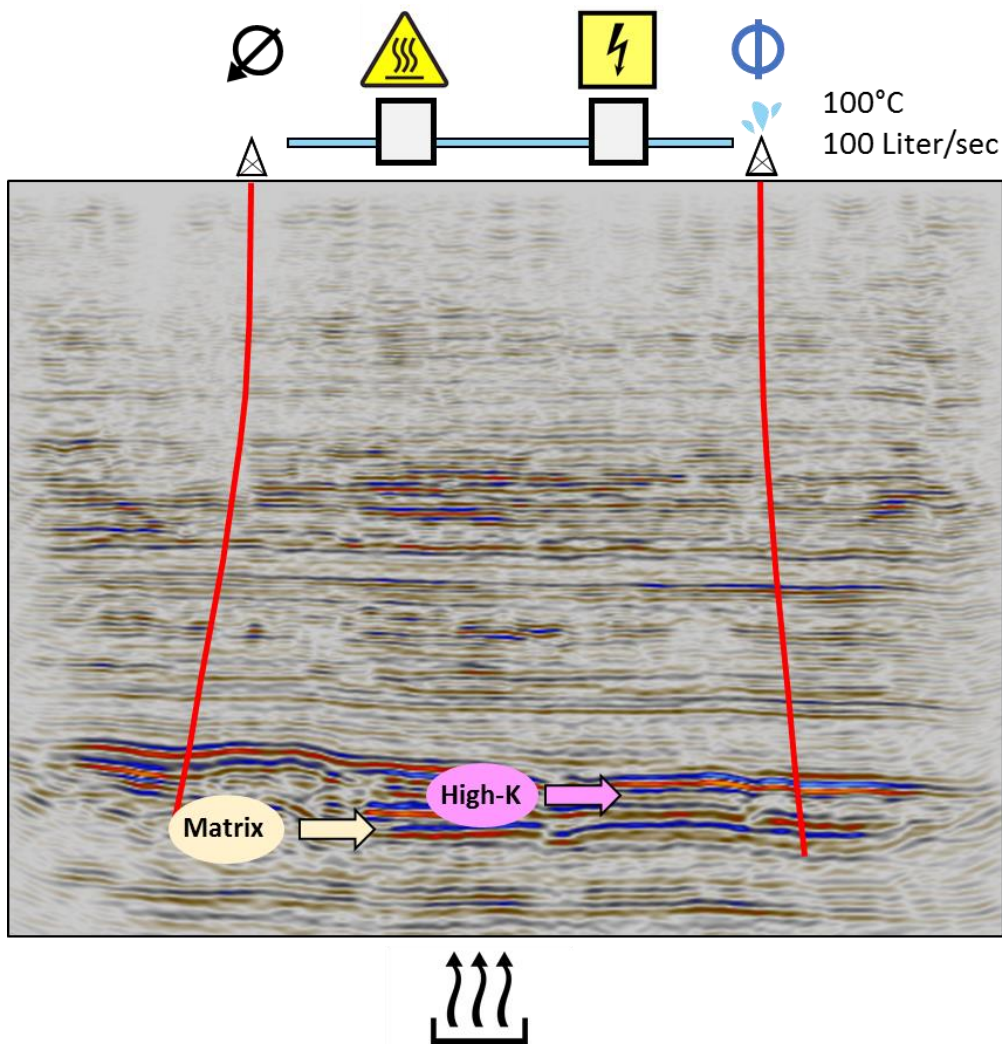


Figure 108: Schematic fluid flow behavior (matrix or high-K) in the subsurface.

7.4 Areas of rapid subsidence

The expansion of geothermal developments south of the greater Munich area is more challenging. This is caused mainly because the reservoir properties of the Upper Jurassic Malm are changing compared to the prolific Munich region. Key observations are: (1) the lack of karstification, (2) a lower degree of dolomitization, and (3) low-permeability fracture and fault zones (Dussel et al., 2018; Wolfgramm et al., 2011). The three “dry” geothermal wells Mauerstetten, Geretsried, and Iking are located in that southern area. Studies from (Ziegler, 1990) proposed rapid subsidence during the Jurassic and Cretaceous for that zone. The alignment is approximately NE-SW following one of the three major Variscan fault orientation trends of the basement (Ziegler, 1990; Ziegler and Dèzes, 2006). Possible reactivation of the old Variscan basement faults caused increased subsidence rates (Wetzel, 2003), variation in accommodation space, and, subsequently, the evolution of a different depositional environment. Compared to the greater Munich area, where shallow-water facies and karstification is present towards the top of the Upper Jurassic Malm (Lemcke, 1987), the southern part is instead dominated by a more distal depositional environment and potential low-permeability facies types.

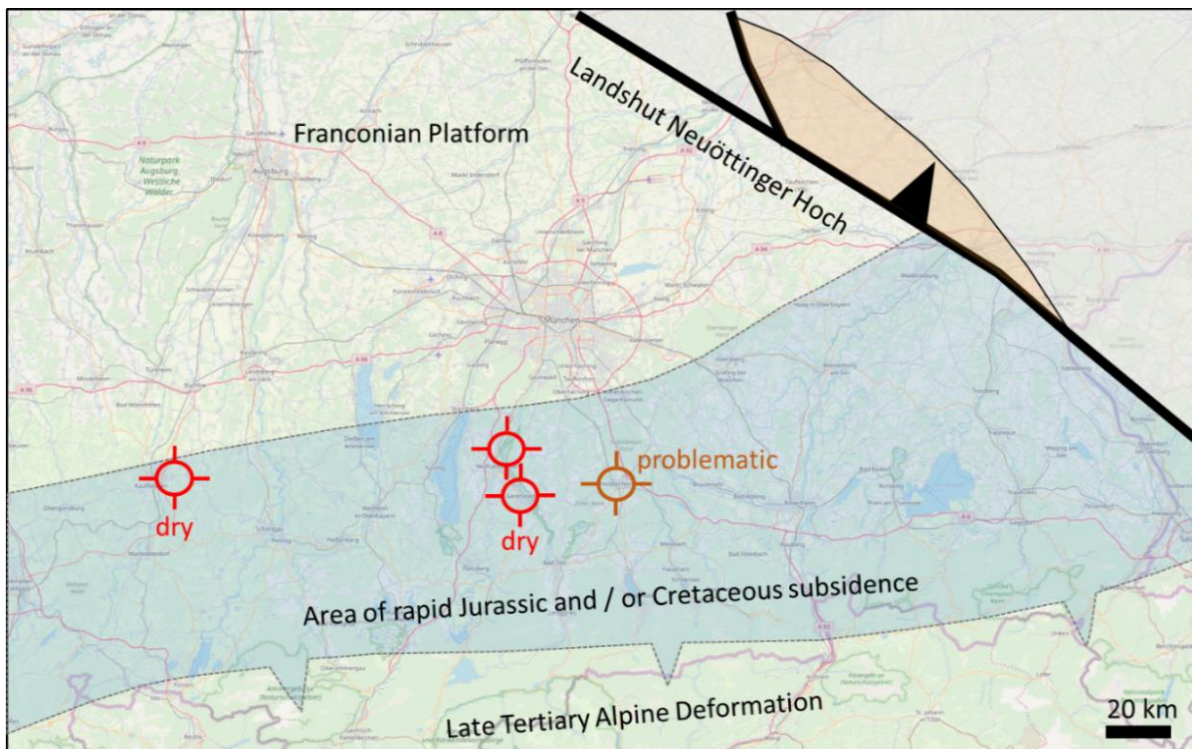


Figure 109: Dry geothermal wells south of Munich (modified from Ziegler, 1990)

Synopsis

Additionally, the following observations support this interpretation.

- (1) The basin-wide correlation from Arlat (2020) showed an increase of total thickness for the Upper Jurassic Malm to the South. The correlation is mostly based on gamma-ray logs and verified by core data if available. The character of the gamma-ray pattern from the southern wells can be described as “blocky” and relatively homogeneous. Along with other indications (e.g., well logs, core data, cuttings, thin sections), this area is interpreted as a low-energy, distal basin environment. Therefore, karstification and abundant shallow-water facies are not likely in that area.
- (2) Dussel (2018) investigated the dry well Geretsried. In Geretsried neither potential karst associated with bioherms nor the large faults produced sufficient permeability. The core data from the sidetrack of well Geretsried reveals very dark, almost black mudstones that are interpreted as distal basin facies. This facies type has not been observed in research well Moosburg SC4, or any other cores associated with this study (Eigler, 2018; Lésic, 2029; Arlat 2020). Therefore, the area of rapid subsidence shown in Figure 109 might represent the southern edge of the carbonate platform.
- (3) Figure 110 shows two seismic dip lines. Survey Königsdorf is located close to the dry geothermal well Geretsried and represents the southern area characterized by rapid subsidence and the distal depositional environment. Freiham is situated in the Munich metropolitan area and represents the central part of the carbonate platform characterized by shallow-water facies and karstification towards the top of the Upper Jurassic (e.g., Malm Zeta). Most of the seismic facies in the Königsdorf dip line can be described as chaotic seismic facies with a weak reflectivity. Other seismic features like reflector terminations are rather subtle. In the Freiham dip line, however, strong reflectivity with a parallel high amplitude seismic facies are present in the upper part (Malm Zeta). The parallel high amplitude seismic facies is onlapping to the chaotic seismic facies and is interpreted as well-bedded intra-basin facies. The chaotic seismic facies represents the biohermal buildups that are frequently karstified and dominated by shallow water facies at the top (dispositional sequence S3). The fact that no buildups are present in the southern Königsdorf area can be interpreted as a change of the depositional environment. In that distal depositional low-energy environment, no geothermal reservoir types are present.

Synopsis

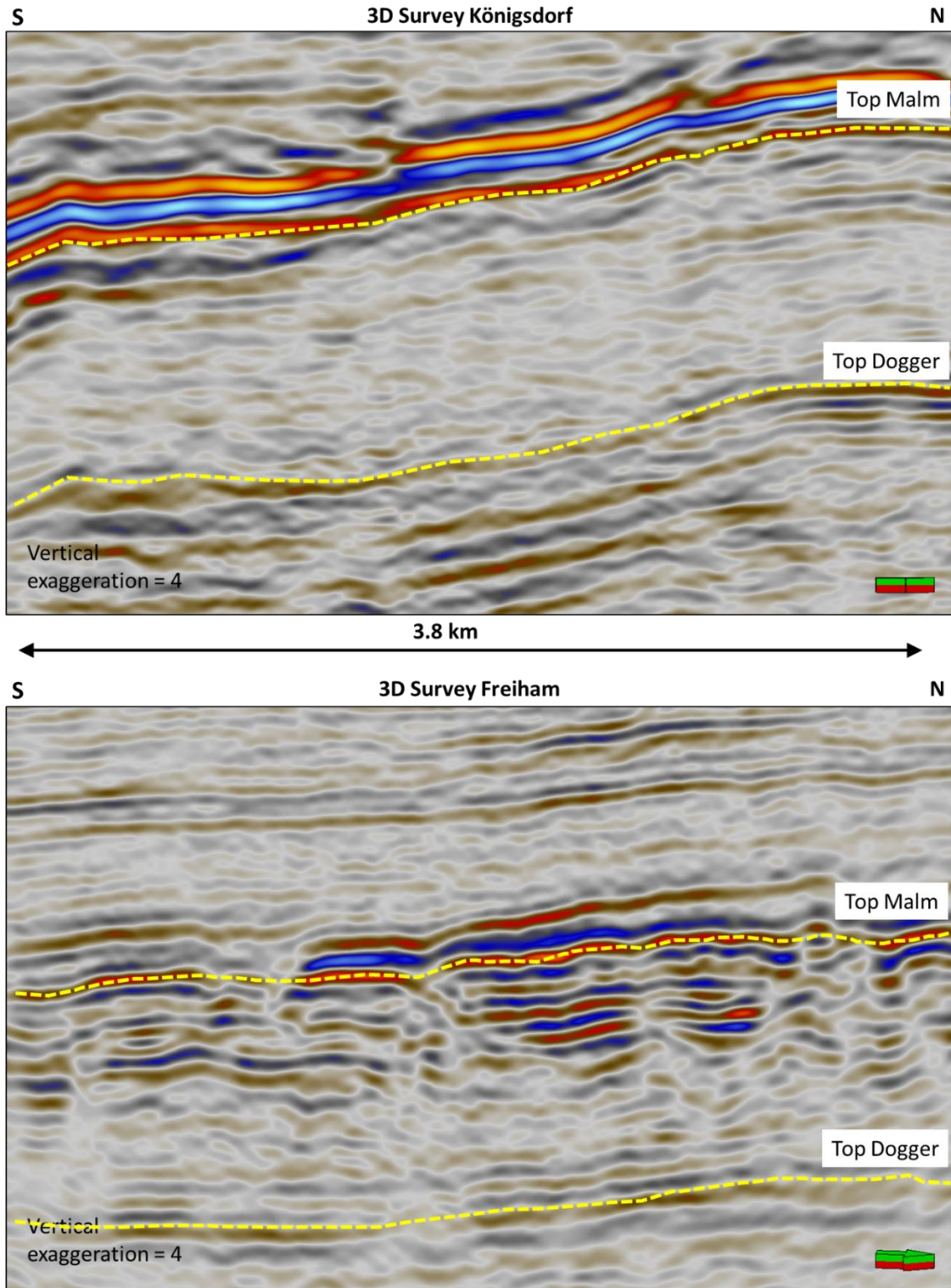


Figure 110: Comparison of seismic dip line from Freiham and Königsdorf.

8. SUMMARY AND CONCLUSIONS

Twentytwo lithofacies types were identified for the Upper Jurassic Malm and the Upper Jurassic/Cretaceous Purbeck Formation of research well Moosburg SC4 and can be grouped into four lithofacies associations: (1) basin, (2) bioherm, (3) bioherm debris, and (4) shallow-water. Nine borehole image facies types can be recognized unambiguously, including four distinct types of stratal surfaces. The vertical stacking of borehole image facies can be interpreted in terms of a transgressive and regressive sequence. Based on core description (Moosburg SC4), borehole image logs, gamma-ray well logs, and 3D seismic interpretation, three large scale sequences can be identified for the Upper Jurassic Malm (S1 to S3), and one large scale sequence for the Purbeck Fm (S4). Small scale cycles and cycle sets were only observed at the late HST of large-scale sequence S3, but are frequently present in the Purbeck Fm (S4). Seven potential geothermal reservoir types were characterized. Three dip-oriented correlation lines (local- regional and basin-scale) show an increase of thickness for the Upper Jurassic from the NE to the SW, especially depositional sequence S3. The 3D seismic interpretation of the study allows to differentiate between the potential reservoir and non-reservoir facies, using the sum of magnitude attribute.

The 1D analysis revealed that facies types are not randomly distributed but follow systematic rules instead. The key to understanding and predict facies distribution is the sequence-stratigraphic framework. Facies and sequence stratigraphic observations from the 1D core analysis can be transferred to the borehole image logs by the additional integration of stratal surfaces. The gamma-ray well log patterns are used to delineate genetically linked depositional units using different scales. Facies distribution within these depositional units follows the same systematic rules, and can, therefore, be interpreted even if the resolution of the borehole image logs is limited in tight intervals. The sequence-stratigraphic framework is also crucial to understand the distribution and character of the potential geothermal reservoir types because they are associated with the depositional facies and the sequence stratigraphic context (especially the presence of shallow water facies, exposure and karstification). The 2D correlation confirms the presence of the three large scale sequences S1-3 in the subsurface of the greater Munich area and beyond. It shows a deepening trend of the depositional environment from the NE to the SW and that the presence of paleohighs affects the accommodation space and, therefore, the total thickness of the Upper

Summary and Conclusions

Jurassic carbonates. The 2D-3D analysis shows that this trend has important implications for the development and distribution of geothermal reservoir facies. The lack of high permeability geothermal reservoir facies south of Munich, either structural or facies related, seems to be associated with the change to a distal, basin-like depositional environment.

The integration of dynamic data and the ranking of reservoir drivers brought new insights into the character of subsurface flow zones and fluid flow behavior. The Upper Jurassic geothermal system of the core study area (3D survey) is a combination of stratigraphic and structural traps. Because the capacity of the producer well (e.g., high permeability fault zone) is only as good as the capacity of injector well (e.g., multiple stratigraphic targets), a sequence-stratigraphic framework is paramount to understand and predict geothermal sweet spot distribution. It is also fundamentally important to avoid potential inter-well connectivity via high-k streaks, often located at sequence boundaries, and to prevent an early thermal breakthrough.

This study shows that the applied workflow and the integration of sequence stratigraphy with paleo-tectonics (e.g., potential reactivation of Variscan faults) are an essential element for successful geothermal exploration and development of Upper Jurassic carbonates in the Molasse Basin.

ACKNOWLEDGMENTS

First of all, I want to thank Prof. Dr. Aigner for being an inspiring mentor and for his unique way of supervising my theses. During the last few years, I learned many valuable lessons in life, also apart from the technical part of this thesis. We had several backslashes from 2013 onwards, and I am truly thankful that he made everything possible to make this geothermal project come true. Persistence pays off! Thank you very much Tom!

I am also very grateful for the co-supervision and the evaluation of this work by Prof. Dr. James Nebelsik. Dr. Hartmut Schulz and Prof. Dr. Peter Süss is thanked for the evaluation of this dissertation.

This thesis is the result of a research collaboration between the Geothermal Alliance Bavaria (GAB) and the sedimentological research group from the University of Tübingen. I would like to thank Dr. Kai Zosseder for his support and excellent cooperation, and the GAB for funding. A very big thank goes out to my highly appreciated colleagues Daniela Pfrang, Daniel Bohnsack, Martin Potten, and Robin Seithel, for their contribution and the uncomplicated and effective teamwork. I am also very grateful to the Reiner Lemoine Foundation for funding and for the chance to participate in the energy transition actively.

Dr. Achim Schubert and the team from Erdwerk is thanked for their support. Especially the fruitful discussion and ideas from Ulrich Steiner, Killian Beichen (BHI interpretation), and Daniel Bendias (3D seismic interpretation) have enriched the outcome of this study. I also want to thank Dr. Mike Drummond (TaskFronterra), for his advice and for sharing his longstanding experience in carbonate sedimentology and borehole image interpretation. I am very grateful to Timo Korth (ALT Luxemburg) for providing the WellCAD License and for the exceptional support during the last 3 years. Schlumberger is thanked very much for the Petrel software.

Michael Eigler, Tojo Chirakal, Nina Lesić, and Oliver Arlat brought with their research and thesis new light into this study. The cooperation was a real enrichment and great time, thank you very much!

I was fortunate to meet Dr. Marin Nowak (again) and Dr. Dietmar Jung at the LfU in Hof, and I am very thankful for their advice and ongoing support.

My Ph.D. colleague Matthias Warnecke is thanks very much for sharing his experience and for his support at the University. I also want the thank Dr. Renate Kostrewa very much, for her help and great discussions during the last years, as well as Dr. Eva Blendinger and Matthias Schuh. The advice and experience from Dr. André Jung were highly appreciated and helped me to structure and focus my work.

And of course, I want to thank my family! Without your help, patience, and support, I could not have made it. Thank you!

REFERENCES

- Agemar, T., Schellschmidt, R. and Schulz, R. (2012) Subsurface temperature distribution in Germany. *Geothermics*, 44, 65–77.
- Aigner, T. and Schauer, M. (1998) Exploration for industrial minerals and rocks using "dynamic stratigraphy": example ultra-pure limestones. *Zeitschrift für angewandte Geologie*, 44, 159–193.
- Akbar, M., Petricola, M., Watfa, M., Badri, M., Charara, M., Boyd, A., Cassell, B., Nurmi, R., Delhomme, J.-P. and Grace, M. (1995) Classic interpretation problems: evaluating carbonates. *Oilfield Review*, 7, 38–57.
- Al-Harthy, A., Al-Sinani, I., Al-Raisi, M. and Saud, A. (2012) Enhanced Dynamic Simulation Through Continuous Fracture Modelling of Carbonate Reservoirs, Oman. SPE Society of Petroleum Engineers, 161647, 1–16.
- Allen, P.A. and Homewood, P. (1986), *Foreland basins*, Blackwell Scientific Publications, Oxford, Boston, 453 pp.
- Allenbach, R. (2002) The ups and downs of "Tectonic Quiescence"—recognizing differential subsidence in the epicontinental sea of the Oxfordian in the Swiss Jura Mountains. *Sedimentary Geology*, 150, 323–342.
- Arlat, O. (2020), *Regional Geologic Trends and Geothermal Reservoir Potential of Upper Jurassic Carbonates*. Master Thesis, Tübingen, Germany, 204 pp, unpublished.
- Bachmann, G.H. and Müller, M. (1992) Sedimentary and structural evolution of the German Molasse Basin. *Eclogae Geologicae Helveticae*, 85, 519–530.
- Bachmann, G.H., Müller, M. and Weggen, K. (1987) Evolution of the Molasse Basin (Germany, Switzerland). *Tectonophysics*, 137, 77–92.
- Bartenbach, M. (2008), *Facies analysis and 3D-modeling of Upper Jurassic Carbonates: Implications for resource- and reservoir geology (Blaubeuren area, SW-Germany)*. Master Thesis, Tübingen, Germany, 149 pp.
- Bendias, D. (2017), *Sedimentology and Architecture of Deepwater Turbidite Systems Offshore Mozambique – from Concept to Application*, PESGB Africa Conference, London, UK.

Blakey, R.C. (2008) Gondwana paleogeography from assembly to breakup - A 500 m.y. odyssey., 1–28.

Böhm, F. (2012), Die Lithofazies des Oberjura (Malm) im Großraum München und deren Einfluss auf die tiefengeothermische Nutzung. Inauguraldissertation zur Erlangung des Doktorgrades des Fachbereichs Geowissenschaften der Freien Universität Berlin. Dissertation, Berlin, 148 pp.

Böhm, F., Birner, J., Steiner, U., Koch, R., Sobott, R., Schneider, M. and Wang, A. (2011) Tafelbankiger Dolomit in der Kernbohrung Moosburg SC4: Ein Schlüssel zum Verständnis der Zuflussraten in Geothermiebohrungen des Malmaquifers (Östliches Molasse-Becken, Malm Süddeutschland). *Z Geol Wissenschaft*, 39, 117–157.

Böhm, F., Koch, R., Höferle, R. and Baasch, R. (2010) Der Malm in der Geothermiebohrung Pullach Th2–Faziesanalyse aus Spülproben (München, S-Deutschland). *Geol. Bl. NO-Bayern*, 60, 17–49.

Böhm, F., Savvatis, A., Steiner, U., Schneider, M. and Koch, R. (2013) Lithofazielle Reservoircharakterisierung zur geothermischen Nutzung des Malm im Großraum München. *Grundwasser*, 18, 3–13.

Bold, M. (2010), Dimension and geometry analysis of the Upper Jurassic sponge-microbial bioherms of the Swabian Alb (SW-Germany). Master Thesis, Tübingen, Germany, 96 pp.

Brown, A.R. (1996) Seismic attributes and their classification. *The Leading Edge*, 15, 1090.

Catuneanu, O., Galloway, W.E., St. Kendall, C.G.C., Miall, A.D., Posamentier, H.W., Strasser, A. and Tucker, M.E. (2011) Sequence Stratigraphy: Methodology and Nomenclature. *Newsl. Stratigr.*, 44, 173–245.

Chen, Q. and Sidney, S. (1997) Seismic attribute technology for reservoir forecasting and monitoring. *The Leading Edge*, 16, 445–456.

Chiracal, T. (2019), Size and Dimensions of Biohermal Build-ups from the Swabian Alb, Tübingen, Germany, research project, unpublished.

Chitale, V.D., Johnson, C., Entzminger, D. and Canter, L. (2010) Application of a modern electrical borehole imager and a new image interpretation technique to

- evaluate the porosity and permeability in carbonate reservoirs: A case history from the Permian Basin, United States. In: Dipmeter and borehole image log technology (Eds. M. Pöppelreiter, C. García-Carballido and M. Kraaijveld), AAPG Memoir 92, 295–307.
- Coats, K.H. (1989) Implicit Compositional Simulation of Single-Porosity and Dual-Porosity Reservoirs. SPE Society of Petroleum Engineers, 1–37.
- Deutsche Stratigraphische Kommission (2016) Stratigraphische Tabelle von Deutschland. Deutsches GeoForschungsZentrum, Berlin, 1.
- Duhon, L. and Topping, D. (2017) Halliburton Reservoir Innovations. Imaging Carbonates. A Formation Evaluation Technology Journal, 1, 1–76.
- Durkin, P.R., Boyd, R.L., Hubbard, S.M., Shultz, A.W. and Blum, M.D. (2017) Three-Dimensional Reconstruction of Meander-Belt Evolution, Cretaceous McMurray Formation, Alberta Foreland Basin, Canada. Journal of Sedimentary Research, 87, 1075–1099.
- Dussel, M., Moeck, I., Wolfgramm, M. and Straubinger, R. (2018) Characterization of a Deep Fault Zone in Upper Jurassic Carbonates of the Northern Alpine Foreland Basin for Geothermal Production (South Germany). PROCEEDINGS, 43rd Workshop on Geothermal Reservoir Engineering Stanford University, Stanford, California, 1–8.
- Eigler, M. (2018), Brenztal-Trümmerkalk Facies Analysis, Sequence Stratigraphy and 3D-Modelling. (Mergelstetten Quarry, SW Germany). Master Thesis, Tübingen, Germany, 164 pp.
- Emery, D. and Myers, K.J. (1996), Sequence Stratigraphy, Blackwell Science Limited, 297 pp.
- Fritz, G.K. (1958) Schwammstotzen, Tuberolithe und Schuttbreccien im weißen Jura der schwäbischen Alb. Eine vergleichende petrogenetische Untersuchung. Arbeiten aus dem Geologisch-Paläontologischen Institut der Technischen Hochschule Stuttgart, Neue Folge, 13, 1–119.
- Fügel, F. (2009), Facies- and 3D-Modelling of an Upper Jurassic Bioherm-Cementmarl-Complex (Allmendingen Quarry, SW-Germany). Master Thesis, Tübingen, Germany, 128 pp.

- Garcia-Carbadillo, C., Boon, J. and Tso, N. (2010) Data management and quality control of dipmeter and borehole image- log data. In: Dipmeter and borehole image log technology (Eds. M. Pöppelreiter, C. García-Carballido and M. Kraaijveld). AAPG Memoir 92, 39-50.
- Geyer, O.F. and Gwinner, M.P. (1984) Die Schwäbische Alb und ihr Vorland (3rd ed.). Sammlung geologischer Führer, 67, 271 pp.
- Guo, J.-C., Nie, R.-S. and Jia, Y.-L. (2012) Dual permeability flow behavior for modeling horizontal well production in fractured-vuggy carbonate reservoirs. Journal of Hydrology, 464-465, 281–293.
- Gwinner, M.P. (1976) Origin of the Upper Jurassic of the Swabian Alb. Sedimentology, 5, 1–75.
- Gygi, R.A. (1986) Mineralostratigraphy, litho- and biostratigraphy combined in correlation of the Oxfordian (Late Jurassic) formations of the Swiss Jura range. Eclogae Geologicae Helveticae, 79, 385–454.
- Handford, C.R. and Loucks, R.G. (1993) Carbonate Depositional Sequences and Systems Tracts--Responses of Carbonate Platforms to Relative Sea-Level Changes: Chapter 1. AAPG Memoir, 57, 545 pp.
- Haq, B.U., Hardenbol, J.A.N. and Vail, P.R. (1987) Chronology of fluctuating sea levels since the Triassic. Science (New York, N.Y.), 235, 1156–1167.
- Homuth, S., Götz, A.E. and Sass, I. (2015) Reservoir characterization of the Upper Jurassic geothermal target formations (Molasse Basin, Germany): role of thermofacies as exploration tool. Geoth. Energ. Sci., 3, 41–49.
- Kearns, C. and Tinker, S.W. (1997), Sequence Stratigraphy and Characterization of Carbonate Reservoirs, SEPM Short Course, 40, 130 pp.
- Keeton, G.I., Pranter, M.J., Cole, R.D. and Gustason, E.R. (2015) Stratigraphic architecture of fluvial deposits from borehole images, spectral-gamma-ray response, and outcrop analogs, Piceance Basin, Colorado. Bulletin, 99, 1929–1956.
- Koch, R. and Heuschkel, S. (2016) Flachwasser Partikel-Kalke (Karbonatsande) des Malm Delta/Epsilon am SO-Rand des Nördlinger Ries (S-Dtl., Steinbruch Bräulesberg, Märker Kalk). Geologische Blätter für Nordost-Bayern, 66, 141–163.

- Koch, R., Senowbari-Daryan, B. and Strauss, H. (1994) The Late Jurassic 'Massenkalk Fazies' of southern Germany: calcareous sand piles rather than organic reefs. *Facies*, 31, 179–208.
- Leinfelder, R. R. (1993) Upper Jurassic Reef Types and Controlling Factors. a preliminary report. *Biogene Sedimentation DFG*, 5, 1–45.
- Leinfelder, R. R., Werner, W., Nose, M., Schmid, D.U., Krautter, M. and al, e. (1996) Paleocology, Growth Parameters and Dynamics of Coral, Sponge and Microblite Reefs from the Late Jurassic. *Göttinger Arbeiten, Geol. Paleo*, 2, 227–248.
- Leinfelder, R.R., Krautter, M., Laternser, R., Nose, M., Schmid, D.U., Schweigert, G., Werner, W., Keupp, H., Brugger, H. and Herrmann, R. (1994) The origin of Jurassic reefs: current research developments and results. *Facies*, 31, 1–56.
- Leinfelder, R. R., Nose, M., Schmid, D. U. and Werner, W. (1993) Microbial crusts of the Late Jurassic: composition, palaeoecological significance and importance in reef construction. *Facies*, 29, 195–230.
- Lemcke, K. (1987) Zur Frage der alten Verkarstung des Malm im Untergrund des deutschen Molassebeckens und an dessen Nordwestrand. *Bull. Ver. schweiz. Petroleum-Geol. u- -Ing.*, 125, 33–46.
- Lemcke, K. (1988) Das bayerische Alpenvorland vor der Eiszeit. *Geologie von Bayern* 1, 175 pp.
- Lesić, N.-M. (2019) The 'Purbeck Formation' of the Molasse Basin (South-Germany). Subsurface Facies, Log and Sequence Analysis. MSc. Thesis, Eberhard-Karls University, Tuebingen, 1–107.
- Lucia, F.J. (2007), Carbonate reservoir characterization. An integrated approach. 2nd edn., Springer, Berlin, New York, xii, 336 pp.
- Mai, A. and Kantzas, A. (2007) Porosity Distributions in Carbonate Reservoirs using Low-Field NMR. *Journal of Canadian Petroleum Technology*, 46, 30–36.
- Meyer, R.K.F. (1994a) „Moosburg 4“, die erste Kernbohrung durch den Malm unter der bayerischen Molasse. *Erlanger geologische Abhandlungen*, 123, 51–81.
- Meyer, R.K.F. and Schmidt-Kaler, H. (1989) Paläogeographischer Atlas des süddeutschen Oberjura (Malm). *Geologisches Jahrbuch*, A/115, 3–77.

- Meyer, R. K. F. and Schmidt-Kaler, H. (1990) Paläogeographie und Schwammriffentwicklung des süddeutschen Malm—ein Überblick. *Facies*, 23, 175–184.
- Miall, A.D. (1985) Architectural-Element Analysis A New Method of Facies Analysis Applied to Fluvial Deposits. *Earth-Science Reviews*, 22, 261–308.
- Miller, C.R., James, N.P. and Kyser, T.K. (2013) Genesis of Blackened Limestone Clasts At Late Cenozoic Subaerial Exposure Surfaces, Southern Australia. *Journal of Sedimentary Research*, 83, 339–353.
- Mitchum, R.M. and Vail, P.R. (1977) Seismic stratigraphic interpretation procedures. In: *Seismic stratigraphy-Applications to hydrocarbon exploration* (Ed. C.E. Payton), AAPG Memoir 26, 135–143.
- Moeck, I.S. (2014) Catalog of geothermal play types based on geologic controls. *Renewable and Sustainable Energy Reviews*, 37, 867–882.
- Nian, T., Jiang, Z. and Song, H. (2018) Borehole image electrofacies with a comparative carbonate petrography analysis: An outcrop well study associated with reservoir application in the Ordovician Tarim Basin. *Interpretation*, 6, 723-737.
- Niebuhr, B. and Pürner, T. (2014) Plattenkalk und Frankendolomit—Lithostratigraphie der Weißjura-Gruppe der Frankenalb (außeralpiner Oberjura, Bayern). *Schriftenreihe der Deutschen Gesellschaft für Geowissenschaften*, 83, 5–72.
- Olivier, N., Pittet, B. and Mattioli, E. (2004) Palaeoenvironmental control on sponge-microbialite reefs and contemporaneous deep-shelf marl-limestone deposition (Late Oxfordian, southern Germany). *Palaeogeography, Palaeoclimatology, Palaeoecology*, 212, 233–263.
- Pawellek, T. (2001) Fazies-, Sequenz-, und Gamma-Ray-Analyse im höheren Malm der Schwäbischen Alb (SW-Deutschland) mit Bemerkungen zur Rohstoffgeologie (hochreine Kalke). *Tübinger geowissenschaftliche Arbeiten: Paläontol Stratigr*; 61; 1 – 246.
- Pawellek, T. and Aigner, T. (2003a) Apparently homogenous “reef”-limestones built by high-frequency cycles. *Sedimentary Geology*, 160, 259–284.

Pawellek, T. and Aigner, T. (2003b) Stratigraphic architecture and gamma ray logs of deeper ramp carbonates (Upper Jurassic, SW Germany). *Sedimentary Geology*, 159, 203–240.

Pawellek, T. and Aigner, T. (2004) Dynamic stratigraphy as a tool in economic mineral exploration: ultra-pure limestones (Upper Jurassic, SW Germany). *Marine and Petroleum Geology*, 21, 499–516.

Pearson, R.A. and Hart, B.S. (2004) Three-Dimensional Seismic Attributes Help Define Controls on Reservoir Development: Case Study from the Red River Formation, Williston Basin. In: *Seismic Imaging of Carbonate Reservoirs and Systems* (Eds. G. Eberli, J.L. Masferro and F.J. Sarg), AAPG Memoir 81, 43–57.

Pomar, L. (2001) Types of carbonate platforms: a genetic approach. *Basin Research*, 313–334.

Ponsot, C.M. and Vail, P.R. (1991b) Sequence stratigraphy of the Jurassic: New data from the Paris - London Basin compiled from well logs. *AAPG Bulletin*, 75., 665 pp.

Popov, P., Qin, G., Bi, L., Efendiev, Y., Kang Z. and Li, K.J. (2009) Multiphysics and Multiscale Methods for Modeling Fluid Flow Through Naturally Fractured Carbonate Karst Reservoirs. *SPE Society of Petroleum Engineers*, 119104, 218–231.

Pöppelreiter, M., Garcia-Carbadillo, C. and Kraaijveld, M. (2010) Borehole image-log technology: Application across the exploration and production life cycle. In: *Dipmeter and borehole image log technology* (Eds. M. Pöppelreiter, C. García-Carballido and M. Kraaijveld), AAPG Memoir 92, 1–13.

Prensky, S. (1999) Advances in borehole imaging technology and applications. In: *Borehole Imaging: Applications and Case Histories* (Eds. M.A. Lovell, G. Williamson and P.K. Harvey), Special Publication, 1–44.

Pross, J., Link, E., Ruf, M. and Aigner, T. (2006) Delineating Sequence Stratigraphic Patterns in Deeper Ramp Carbonates. Quantitative Palynofacies Data from the Upper Jurassic (Kimmeridgian) of Southwest Germany. *Journal of Sedimentary Research*, 76, 524–538.

Purwanto, K.E. (2002), Reservoir characterization using borehole images from behind: outcrop wells, Rock Springs Uplift, Wyoming, PhD thesis, Colorado School of Mines, 192 pp.

Quenstedt, F.A. (1858), *Der Jura*, Tübingen, Germany, 842 pp.

Reid, S.K. and Dorobek, S.L. (1993) Sequence stratigraphy and evolution of a progradational, foreland carbonate ramp, Lower Mississippian Mission Canyon Formation and stratigraphic equivalents, Montana and Idaho. In: *Sequence stratigraphy and evolution of a progradational, foreland carbonate ramp, Lower Mississippian Mission Canyon Carbonate Sequence Stratigraphy—Recent Developments and Applications* (Eds. R.G. Loucks and F.J. Sarg), AAPG Memoir 57, 327–352.

Rüdiger, T. and Schulz, R. (2007), *Facies Differentiation of the Malm by Interpretation of Reflection Seismic Profiles and a Moving Source VSP Experiment*, Unterhaching, Germany, 7 pp.

Ruf, M., Link, E., Pross, J. and Aigner, T. (2005a) A multi-proxy study of deeper-water carbonates (Upper Jurassic, southern Germany): combining sedimentology, chemostratigraphy and palynofacies. *Facies*, 51, 327–349.

Ruf, M., Link, E., Pross, J. and Aigner, T. (2005b) Integrated sequence stratigraphy: Facies, stable isotope and palynofacies analysis in a deeper epicontinental carbonate ramp (Late Jurassic, SW Germany). *Sedimentary Geology*, 175, 391–414.

Schick, H. (2004) Subdivision and type section of the “Lacunosamergel-Formation” (Upper Jurassic, Swabian Alb, Germany). *Stuttgarter Beiträge zur Naturkunde, Serie B*, 346, 1-25.

Schlager, W. (1993) Accommodation and supply—a dual control on stratigraphic sequences. *Sedimentary Geology*, 86, 111–136.

Schlager, W. (2005), *Carbonate Sedimentology and Sequence Stratigraphy. Concepts in Sedimentology and Paleontology*, Society of Economic Paleontologists and Mineralogists (SEPM), 200 pp.

Scotese, C.R. (2001), *Atlas of Earth History. PALEOMAP Project*. <http://www.scotese.com>.

Seilacher, A. (2007), *Trace Fossil Analysis*, Springer-Verlag Berlin Heidelberg, 226 pp.

Seithel, R., Müller, B., Zosseder, K., Schilling, F. and Kohl, T. (2018) Betrachtung der Seismizität um Geothermie-Anlagen im geomechanischen Kontext. *Geothermische Energie*, 89, 24–27.

Serra, O. (1989) Formation Microscanner Image Interpretation. Schlumberger Educational Service, 1–117.

Sissingh, W. (1997) Tectonostratigraphy of the North Alpine Foreland Basin: correlation of Tertiary depositional cycles and orogenic phases. *Tectonophysics*, 1997, 223–256.

Steiner, U. and Böhm, F. (2011), Lithofacies and structure signatures of ImageLog in carbonates and their implications for reservoir characterisation in Southern Germany, Valencia, Spain.

StMWIVT (2010) Bayerischer Geothermieatlas, 2010.

Strasser, A. (1986) Ooids in Purbeck limestones (lowermost Cretaceous) of the Swiss and French Jura. *Sedimentology*, 33, 711–727.

Strasser, A. and Davaud, E. (1983) Black pebbles of the Purbeckian (Swiss and French Jura): lithology, geochemistry and origin. *Eclogae Geologicae Helveticae*, 76, 551–580.

Tinker, S.W., Caldwell, D.H., Cox, D.M. and Zahm, L.C. Brinton, L. (2004) Integrated Reservoir Characterization of a Carbonate Ramp Reservoir, South Dagger Draw Field, New Mexico: Seismic Data Are Only Part of the Story. *AAPG Memoir*, 81, 91–105.

Trice, R. (1999) A methodology for applying a non-unique, morphological classification to sine wave events picked from borehole image log data. In: *Borehole Imaging: Applications and Case Histories* (Eds. M.A. Lovell, G. Williamson and P.K. Harvey), Special Publication, 159pp.

Van Wagoner, J.C., Mitchum, R.M., Campion, K.M. and Rahmanian, V.D. (1990) Siliciclastic sequence stratigraphy in well logs, cores, and outcrops. *American Association of Petroleum Geologists Methods in Exploration Series*, 0–55.

Van Wagoner, J.C., Posamentier, H.W., Mitchum, R.M., Vail, P.R., Sarg, J.F., Loutit, T.S. and Hardenbol, J. (1988) An overview of the fundamentals of sequence stratigraphy and key definitions. *Society of Economic Paleontologists and Mineralogists Special Publication*, 42, 39–45.

- Villinger, E. and Fleck, E. (1995) Symbolschlüssel Geologie (Teil 1) und Bodenkunde Baden-Württemberg. Informationen des geologischen Landesamt Baden-Württemberg, 5, 68.
- Wagenplast, P. (1972) Okologische Untersuchung der Fauna aus Bank- und Schwammfazies des Weißen Jura der Schwabischen Alb. Arb. Inst. Geol. Paläont. Universität Stuttgart, 67, 1–99.
- Walker, R.G. and James, N.P. (1992), Facies Models; Response to sea Level Change, 409 pp.
- Warnecke, M. and Aigner, T. (2019) Influence of subtle paleo-tectonics on facies and reservoir distribution in epeiric carbonates: Integrating stratigraphic analysis and modelling (U. Muschelkalk, SW Germany). *Sedimentary Geology*, 383, 82–100.
- Weissert, H. and Mohr, H. (1996) Late Jurassic climate and its impact on carbon cycling. *Palaeogeography, Palaeoclimatology, Palaeoecology*, 27–43.
- Werner, F. and Wetzel, A. (1982) Interpretation of biogenic structures in oceanic sediments. *Bulletin de l'Institut Géologique du Bassin d'Aquitaine*, 275–288.
- Wetzel, A., Allenbach, R. and Allia, V. (2003) Reactivated basement structures affecting the sedimentary facies in a tectonically “quiescent” epicontinental basin: an example from NW Switzerland. *Sedimentary Geology*, 157, 153–172.
- Wolfgramm, M., Dussel, M., Lueschen, E., Schulz, R., Thomas, R. and Koch, R. (2011) Zuflusszonen im Malm – Untersuchungen des geothermischen Hauptgrundwasserleiters im süddeutschen Molassebecken. *bbr Sonderheft Geothermie*, 75–82.
- Wolpert, P.J., Aigner, T., Beichel, K., Steiner, U. and Savvatis, A. (2019), Linking 3D Seismic Interpretation and Borehole Image Facies to Unravel Sequence Stratigraphic Architecture of Jurassic Carbonates, EAGE Annual Conference, London, UK.
- Wolpert, P.J. and Poppelreiter, M.C. (2019) Borehole-image-log characterization of deltaic deposits from a behind-outcrop well: Opportunities and limitations. *Journal of Sedimentary Research*, 89, 1207–1230.
- Ziegler, B. (1977) The “White” (Upper) Jurassic in southern Germany. *Stuttg. Beitr. Naturkd.*, 1–79.

Ziegler, M.A. (2001) Late Permian to Holocene paleofacies evolution of the Arabian Plate and its hydrocarbon occurrences. *GeoArabia*, 6, 445–504.

Ziegler, P. (1990) *Geological atlas of Western and Central Europe*. Shell Internationale Petroleum Maatschappij, B.V., The Hague.

Ziegler, P.A. and Dèzes, P. (2006) Crustal evolution of Western and Central Europe. *Geological Society, London, Memoirs*, 32, 43–56.